



PhD Program in Neuroscience

Instituto de Neurociencias (CSIC-UMH)

Genetic robustness of EMT-TFs in zebrafish heart laterality

Noemi Castroviejo Jiménez

Thesis director

Prof. Maria Ángela Nieto Toledano

University Miguel Hernández de Elche



This Doctoral Thesis, entitled " Genetic robustness of EMT-TFs in zebrafish heart laterality " is presented under the **conventional thesis form with the following quality indicator(s)**:

- **N. Castroviejo**, O. H. Ocaña, L. Rago, H. Coskun, A. Arcas, J. Galceran, and M. A. Nieto. 2020. "Reply to: Zebrafish *prrx1a* mutants have normal hearts." Nature 585, E17–E19, 2020. Doi: [10.1038/s41586-020-2675-0](https://doi.org/10.1038/s41586-020-2675-0)



Sant Joan d'Alacant, 7th April 2022

Prof. Ms. M. Ángela Nieto Toledano, Director of the doctoral thesis entitled "**Genetic robustness of EMT-TFs in zebrafish heart laterality**".

INFORM/S:

That Ms. Noemi Castroviejo Jiménez has carried out under my supervision the work entitled "**Genetic robustness of EMT-TFs in zebrafish heart laterality**" in accordance with the terms and conditions defined in her Research Plan and in accordance with the Code of Good Practice of the University Miguel Hernández of Elche, satisfactorily fulfilling the objectives foreseen for its public defence as a doctoral thesis.

I sign for appropriate purposes, at Sant Joan d'Alacant, 7th of April of 2022

Thesis director

Prof. Ms. M. Ángela Nieto Toledano



Sant Joan d'Alacant, 7th April 2022

Dr. Ms. Elvira de la Peña García, Coordinator of the Neurosciences PhD Program at the Institute of Neurosciences in Alicante, a joint centre of the Miguel Hernández University (UMH) and the Spanish National Research Council (CSIC),

INFORMS:

That Ms. Noemi Castroviejo Jiménez has carried out under the supervision of our PhD Program the work entitled "Genetic robustness of EMT-TFs in zebrafish heart laterality" in accordance with the terms and conditions defined in its Research Plan and in accordance with the Code of Good Practice of the University Miguel Hernández de Elche, fulfilling the objectives satisfactorily for its public defence as a doctoral thesis.

Which I sign for the appropriate purposes, in Sant Joan d'Alacant, 7th of April of 2022

Dr. Ms. Elvira de la Peña García

Coordinator of the PhD Program in Neuroscience



Funding/Grants/Scholarship:

The completion of this Doctoral Thesis has been carried out thanks to a “Formación de Profesorado Universitario (FPU)” pre-doctoral scholarship financed by the Ministry of Universities with reference FPU15-01057 (2017-2021), and a contract of higher degree in technical and professional activities funded by the National R&D Plan project with reference RTI2018-096501-B-I00 (2021-Present).

The research has been funded by the following research projects:

- “Common molecular pathways in epithelial-mesenchymal transition and left-right asymmetries” – European Research Council (ERC Advanced grant. AdG322694) (2013-2018).
- “La complejidad de la plasticidad epitelial: implicación en fisiología, patología y estrategias terapéuticas” – RTI2018-096501-B-I00 (2019-Present)

*"Talent is worthless
unless exercised"*

Dimmu Borgir

TABLE OF CONTENTS

TABLE OF CONTENTS.....	1
LIST OF SYMBOLS AND ABBREVIATIONS	5
ABSTRACT.....	9
RESUMEN	13
INTRODUCTION	17
1. Left-Right Asymmetry	19
1.1. Breaking of bilateral symmetry and fluid flow in the L/R organizer	20
1.1.1. Initial symmetry breaking	20
1.1.2. Generation of asymmetric flow	20
1.1.3. Sensing asymmetric flow	20
1.1.4. Asymmetric gene expression around the LRO.....	20
1.2. Asymmetric gene expression in the lateral plate mesoderm	23
1.2.1. Self-enhancement and lateral-inhibition feedback system	20
1.2.2. Asymmetric expression in the LPM.....	20
1.3. Organ laterality	25
2. Cardiac Development.....	26
2.1. Zebrafish heart morphogenesis.....	26
2.2. Mouse heart morphogenesis	28
2.3. Contribution of first and second heart fields to the vertebrate heart.....	29
2.4. Cardiac transcription factors	31
2.5. Asymmetric heart morphogenesis.....	32
2.5.1. Cardiac asymmetries preceding looping.....	32
2.5.2. Heart looping steps	33
2.5.3. Intrinsic vs. extrinsic mechanism driving asymmetric heart laterality	34
2.6. Heart laterality defects	37
3. Epithelial to Mesenchymal Transition in Development and Disease.....	39
3.1. EMT during heart development	41
3.2. EMT inducers.....	42
3.2.1. SNAIL.....	43
3.2.2. PRRX.....	44
3.2.3. EMT-TFs and L/R asymmetry	45

OBJECTIVES	49
General Objective.....	51
Specific Objectives.....	51
MATERIALS AND METHODS	53
1. Zebrafish Embryos	55
1.1. Genotyping mutant lines	57
2. Injections in Zebrafish	57
2.1. CRISPR-Cas9 injections	57
2.2. CRISPR-Cas13d injections	58
3. Whole-mount in <i>situ</i> Hybridisation (Colorimetric and Fluorescent)	59
3.1. Design of probes for ISH	60
4. Whole-mount Immunofluorescence	61
5. <i>In silico</i> Analysis	62
6. Fixed Sample – Image Acquisition and Processing	62
6.1. Microscopy image acquisition	62
6.2. Processing of image data.....	63
6.2.1. <i>spaw</i> , jogging and heart laterality.....	63
6.2.2. Posterior pole displacement and looping angle	63
6.2.3. Area of atrium and cilia length.....	63
6.2.4. Quantification of number of cells (L/R <i>Prrx1</i> in <i>TgBAC(tbx5a:eGFP)</i>).....	63
7. <i>In vivo</i> Time Lapse	64
7.1. Acquisition.....	64
7.2. Processing of time-lapse data	64
8. Statistical Analysis and Figures Design	65
RESULTS	67
1. <i>Prrx1a</i> in Heart Laterality	69
1.1. <i>prrx1a</i> is asymmetrically expressed in cardiac precursors	69
1.2. G0- <i>prrx1a</i> crispants show mesocardia and additional heart defects.....	73
1.3. <i>Prrx1a</i> can be dispensable but plays a specific role in heart laterality	78
2. Genetic Cooperation of EMT-TFs in Zebrafish Heart Laterality	84
2.1. Other EMT-TFs, <i>prrx1b</i> , <i>snail1b</i> and <i>twist1a</i> are also asymmetrically expressed in heart precursors	84
2.2. Cooperation between EMT-TFs in heart laterality	90
2.2.1. Functional analysis of individual TFs	90
2.2.2. Functional analysis of combinations of EMT-TFs	93

2.3. Lack of heart laterality phenotype or low penetrance in individual EMT-TF stable mutants	94
2.4. Cooperation explains the lack or incomplete penetrance of heart laterality phenotype in individual EMT-TFs stable mutants	96
DISCUSSION	101
1. <i>prrx1α</i> -LOF reagents specifically impair heart laterality in zebrafish	104
2. Additional TFs expressed in the aLPM are also involved in driving heart laterality in zebrafish.....	107
3. Heart laterality is a robust process supported by the cooperation of EMT-TFs in the aLPM	110
CONCLUSIONS	115
CONCLUSIONES.....	115
BIBLIOGRAPHY.....	121
ANNEX.....	159
ACKNOWLEDGEMENTS	173

LIST OF SYMBOLS AND ABBREVIATIONS

- **A/D:** Anterior-Dorsal
- **A/P:** Anterior-Posterior
- **A:** Deoxyadenosine
- **AF:** Atrial Fibrillation
- **aLPM:** anterior Lateral Plate Mesoderm
- ***amhc:*** atrial myosin heavy chain
- **AP:** Arterial Pole
- **aSHF:** anterior SHF
- **AVC:** Atrioventricular Canal
- **ba:** branchial arches
- **BA:** Bulbus Arteriosus
- **BAC:** Bacterial Artificial Chromosome
- **BM:** Basement Membrane
- **BMP/Bmp/bmp:** Bone Morphogenetic Protein or gen
- **bpm:** beats per minute
- **BSA:** Bovine Serum Albumin
- **Ca²⁺:** Calcium
- **Cas9:** CRISPR-associated protein 9
- **CD:** Cardiac Disc
- **cf:** caudal fin
- **cg:** cranial ganglia
- **CHD:** Congenital Heart Defects
- **CM:** Cardiomyocytes
- **CNCC:** Cardiac Neural Crest Cells
- **cns:** central nervous system
- **CPCs:** Cardiac Progenitors Cells
- **CRISPR:** Clusters of Regularly Interspaced Short Palindromic Repeats
- **D/V:** Dorso-Ventral
- **DAPI:** 4',6-diamidine-2' - phenylindole dihydrochloride
- **DEPC:** Diethylpyrocarbonate
- **DFCs:** Dorsal Forerunner Cells
- **dgRNA:** duplex guide RNAs
- **DIG:** Digoxigenin
- **DM:** Dorsal Mesocardium
- **dpf:** days post-fertilization
- **dRFP:** destabilized Red Fluorescence Protein
- **DSB:** Double Strand Break
- **E:** Embryonic day
- **ECM:** Extracellular Matrix
- **EMT:** Epithelial-Mesenchymal Transition
- **EndMT:** Endothelial- Mesenchymal Transition
- **F:** Forward
- **FGF8/Fgf8:** Fibroblast Growth Factor 8
- **FHF:** First Heart Field
- **GO:** Generation 0
- **GWAS:** Genome-Wide Association Study

- **hg**: hatching gland
- **hpf**: hours post fertilization
- **HR**: Homologous Recombination
- ***hst***: *heartstring*
- **HT**: Heart Tube
- **IC**: Inner Curvature
- **Icos**: Intracellular calcium (Ca^{2+}) oscillations
- **IFT**: Inflow Tract
- **ISH**: *In Situ* Hybridization
- **KD**: Knockdown
- **KV**: Kupffer's Vesicle
- **L/R**: Left-Right
- **LOF**: Loss-of-Function
- **LPM**: Lateral Plate Mesoderm
- **LRO**: Left-Right Organizer
- **MEF**: Mouse Embryonic Fibroblast
- **MET**: Mesenchymal-Epithelial Transition
- **miRNAs**: microRNAs
- **MO**: Morpholino
- ***myl7***: *myosin light chain 7*
- **NC**: Neural Crest
- **nch**: notochord
- **NGS**: Normal Goat Serum
- **np**: neural plate
- **nt**: nucleotide
- **O/N**: Overnight
- **OC**: Outer Curvature
- **OFT**: Outflow Tract
- **ORF**: Open Reading Frame
- **PAM**: Protospacer Adjacent Motif
- **PBS**: Phosphate Buffered Saline
- **PBTw**: PBS with Tween-20
- **PBTx**: PBS with Triton X-100
- **PCP**: Planar Cell Polarity
- **PCR**: Polymerase Chain Reaction
- **pd**: pronephric duct
- **PE**: Proepicardial/Proepicardium
- **pf**: pectoral fin
- **PFA**: Paraformaldehyde
- **POD**: Peroxidase
- **PRRX/Prrx/prrx**: Paired-related homeobox
- **PS**: Primitive Streak
- **pSHF**: posterior SHF
- **PTC**: Premature Termination Codon
- **R**: Reverse
- **RA**: Retinoic Acid
- **RNAi**: RNA interference
- **RNP**: Ribonucleoproteins
- **RT**: Room Temperature
- **scRNAseq**: single-cell RNA Sequencing
- **SELI**: Self-Enhancement and Lateral Inhibition
- **sGAGs**: Sulfated glycosaminoglycans
- **sgRNA**: single guide RNAs
- **SHF**: Second Heart Field
- **SHH**: Sonic Hedgehog
- **som**: somites
- **SPIM**: Selective plane illumination microscopy
- **T**: Deoxythymidine
- **TA**: Transcriptional Adaptation

- **TALEN**: Transcription Activator-Like Effector Nucleases
- **tb**: tailbud
- **TF**: Transcription Factor
- **TGD**: Teleost Genome Duplication
- **TGF- β** Transforming Growth Factor beta
- **UTR**: Untranslated Region
- **VP**: Venous Pole
- **YSL**: Yolk Syncytial Layer
- **Zeb/zeb**: Zinc-finger E-box-binding homeobox

ABSTRACT |

ABSTRACT

Most animals exhibit an external bilateral symmetry while there is an interior left-right (L/R) asymmetry regarding the position of the visceral organs, which is fundamental for their proper function. During development, these asymmetries are set up through the establishment of an intricate L/R cascade along the lateral plate mesoderm (LPM). In vertebrates, there are two parallel and mutually repressed pathways. The TGF- β family member Nodal exerts a dual function on the left-hand side. With its downstream target, Pitx2a, a paired-like homeodomain transcription factor (TF), it establishes left identity, and through the activation of several microRNAs, it attenuates the inducers of the epithelial-to-mesenchymal transition (EMT) on the left-hand side. This attenuation allows the predominance of the BMP pathway on the right LPM, where transient higher levels of its targets, EMT inducers such as Prrx1 and Snail1, lead to a differential L/R EMT that drives the leftward displacement of the posterior pole of the heart in vertebrates. Subsequent looping leads to the final position of the heart and laterality features optimal for its function.

In zebrafish, *prrx1a* acute loss-of-function (LOF) leads to a mesocardia phenotype due to the failure in the asymmetric contribution of cells that drives heart laterality. However, it has been shown that different allelic mutants for this EMT-TF present normal hearts. To better understand the role of Prrx1 and the overall process of heart laterality, we have investigated (i) the specificity of the described mesocardia phenotype, and (ii) the mechanism that can lead to the appearance of normal hearts in the *prrx* mutant background. With respect to specificity, using both, several sets of CRISPR/Cas9 RNA guides and a novel CRISPR/Cas13d-mediated strategy that targets the mRNA rather than editing the genome, we have confirmed the mesocardia phenotype. Regarding the mechanism, we have uncovered that both the cardiac TF *tbx5a* and additional EMT-TFs, namely *prrx1b*, *twist1a* and *snail1b*, also show a L/R asymmetric expression in the aLPM and lead to mesocardia after their CRISPR-Cas9-mediated acute loss in generation 0 (G0) embryos. Furthermore, LOF in G0 embryos for combinations of these TFs, reveal their cooperation in the process of heart laterality in the zebrafish. This cooperative behaviour of different EMT-TFs can explain the compensation of the phenotype in the *prrx1a* mutant background and provides robustness to the system, securing the proper position and, therefore, function of the heart.

RESUMEN |

RESUMEN

La mayoría de los animales presentan simetría bilateral externa, pero internamente existen asimetrías izquierda-derecha (I/D) en la disposición de los órganos, que es fundamental para su correcto empaquetamiento y funcionamiento. Durante el desarrollo embrionario, estas asimetrías ocurren tras el establecimiento de una cascada de señalización en el mesodermo lateral (LPM). En el LPM izquierdo, un miembro de la familia TGF- β llamado Nodal, ejerce una función dual. Por una parte, con su efector Pitx2, un factor de transcripción (TF) con homeobox y un dominio como el del gen *paired*, establecen la identidad izquierda. Por otra parte, Nodal activa de forma transitoria microRNAs que atenúan la expresión de factores inductores de transición epitelio-mesénquima (EMT) en el lado izquierdo. Esta atenuación permite la preponderancia de la cascada de señalización de BMP, otro miembro de la familia TGF- β , desde el lado derecho. Los niveles más elevados de sus efectores, factores inductores de la transición epitelio-mesénquima (EMT-TFs) como Snail1 y Prrx1, dan lugar a una EMT asimétrica, mayor desde el lado derecho que produce el desplazamiento del polo posterior del corazón hacia la izquierda, mecanismo que está conservado en los vertebrados. Posteriormente, ocurre el giro del corazón en un proceso denominado “looping” que conduce a la posición final del corazón, fundamental para su desarrollo y funcionamiento correcto.

En el pez cebra, la pérdida de función aguda de *prrx1a*, conduce a un fenotipo de mesocardia, debido a la falta de contribución asimétrica de células, mayor desde el lado derecho que dan lugar a la lateralidad del corazón. Sin embargo, diferentes mutantes de *prrx1a* tienen el corazón en posición normal. Para entender este hecho, hemos estudiado la especificidad del fenotipo de mesocardia, mediante la generación de nuevas guías para el sistema CRISPR/Cas9 más eficientes y hemos utilizado una tecnología CRISPR novedosa basada en Cas13d que, en lugar del editar el genoma, degrada los transcritos del gen correspondiente, lo que nos ha permitido confirmar el fenotipo. En cuanto al mecanismo, hemos descubierto que tanto el TF cardíaco *tbx5a* como otros EMT-TF, concretamente *prrx1b*, *twist1a* y *snail1b*, también mostraban una expresión asimétrica I/D en el aLPM y también conducen a la mesocardia tras su pérdida aguda mediada por CRISPR-Cas9 en embriones de generación 0 (G0). Además, la falta de función en embriones G0 o en mutantes para combinaciones de estos TFs, revela su cooperación en el proceso de lateralidad del corazón en el pez cebra. Este comportamiento cooperativo de los diferentes EMT-TFs puede explicar la compensación del fenotipo en el fondo mutante *prrx1a* y proporciona robustez al sistema, asegurando la posición y, por tanto, el funcionamiento adecuado del corazón.

INTRODUCTION |

1. Left-Right Asymmetry

On their surface, bilaterian animals such as vertebrates appear symmetrical. However, the positioning of visceral organs within the body cavity reveals an underlying and intrinsic left-right (L/R) asymmetry regarding their morphology and position, which is fundamental to their proper function (Hamada, 2020). Being asymmetric favours organ packaging, which has increased the evolutionary fitness of species (Blum and Ott, 2018). As such, heart points to the left, the liver is positioned on the right, pancreas and stomach on the left, the intestine rotates anticlockwise, and left and right lungs have different number of lobes (Figure 1) (Blum and Ott, 2018).

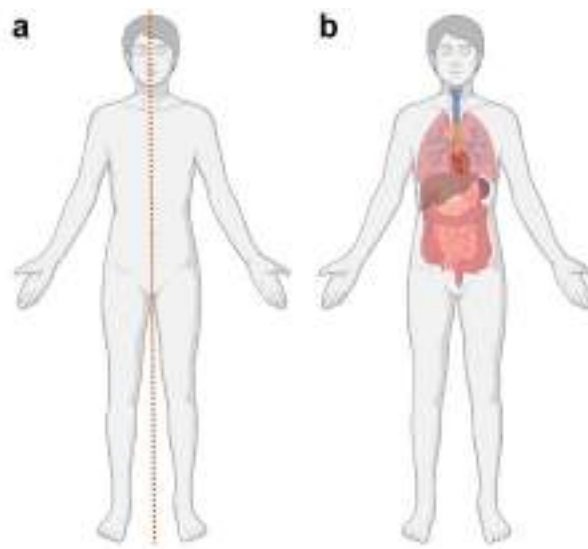


Figure 1 | Internal asymmetry of human body cavity. (a) Animals with external bilateral symmetry have a mirror symmetry in the sagittal plane, which divides the body vertically into right and left halves. **(b)** Asymmetric disposition of internal organs can be appreciated inside the body cavity.

One of the keystones in the developmental biology field is to unravel how these asymmetries arise and change during embryonic development (Levin et al., 2016). It is generally agreed that there are three phases: (i) a symmetry-breaking mechanism which originates a L/R axis oriented relative to the anteroposterior (A/P) and dorsoventral (D/V) ones; (ii) amplification of asymmetric gene expression along the embryo; (iii) and translation of the L/R asymmetric information into asymmetric morphogenesis of the organ primordia (Campione and Franco, 2016).

1.1. Breaking of bilateral symmetry and fluid flow in the L/R organizer

Across vertebrates, at the end of gastrulation, L/R specification is controlled by a transient midline structure at the anterior tip of the primitive streak (PS) of amniote embryos called left-right organizer (LRO) (Ferreira and Vermot, 2017). LRO's architecture is diverse among vertebrates, and it is known as Kupffer's vesicle (KV) in zebrafish, node in the mouse, Hensen's node in the chicken, gastrocoel roof plate in *Xenopus* and notochordal plate in rabbit (Nakamura and Hamada, 2012). Most vertebrates contain motile cilia in their LRO cells, whose rotational movement generates a counterclockwise fluid flow within the node cavity that causes the asymmetric activation of genetic pathways around the LRO's (Dasgupta and Amack, 2016; Smith et al., 2006). Some vertebrates as chicken (Gros et al., 2009), pig or reptiles (Kajikawa et al., 2020) do not rely on this mechanism as they do not contain a ciliated LRO (Blum et al., 2014). Alternatively, in the Hensen's node, there is an asymmetric cell rearrangement due to a leftward movement of cells (Mendes et al., 2014) which breaks L/R symmetry (Cui et al., 2009; Gros et al., 2009). Thus, while the symmetry breaking mechanisms appear to differ among animals, the molecular L/R patterning is conserved (Hamada and Tam, 2020).

1.1.1. Initial symmetry breaking

The initial step of symmetry breaking is the most debated in the field (Vandenberg and Levin, 2013). There are different models (which do not exclude the cilia flow model), as the chromatid segregation model (Sauer and Klar, 2012) or the ion flux hypothesis which claims that L/R symmetry breaking occurs prior to the formation of the LRO (Campione and Franco, 2016). In *Xenopus*, already from 2-4 cell stage, there is a L/R distribution of ion pumps (Qiu et al., 2005) which leads to asymmetric electrochemical gradients (Adams et al., 2006) due to pre-existing chiral microtubule and actin cytoskeletal components oriented in the D/V and A/P axes (Aw et al., 2008; Danilchik et al., 2006). Initial symmetry breaking has been deeply studied in *Xenopus*, and several of these components have been also identified in other species as chickens or zebrafish (Kawakami et al., 2005). Even mouse blastomeres seem not to be L/R equivalent (Roberts et al., 2011; Sun et al., 2012). Therefore, a unified model of early and late contribution to breaking symmetry is possible, with the ciliary flow model or the alternative in chick and other mentioned above, being important for amplifying and backing up pre-existing asymmetric information (Vandenberg and Levin, 2013).

1.1.2. Generation of asymmetric flow

At embryonic day (E)7.5, the mouse ventral node forms as a pit of ciliated cells (**Figure 2a**) (Lee and Anderson, 2008; Shiratori and Hamada, 2006). Those cilia already contain pre-existing positional cues: in the D/V axis, as they are in the ventral side of the cell, and in the A/P axis, as they are tilted towards the posterior side due to their asymmetrically positioned basal bodies (Hashimoto et al., 2010; Nonaka et al., 2005) which depend on core planar cell polarity (PCP) components (Minegishi et al., 2017). In addition, the intrinsic chirality of cilia due to the arrangement of microtubules and dynein arms causes the effective leftward fluid flow (Hamada, 2020).

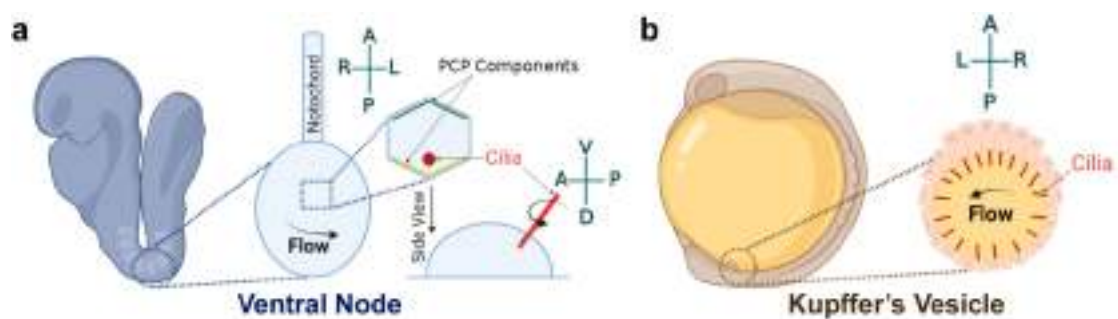


Figure 2 | LRO from mouse and zebrafish embryo. **(a)** Ventral node from mouse embryos whose cilia are positioned in the ventral and posterior part of their pit cells, producing a leftward asymmetric flow. **(b)** Monociliated cells of the Kupffer's vesicle (KV) from zebrafish have different morphologies. A leftward flow is generated leading to asymmetric gene activation.

In zebrafish, the KV is formed by precursor cells, called the dorsal forerunner cells (DFCs) which are specified during gastrulation at the dorsal margin of the embryo (Essner et al., 2005; Oteíza et al., 2008). This LRO caudal to the notochord, is a spherical structure filled with an internal fluid and composed by an average of 50 monociliated cells facing its lumen (**Figure 2b**) (Amack, 2014; Essner et al., 2005; Kramer-Zucker et al., 2005). Indeed, the cellular architecture of the KV is also asymmetric, as there is higher density of cells in the anterior-dorsal (A/D) region (Kreiling et al., 2007; Okabe et al., 2008). This is due to cell tension along its A/P axis that remodels and tightens the anterior KV cells (Wang et al., 2011, 2012) and to the accumulation of components of the extracellular matrix (ECM) secreted by the notochord in the A/D region (Compagnon et al., 2014). Consequently, the fluid flow is faster in this A/D region causing a L/R asymmetric flow (Sampaio et al., 2014).

Introduction

1.1.3. Sensing asymmetric flow

Once the asymmetric flow from the LRO has been generated, the embryo must sense it to evoke the activation of asymmetric genetic cascades (Hamada, 2020). The “two-cilia” hypothesis is based on the fact that mouse ventral node (and zebrafish’s KV (Sampaio et al., 2014)) contains two types of ciliated cells: pit cells with motile cilia in the centre that generate the flow, and crown cells with immotile primary cilia at the periphery to sense changes in the flow (McGrath et al., 2003). It has not been fully demonstrated yet what exactly is perceived by the cells (Grimes and Burdine, 2017), for which there are two prevalent models: (i) the chemosensation model by which particles or vesicles asymmetrically distributed are sensed on the left side (Okada et al., 2005; Tanaka et al., 2005); (ii) and the mechanosensation model by which the force of the flow is sensed instead of a chemical determinant (McGrath et al., 2003; Tabin and Vogal, 2003).

Whatever the cause, the flow triggers the activation of the calcium (Ca^{2+})⁺ channels Pkd2 and Pkd1-like-1 which send laterality cues into adjacent tissues (Field et al., 2011; Schottenfeld et al., 2007; Yoshida et al., 2012). Nevertheless, in the mouse, if mechanosensation originates in primary cilia is not via calcium signalling (Delling et al., 2016), while asymmetric intracellular Ca^{2+} oscillations (icos) are detected in zebrafish (Yuan et al., 2015). Thus, the connection between Ca^{2+} asymmetries and asymmetric gene expression is still under investigation (Grimes and Burdine, 2017).

1.1.4. Asymmetric gene expression around the LRO

Before the asymmetric flow occurs, at the 4-6 somite stage in zebrafish, *southpaw/spaw* (a secreted factor of the transforming growth factor β (TGF β) family, also known as Nodal) and *dand5/charon* (a member of the Cerberus/Dan family of secreted TGF- β repressor and also known as Cerl2) are bilaterally expressed around the LRO (Long et al., 2003). But in response to the asymmetric flow, *dand5* is downregulated in the left side (R>L), causing activation of left-sided *spaw* signalling at the 10-12 somite stage (Hashimoto et al., 2004; Nakamura et al., 2012) (**Figure 3a**). Therefore, a leftward flow is necessary and sufficient to produce the Nodal-dependent symmetry breakage in cilia-dependent vertebrate embryos (Blum et al., 2014).

Remarkably, *Cerl2* is absent in the cilia-independent LRO from reptiles and birds, where Nodal expression is intrinsically asymmetric (L>R) (Yoshida et al., 2016). Thus, different

vertebrates employ different strategies to accomplish the same Nodal asymmetric expression (Blum and Ott, 2018; Hamada, 2020).

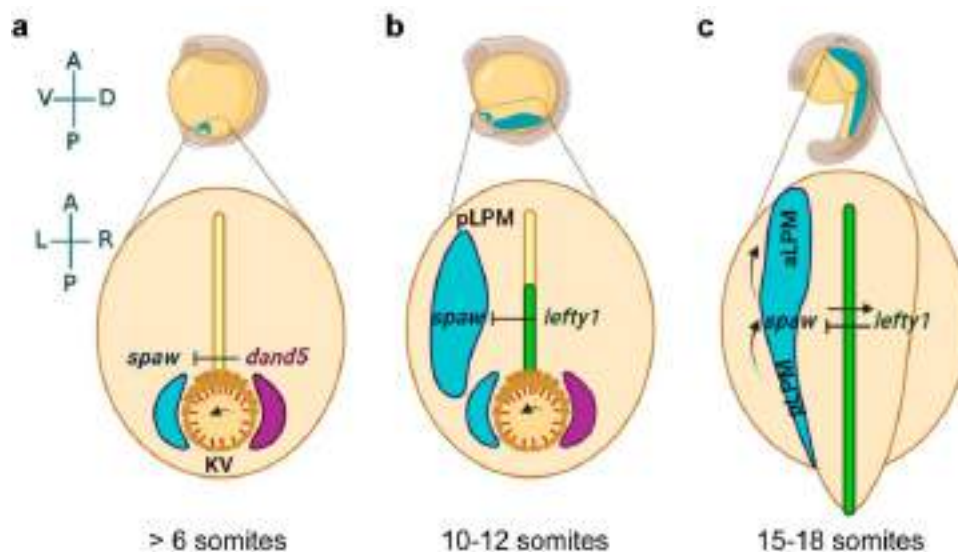


Figure 3 | Establishment of L/R cascade in zebrafish lateral plate mesoderm (LPM). (a) At around the 6-somite stage, the *spaw* inhibitor *dand5* (purple) is bilaterally expressed around the LRO but it is degraded on the left side leading to an increase of *spaw* (blue) expression in the left perinodal region. (b) From the 10-somite stage, *spaw* activates its own expression, which spreads through the left LPM activating the expression of its own inhibitor *lefty1* (green) in the notochord, acting as a barrier. (c) The posterior-to anterior Nodal wave leads to *spaw* expression all along the LPM, activating an asymmetric L/R cascade.

1.2. Asymmetric gene expression in the lateral plate mesoderm

Asymmetries that are originated in the surroundings of the LROs are then transmitted to the lateral plate mesoderm (LPM). Originated during gastrulation, LPM forms lateral to the paraxial mesoderm and it is flanked in the D/V axis by the ectoderm and the endoderm (Figure 4) (Lawson et al., 1991; Rosenquist, 1970; Tam and Beddington, 1987). Both A/P and D/V LPM axes are determined by the asymmetric expression of Nodal and the bone morphogenetic protein (BMP) (Arnold and Robertson, 2009; Hill, 2018). As body segmentation proceeds, the LPM is divided into anterior (aLPM) and posterior (pLPM), giving rise to different embryonic structures (Figure 4) (Prummel et al., 2020).

1.2.1. Self-enhancement and lateral-inhibition feedback system

In the zebrafish, and exclusively on the left-pLPM, *spaw* acts as a left determinant propagated as a wave from posterior to anterior (Wang and Yost, 2008). There are different

Introduction

strategies to maintain this asymmetric expression of *spaw*, including feedback systems such as self-enhancement and lateral-inhibition (SELI) (Figure 3b) (Nakamura et al., 2006). On one hand, Nodal regulates its own expression in the perinodal region and in the left LPM via the Nodal-responsive enhancer ASE (Brennan et al., 2002; Saijoh et al., 2003; Vincent et al., 2004). On the other hand, Nodal activates its own antagonists, the TGF- β family ligands Lefty1/2 (Bisgrove et al., 1999). Thus, *lefty1* acts as a midline barrier repressing *spaw* expression and restringing it to the left side (Figure 3c) (Lenhart et al., 2011; Meno et al., 1998). Besides, BMP signalling is required independently of Nodal to also activate *lefty1* in the midline to secure unilateral Nodal expression and a correct L/R cascade (Smith et al., 2011). This SELI system, a type of Turing reaction-diffusion system, is based on the principle of a faster diffusion of the inhibitor (*lefty1*) than the activator (*spaw*) (Müller et al., 2012; Wang et al., 2016).

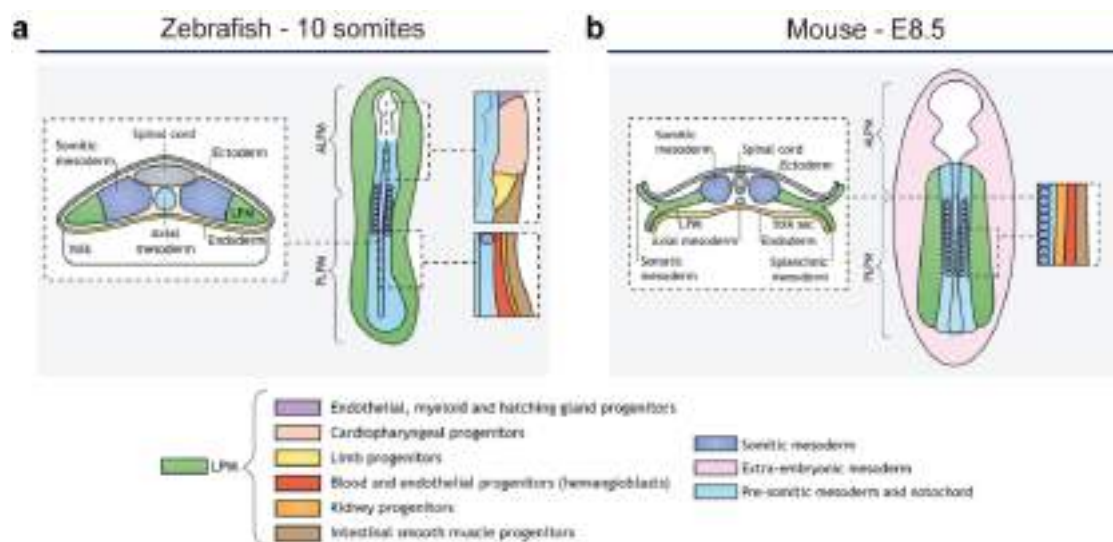


Figure 4 | LPM in zebrafish and mouse embryos. (a) The LPM (green) originates during gastrulation together with the axial and paraxial mesoderm (blue) which are contained between the ectoderm and endoderm. The architecture of LPM bilateral stripes becomes apparent during the segmentation stages when it is divided into anterior (aLPM) - where cardiopharyngeal progenitors reside (pink) - and posterior (pLPM) domains. (b) In amniotes, the post-gastrulation LPM splits into a dorsal somatic layer and a ventral splanchnopleuric layer. Modified from Prummel et al., 2020.

Additionally, Ca^{2+} signals are more prevalent on the left side and may reach the LPM as they might travel through endodermal cells connected through gap junctions (Beyer et al., 2012; Viotti et al., 2012). This calcium spreading leads to an increased secretion of sulphated glycosaminoglycans (sGAGs) in the basement membrane (BM) between the mesoderm and the endoderm (Oki et al., 2007), benefiting Nodal transfer (Norris, 2012).

1.2.2. Asymmetric expression in the LPM

Once Nodal signalling arrives to the left-aLPM activates the expression of Pitx2, a homeodomain transcription factor (TFs), whose expression remains until much later than that of Nodal (Yoshioka et al., 1998). In fact, the Nodal-Pitx2 signalling activated exclusively on the left side is involved in the asymmetric morphogenesis of visceral organs (Ryan et al., 1998).

In zebrafish, chick and mouse, the Nodal wave from pLPM to aLPM upregulates the expression of microRNAs (miRNAs) which transiently attenuate the expression of epithelial-mesenchymal transition (EMT) TFs Prrx1 and Snail1 along the left-LPM in a Pitx2-independent manner (Figure 5) (Rago et al., 2019). Nodal and BMP implement the left and right dominance through the mutual inhibition of their respective targets, securing a proper balance of L/R information (Rago et al., 2019).

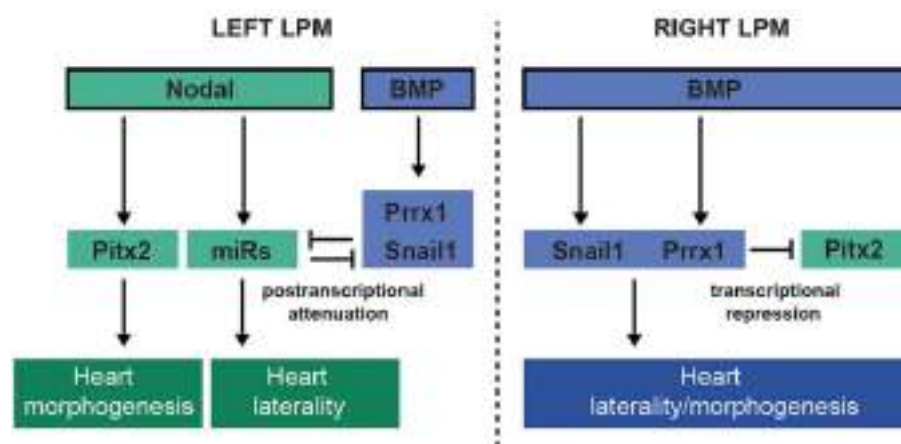


Figure 5 | Asymmetric expression in the LPM. A posterior-to-anterior Nodal wave upregulates miRNAs to transiently attenuate on the left the levels of the BMP-activated EMT-TFs Prrx1 and Snail1. Nodal and BMP exert their respective dominance on the left and right sides through the mutual inhibition of their respective targets, leading to a proper laterality and morphogenesis of the heart. Image from Rago et al., 2019.

1.3. Organ laterality

The L/R asymmetric gene expression along the LPM is transmitted to symmetric organ primordia in different ways: (i) if there is just one organ, as the heart or the gut, they are displaced from the midline through L/R asymmetric directional forces; (ii) if the primordia are bilateral, as the lung, they can undergo differential branching and growth; or (iii) unilateral regression as in the vascular system (Hamada, 2020 and Coskun et al., unpublished).

Introduction

The heart primordium is the first to break symmetry (Desgrange et al., 2018), occupying an asymmetrical position in the chest cavity showing an asymmetric morphology and connection with the vasculature (Grimes and Burdine, 2017). The asymmetric patterning occurs at different scales: organ level (as it is highly influenced by the L/R axis), cellular level (with asymmetric gene expression and cell behaviour) and at the molecular level (with chirality molecules) (Smith and Uribe, 2021). As the heart and the cardiovascular system come from progenitor cells in the LPM (Prummel et al., 2020), they are highly sensitive to L/R patterning defects (Gabriel and Lo, 2020).

2. Cardiac Development

2.1. Zebrafish heart morphogenesis

At the blastula stage, zebrafish cardiac progenitor cells (CPCs) are already specified to become atrial or ventricular myocardium (Keegan et al., 2004; Stainier et al., 1993). During gastrulation, they ingress and migrate forming two bilateral precardiac fields located in the posterior half of the aLPM, with ventricular progenitors medial to the atrial ones (Figure 6a) (Staudt and Stainier, 2012). By 16 hours post fertilization (hpf) (14-somite stage), myocardial differentiation begins with the formation of bilateral precardiac fields separated by the ventral midline and sandwiched between the anterior endoderm and the underlying yolk syncytial layer (YSL) (Yelon et al., 1999). Between 16-20 hpf these heart fields migrate as a polarized epithelium and fuse in the midline, forming the cardiac disc (CD) with endocardial progenitors lined among the atrial cells at the periphery and ventricle cells at the core (Figure 6b) (Bakkers, 2011; Trinh and Stainier, 2004). Meanwhile, CPCs that reside laterally to the CD in the aLPM remain undifferentiated (Figure 6b) (Smith and Uribe, 2021). From this ring-shaped heart, at 21-23 hpf a cone extends out forming a primitive heart tube (HT) (Stainier et al., 1993) with its venous pole (VP) being displaced towards the left in a process called cardiac jogging (Figure 6c) (Chen et al., 1997). By 24 hpf, the linear HT with a well-differentiated but rudimentary atrium and ventricle starts to pump while there is an addition of cells to the arterial pole (AP) and the VP (Kemmler et al., 2021). Cardiac jogging which is the leftward displacement of the HT respect to the A/P axis, is visible until 28hpf (Figure 6c) (Chen et al., 1997). A leftward displacement is maintained by the L/R asymmetric forces exerted by the incorporation to the VP of more cells from the right-hand side (Ocaña et al., 2017). From 30 hpf to 48 hpf the looping of the heart becomes apparent, with the left shift of the VP mentioned above and the rightward bending of the ventricle (Lombardo

et al., 2019) producing a flat S-shaped heart with a clear L/R asymmetry (Figure 6d). By 48hpf, both chambers of the looped heart are lined by the endocardium and separated by the atrioventricular canal (AVC) (Beis et al., 2005). In addition, chamber curvatures appear as a result of a process called ballooning that forms the convex outer and concave inner curvatures (OC and IC, respectively) (Figure 6e) (Auman et al., 2007).

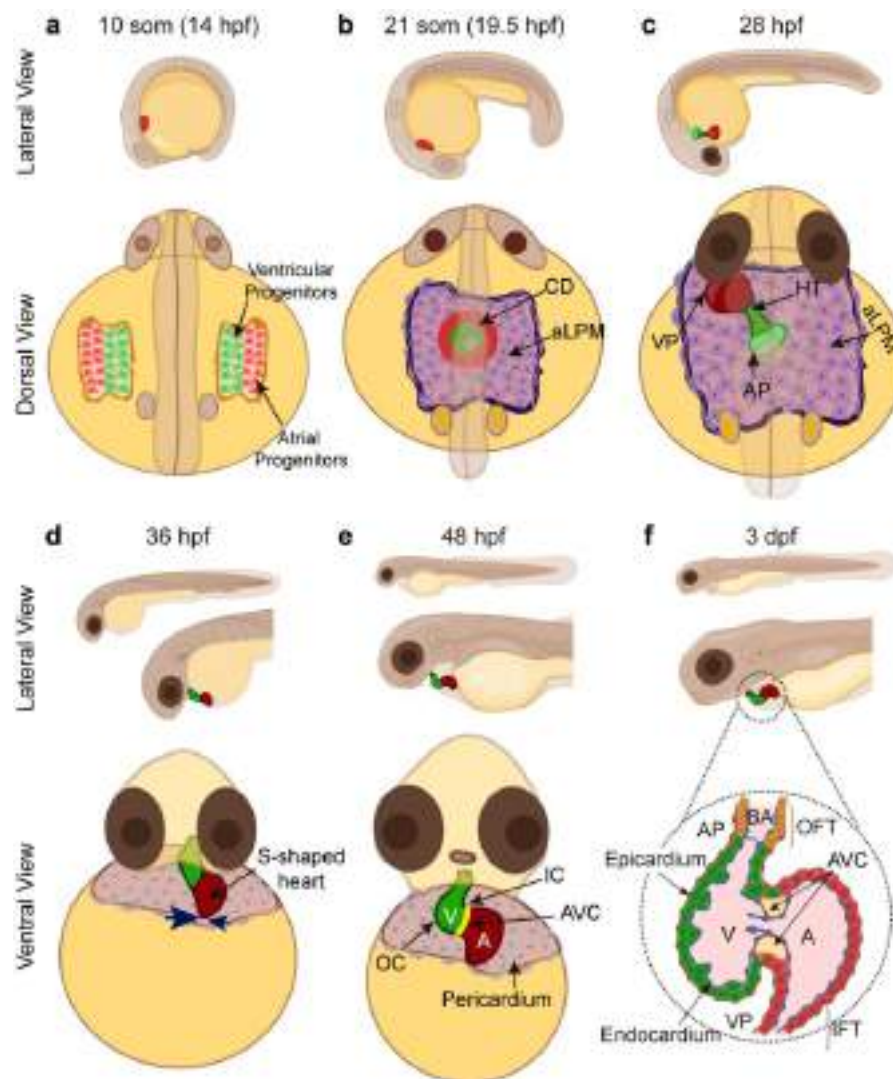


Figure 6 | Heart morphogenesis in zebrafish. (a) At the 10-somite stage, bilateral precardiac fields with specified atrial (red) and ventricular (green) progenitors are positioned in the aLPM. (b) At the 21-somite stage, a cardiac disk (CD) is observed after fusion in the midline of the two medial aLPM, while the lateral (in purple) remains undifferentiated. (c) Before 28 hpf, the CD elongates forming a primitive heart tube (HT) with the venous pole (VP) displaced towards the left and surrounded by lateral aLPM cells. Anterior pole (AP). (d) At 36 hpf, anterior migration of the HT and L/R asymmetric addition of cells from the lateral aLPM maintain the leftward displacement (dark blue arrows) of the VP leading to a S-shaped heart. (e) By 48 hpf, the heart is in the pericardial cavity with a ventricle (V) and atrium (A) separated by the atrioventricular canal (AVC, in yellow) and with a clear inner (IC) and outer curvature (OC). (f) From 3 dpf, the three layers of the heart (epicardium, myocardium and endocardium) can be appreciated. Bulbus arteriosus (BA) and the valves of the heart outflow tract (OFT), inflow tract (IFT) and AVC are also visible.

Introduction

During 3-5 days post-fertilization (dpf) further heart maturation processes lead to the appearance of: (i) an outflow tract (OFT) embracing the trabeculated ventricle which ends in the bulbus arteriosus (BA) acting as a pressure capacitor (Grimes and Kirby, 2009); (ii) an atrium followed by an inflow tract (IFT) region where the pacemaker in the *sinus venosus* regulates heart beating (Tessadori et al., 2012); (iii) the epicardium derived from the transient proepicardium (PE) (Andrés-Delgado et al., 2019) as well as the development of the valves of the AVC, OFT and IFT (Martin and Bartman, 2009) (Figure 6f). By 5 dpf, the atrium moves medially and repositions itself behind the ventricle (Singleman and Holtzman, 2012).

2.2. Mouse heart morphogenesis

During gastrulation, mouse CPCs which are not yet committed to a cardiac fate (Tzouanacou et al., 2009) ingress and locate close to the anterior PS, near the cranial-mesodermal progenitors (Kinder et al., 2017).

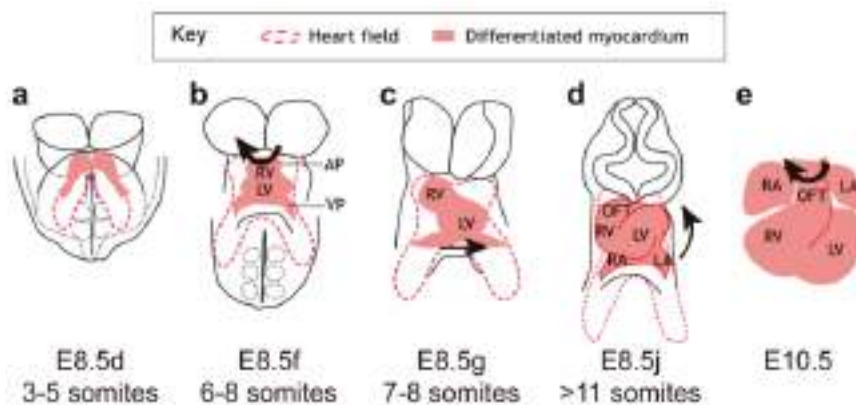


Figure 7 | Heart morphogenesis in mice. (a) At E8.5d, CM first differentiate forming the myocardium of the cardiac crescent. (b) At E8.5f, the HT is straight with the right ventricle (RV) lying cranially to the left ventricle (LV). Rotation of the arterial pole (AP) is indicated by the arrow. Venous pole (VP). (c) From E8.5g, the RV is progressively readjusted to the right side while there is an asymmetric ingression of CPCs from the surrounding heart field at the VP. The leftward shift of the VP is represented by an arrow. (d) At E8.5j, a helical shape of the looped HT is observed with a clear outflow tract (OFT), RV, LV, right (RA) and left atrium (LA). (e) At E10.5, the AP and VP converge (arrow at E8.5j), while rotation of the OFT continues (curved arrow). Image modified from Desgrange et al., 2018.

Around E7.5, epithelial CPCs differentiate within the splanchnic mesoderm of the aLPM and migrate towards the midline forming the myocardium of the bilateral cardiac crescent (Figure 7a) (Ivanovitch et al., 2017; Vincent and Buckingham, 2010). Along with foregut closure, right and left fields from the cardiac crescent bulge and migrate to the midline fusing and forming a dorsally opened primitive HT constituted by an inner endocardial layer and outer myocardial layer (Brade

et al., 2013). By E8.5f, the right ventricle is aligned cranially with the left ventricle and the beating HT is dorsally closed (**Figure 7b**) (Kelly et al., 2014; Zaffran et al., 2004). While looping is taking place, the dorsal mesocardium (DM) breaks down (Le Garrec et al., 2017), leaving the HT attached to the dorsal pericardial wall only to the poles of the heart where CPCs are being incorporated (Domínguez et al., 2012; Kelly et al., 2001). At E8.5g, the rightward rotation of the AP (Le Garrec et al., 2017) and the leftward displacement of the VP results in the rightward tilting of the heart (**Figure 7c**) (Desgrange et al., 2018; Ocaña et al., 2017). Cardiac chambers grow out through a process called ballooning leading to the formation of the right and left ventricles and the atria (Christoffels et al., 2000). Simultaneously, the PE starts to grow over the outer surface of the heart to form the epicardium (Cao et al., 2020; Komiyama et al., 1987). By E8.5j, the heart presents a helical shape being the right ventricle position aside the left ventricle (**Figure 7d**). At E10.5, when looping is completed, the OFT is in line with the atria (**Figure 7e**) (Desgrange et al., 2018).

2.3. Contribution of first and second heart fields to the vertebrate heart

Heart relies on the contribution of cells from different progenitor pools, including the pharyngeal mesoderm, PE cells, cardiac neural crest cells (CNCC) and cardiogenic mesoderm. Importantly, it is formed by the contribution of early and late-differentiating aLPM progenitors called first (FHF) and second heart fields (SHF), respectively (Knight and Yelon, 2016; Meilhac and Buckingham, 2018).

At early stages of chordate development, there is a common precursor field called the cardiopharyngeal field (CPF), which contains the SHF and branchiomeric progenitor cells (Diogo et al., 2015) (**Figure 8a**). In zebrafish, the medially located aLPM contributes to the FHF and the lateral aLPM which migrates anteriorly contributes to part of the SHF, the pericardial sac, the pharyngeal arches, and the peritoneum (Mao et al., 2021). The initial CD and HT consists of an endocardium covered by cardiomyocytes (CM) derived from the FHF which can be detected with differentiation markers such as *myosin light chain 7 (myl7)* (**Figure 8b**) (Hinits et al., 2012; Schindler et al., 2014). From 24 hpf onwards, elongation of the HT is caused by the addition of CM and smooth-muscle cells coming from different SHF-progenitors (Hami et al., 2011; Lazic and Scott, 2011; Mosimann et al., 2015). One subset gives rise to the IFT at the base of the atrium of the mature heart (Derrick et al., 2021a; Fukui et al., 2018; de Pater et al., 2009; Witzel et al., 2012) and the other contributes to the AP and, eventually, to the OFT of the ventricle (**Figure 8c**) (Felker et al., 2018; George et al., 2015; Grimes and Kirby, 2009; Guner-Ataman et al., 2013; Holowiecki

Introduction

et al., 2020; Nevis et al., 2013; Paffett-Lugassy et al., 2017; Witzel et al., 2017; Zeng and Yelon, 2014; Zhou et al., 2011). Between 18 and 48 hpf, aLPM cells only divide once or twice and are not organised within precursors fields with fixed topology in the A/P or L/R axis (Mao et al., 2021). After 48 hpf, CM proliferation progressively increases (Staudt and Stainier, 2012).

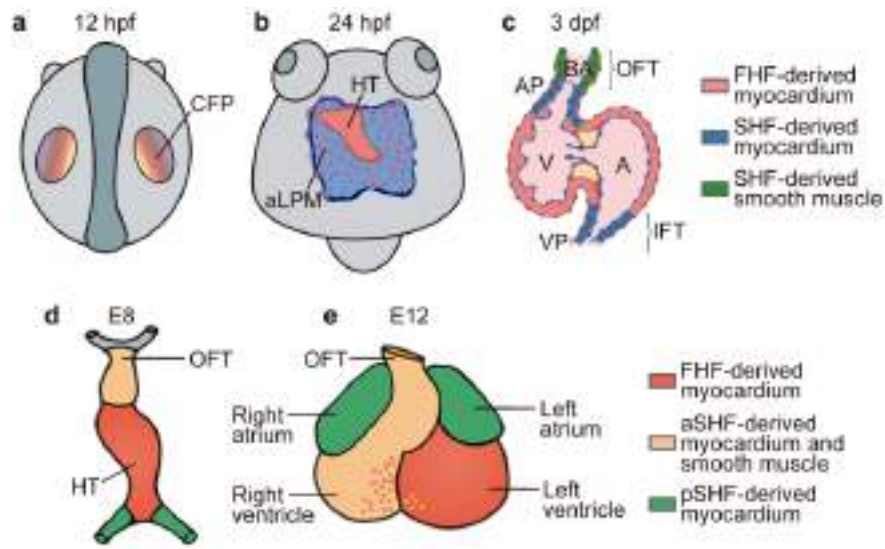


Figure 8 | FHF and SHF in zebrafish and mouse heart. (a) The cardiopharyngeal field (CPF), a mixed population of branchiomeric and heart precursors is localized at 12 hpf in the aLPM of zebrafish. **(b)** By 24 hpf, the medial aLPM gives rise to the primary HT, derived from the FHF (pink), and is surrounded by undifferentiated aLPM. **(c)** This lateral and undifferentiated aLPM contributes to both poles of the heart as part of the SHF contribute to the myocardium (blue) and smooth muscle of the bulbus arteriosus (BA) (green) at 3 dpf. **(d)** In mouse embryos, the primary HT is composed of cells derived from the FHF (red). **(e)** Addition of anterior SHF to the AP (orange) and posterior SHF to the VP (green) leads to the formation of the different chambers. Modified from Prummel et al., 2020.

The mouse embryonic heart is also derived from multiple cell lineages. Single-cell RNA sequencing (scRNAseq) of the anterior cardiac region identified clusters associated with the FHF, SHF and an intermediate differentiation state (Tyser et al., 2021). FHF gives rise to the majority of primary HT cells (Figure 8d) and will form the left ventricle and parts of the atria (Meilhac et al., 2004). On the other hand, undifferentiated SHF-progenitors, which lie dorso-medially to the cardiac crescent in the pharyngeal mesoderm, form an epithelial layer in the dorsal pericardial wall (Francou et al., 2017; Vincent and Buckingham, 2010). SHF is divided into anterior (aSHF) and posterior (pSHF) that differentiate into the OFT and right ventricle, and the IFT and atria, respectively (Figure 8e) (Cai et al., 2003; Galli et al., 2008; Ivanovitch et al., 2017; Kelly et al., 2014; Mjaatvedt et al., 2001; Rana et al., 2014; Waldo et al., 2001). The increase in CM number is primarily achieved by cell addition and not by proliferation (Kelly, 2012).

Although the two-chambered zebrafish heart is simpler than that of the mouse, which bears double-circulation and four-chambers, the signalling pathways used for SHF addition are conserved (Knight and Yelon, 2016; Rochais et al., 2009). These include fibroblast growth factor 8 (Fgf8) and retinoic acid (RA), respectively promoting or limiting the process (Derrick et al., 2021a; Duong et al., 2021; Ryckebusch et al., 2008).

2.4. Cardiac transcription factors

One of the key determinants of vertebrate heart development is Nkx2.5, a homeobox-containing TF implicated in the determination of the aLPM, CM differentiation, chamber contribution and heart morphogenesis (Chen and Fishman, 1996). It is expressed in both heart fields, upstream of the BMP signal to preserve the identity of the SHF (Prall et al., 2007) and regulating its proliferation (Colombo et al., 2018; Guner-Ataman et al., 2013). Similarly, Gata factors are key for SHF regulation, including proliferation, OFT contribution and septation (Arceci et al., 1993; Reiter et al., 1999).

Tbx5, a member of the T-box TF family (Alzein et al., 2021; Ryan and Chin, 2003; Steimle and Moskowitz, 2017) is another crucial factor, as it is involved in the maturation of CM, in PE specification (Liu and Stainier, 2010), atrial septation (Xie et al., 2012), the establishment of the conduction system (Moskowitz et al., 2004) and L/R laterality (Sulaiman et al., 2016). Loss of *tbx5* function in zebrafish causes and expansion of FHF contribution as Tbx5 is pivotal for SHF differentiation (Mosimann et al., 2015) and mesocardia (HT in the midline) (Garrity et al., 2002). In mouse, FHF-Tbx5+ cells contribute to the cardiac crescent, as it is expressed in the left ventricle, while SHF-Tbx5+ cells contribute to the posterior portion of the HT, corresponding to the *sinus venous* and future atria (Bruneau et al., 1999; Devine et al., 2014). Indeed, mouse homozygous for *Tbx5* have a linear HT and absence of the forelimbs leading to embryonic lethality by E10.5 (Bruneau et al., 2001). Nevertheless, Tbx5 downstream targets in the context of cardiac development are still unknown (Steimle and Moskowitz, 2017).

Interestingly, the three cardiac TFs (Nkx2.5, Tbx5 and Gata) control the differentiation of CPCs and interact with each other to induce the expression of downstream cardiac genes in the network, providing an extra level of complexity (Luna-Zurita et al., 2016). In fact, these genes are not lineage-restricted as they are implicated in myocardial cell differentiation as well as in defining CPCs (Meilhac and Buckingham, 2018). A lot of effort has been invested to trace heart progenitors within the aLPM, which is a very dynamic tissue (Felker et al., 2018). Only timing of

Introduction

recruitment would distinguish cells of the FHF and SHF as they have several markers intermingled during the implementation of differentiation programs (Tyser et al., 2021) as it occurs for the CPF (Diogo et al., 2015).

2.5. Asymmetric heart morphogenesis

Heart looping, preceded by asymmetric gene expression, is the first sign of asymmetric organogenesis (Patten, 1922). Therefore, this organ furnishes an interesting model to decipher L/R asymmetric morphogenesis during development (Desgrange et al., 2018).

2.5.1. Cardiac asymmetries preceding looping

In zebrafish, when the CD is formed (22 somite stage), *spaw* and *lefty2* are exclusively expressed in the left LPM (Smith et al., 2008). BMP signalling is also relevant as it plays diverse and subsequent roles in L/R patterning (Smith and Uribe, 2021). Nevertheless, whether it is asymmetrically expressed in the CD is debated, as *bmp4* and its effectors phospho-smad 1/5/8 are highly expressed on the left side according to Chen et al., 1997, Lenhart et al., 2013, Smith et al., 2008 and Chocron et al., 2007 but Veerkamp et al., 2013, described BMP signalling enriched on the right-hand side. Nevertheless, BMP is expressed bilaterally along the LPM as already shown in **Figure 5**. The speed of migration of zebrafish's CPCs that contribute to the CD and HT are already asymmetric, as posterior CPCs displace at a higher rate than those of the anterior region causing the rightward rotation of the CD (Campos-Baptista M. et al., 2008; Smith et al., 2008). This differential migration rate depends on the chemoattractant effect on BMP signalling guiding the leftward jogging (Smith et al., 2008). *spaw* also modulates the asymmetric expression with higher levels on the left of the cytoskeletal gene *α-actin1b* (Noël et al., 2013) and represses nonmuscle myosin II with higher levels on the right (Veerkamp et al., 2013). Additionally, there is an asymmetric expansion of the ECM cross-linking protein *hapln1a* on the left-side of the CD within the myocardial-endocardial layer (Derrick et al., 2021b). All this asymmetric morphogenesis corresponds to cells from the FHF (Desgrange et al., 2018). On the other hand, SHF precursors in the aLPM are asymmetrically distributed as twice CPCs are on the right compared to the left giving rise to more CM as *tbx5a* may suppress cardiac proliferation on the left side (Mao et al., 2021). Besides, left-CPCs have higher migration speed and track length as *tbx5a* functions in maintaining L/R asymmetry in migration dynamics (Mao et al., 2021).

At 24 hpf, jogging occurs in a *spaw*-dependent manner (Grimes et al., 2020). Simultaneously, cells from the left side contribute to the dorsal HT, while cells from the right-side

form the ventral part resulting in the conversion of a L/R polarity to a D/V one (Baker et al., 2008; Rohr et al., 2008 and Smith et al., 2008). As a matter of fact, *meis2b*, which is expressed in the posterior CD and the left side of the HT regulates atrial morphogenetic growth as it delimits the two atrial compartments of the zebrafish heart analogous to the left and right atria in mammals (Guerra et al., 2018). In fact, *spaw*-dependent and left-restricted *has2* expression in the VP cells works synergistically with *hapln1a* to assist atrial morphogenesis (Derrick et al., 2021b; Smith et al., 2008).

The equivalent of the zebrafish's CD clockwise rotation in chicken and mouse would be the rightward rotation of their AP (Le Garrec et al., 2017; de la Cruz and Markwald, 1998) which also would contribute to a change of polarity from L/R to D/V (Campione et al., 2001). Similarly, cytoskeletal genes or their components are asymmetrically expressed in the HT (Itasaki et al., 1991) as *Has2* or *Acta1* (Camenisch et al., 2000).

2.5.2. Heart looping steps

Looping defines the morphogenetic process which bring heart chambers from a straight HT closer together to their final topographical localization to establish a correct blood circulation (Patten, 1922). It depends on: (i) intrinsic mechanisms related to growth rate (Kennaway et al., 2011) and its orientation with respect to the axis of the tube at individual or tissue level (Kawahira et al., 2020); and (ii) extrinsic mechanisms related to external forces and processes/cues (Desgrange et al., 2018).

In higher vertebrates, cardiac looping encompasses several steps (Männer, 2009). At the beginning the heart is a straight tube (**Figure 9a**) that will progressively undergo a ventricular bending adapting a convex C-shaped towards the right side (ventricular D-looping or C-looping) as the midsagittal plane become the OC (**Figure 9b**) (De La Cruz et al., 1989; Männer, 2000). Afterwards, there is a reduction in the distance between the IFT and OFT which brings the ventricle caudal to the atria leading to the S-shaped loop (**Figure 9c**) (Taber et al., 1995) with an anisotropic growth of CM being key for this process (Kidokoro et al., 2008; Shi et al., 2014). Finally, a terminal repositioning leads to a reverse rightward torsion resulting in a helix shape (Männer, 2009; Singleman and Holtzman, 2012).

Introduction

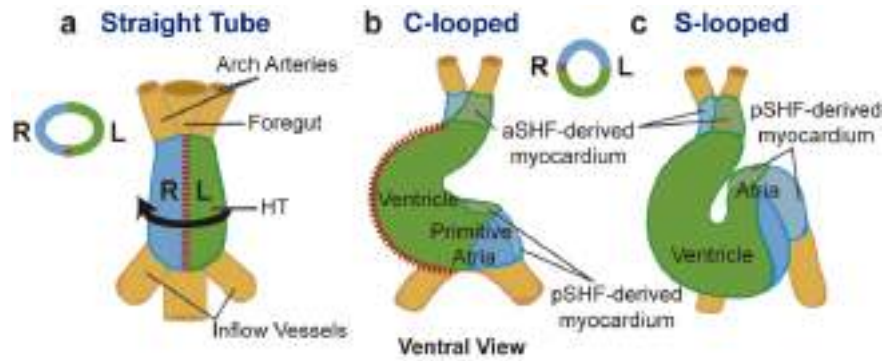


Figure 9 | Cardiac looping in high vertebrates. (a) The primary HT is positioned ventral to the foregut and is open dorsally. (b) It suffers a ventral bending followed by a rotation to the right. This twist brings the left side of the tube to the front (marked by dotted lines) and the IC to the left side adopting a C-shaped. (c) Subsequent addition of cells from the SHF to the IFT and OFT favours looping leading to a S-shaped loop.

In zebrafish, cardiac looping starts after jogging at 28hpf, the equivalent to the initial bending in amniotes (Grimes et al., 2020). Firstly, there is an early S-looping phase between 30-42 hpf which involves the D-bending of the ventricle along the OC which is favoured by the elongation of its CM as a result of blood flow (Auman et al., 2007) and an atrial bending with an OC towards the left. Secondly, an advanced S-looping phase 42-54 hpf involves the cranial shift of the atrium leading to both chambers being aligned perpendicular to the mid-sagittal plane and completed after anisotropic ballooning of the ventricle and atrium (Lombardo et al., 2019; Tessadori et al., 2021). Simultaneously to S-looping, there is planar bending of the heart, a torsional deformation more vigorous within the region of the AP (Lombardo et al., 2019). The second S-shaped loop stage of amniotes should not be confused with the early phase of heart looping in zebrafish that lead to a S-shaped heart (Desgrange et al., 2018).

2.5.3. Intrinsic vs. extrinsic mechanism driving asymmetric heart laterality

Although cardiac looping morphogenesis in zebrafish has some differences compared to higher vertebrates, it may be driven by the same biophysical forces (Lombardo et al., 2019). There are two models to explain how the heart undergoes C-shaped looping. The classical one invokes ventral bending driven by D/V cellular changes from cells of the HT itself (intrinsic mechanisms) (Shi et al., 2014) followed by a rotation to the right forming the well-known C-shaped loop (Figure 10a) (Männer, 2000; Kirby, 2007). The other model proposes physical buckling, where the HT confined into the pericardial cavity suffers mechanical constraints promoting growth in a L/R asymmetric manner (extrinsic mechanism) (Figure 10b) (Bayraktar and Männer, 2014; Le Garrec et al., 2017). The intensity of buckling is proposed to be the result of the breakdown of the DM

while the direction would be driven by the amplification of small L/R variations at the poles due to asymmetric patterning in CPCs (Desgrange et al., 2020; Le Garrec et al., 2017; Ocaña et al., 2017).

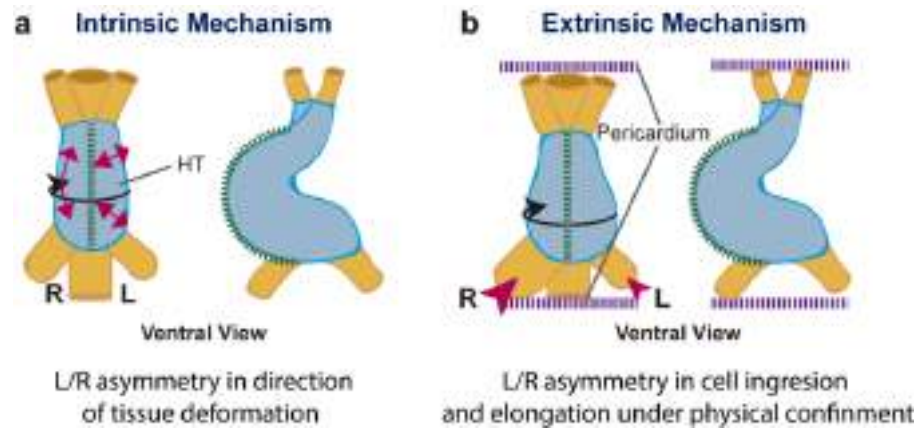


Figure 10| Extrinsic vs. intrinsic mechanisms of heart looping. (a) The intrinsic mechanism relies on the L/R asymmetry of the CM in the HT in the direction of tissue deformation (pink arrows), leading to the torsion of the heart forming the C-shaped loop. **(b)** The extrinsic mechanism relies on the physical confinement of the HT in the pericardial cavity (purple lines) and the asymmetric contribution of CPCs to the poles of the heart (pink arrows), which dictate the rotation of the HT forming the C-shaped loop.

Supporting intrinsic mechanisms, isolated chick and fish heart explant cultures form a C-shaped which is prevented by pharmacological inhibition of actomyosin cytoskeleton (Manning and McLachlan, 1990; Noël et al., 2013; Shi et al., 2014). Besides, chick myocardial cells are intrinsically chiral, as N-cadherin and myosin-II are enriched specifically on the boundaries of cells leading to a dominant clockwise rotation of the HT (Ray et al., 2018). In fact, initial C-looping in chick embryo is accomplished by a L/R asymmetry in the direction of tissue deformation of the right myocardium (**Figure 10a**) leading to an F-actin-dependent cellular reorganization (Kawahira et al., 2020). Quantification of looping is more compatible with the initial bending rather than with looping, as isolated C-shape stage hearts were not able to loop further (Ramasubramanian et al., 2013). During looping in zebrafish, BMP acts as an intrinsic signalling during planar bending as its pharmacological inhibition causes S-looping defects (Lombardo et al., 2019). Besides, there is a *tbx5a*-dependent twist of the HT, as both chambers suffer an asymmetric rotational movement towards the AVC while CM rearrange towards the OC. This clockwise rotation of the ventricle is in the same direction as the rotation of the CD (Smith et al., 2008) and that of the OFT (Lombardo et al., 2019). Remarkably, SHF cells incorporation to the poles seems to be dispensable for this twisting (Tessadori et al., 2021).

Introduction

With respect to the extrinsic cues, this mechanism has been tested in mechanical simulations with non-biological material (Bayraktar and Männer, 2014; Männer, 2004) as well as through computational simulations and 3D images (Le Garrec et al., 2017; Taber et al., 2010; Voronov et al., 2004). If while the heart is growing longitudinally the distance between both poles of the heart is fixed, it will suffer deformation (**Figure 10b**). If the growth pattern is in the same plane than the tube axis it would be as in zebrafish a flat-S shape, while if the planar configuration is broken it would produce a helical shape as in amniotes (Desgrange et al., 2018).

In vertebrates, asymmetric cell contributions from the aLPM, with more CPCs from the right side (Mao et al., 2021; Ocaña et al., 2017), produce the leftward displacement of the posterior pole of the heart in a actomyosin-dependent manner (Ocaña et al., 2017). As the pericardial sac is contiguous with the VP, it could provide some level of mechanical constraints (Ocaña et al., 2017). Likewise, several studies in chicken uncovered that after the rightward rotation of the AP there is a leftward displacement of the VP carried out by asymmetric forces elicited by differential cell contribution, proliferation and cytoskeletal contraction (Kidokoro et al., 2008; Ocaña et al., 2017; Stalsberg and Dehaan, 1969). In the mouse, leftward displacement of the VP and the rightward looping occurs as a combination of detachment of DM and a L/R asymmetric EMT that contributes more cells from the right to the VP (Le Garrec et al., 2017; Ocaña et al., 2017). Indeed, it was known that cranial pSHF contributes asymmetrically to right and left sides of the heart (Domínguez et al., 2012) and it has also recently been observed that there is a higher proliferation (Desgrange et al., 2020) and insertion (Esteban et al., 2021) of right-SHF cells in the IFT which precedes looping and enforces asymmetric forces. In fact, SHF deployment in the dorsal pericardial wall is a source of mechanical force that leads to epithelial tension (Francou et al., 2017). This is all compatible with the mesocardia observed in *Snail1* conditional mutants (Ocaña et al., 2017). Therefore, when the addition of CM to both poles is defective, the expression of SHF-markers including *Hand1*, *Hand2*, *Isl1*, *Mef2c*, *Nkx2-5*, *Tbx5* or *Snail1* are impaired and the HT shows looping defects (Bruneau et al., 2001; Cai et al., 2003; George et al., 2015; Lazic and Scott, 2011; Lin et al., 1997; Ocaña et al., 2017; Risebro et al., 2006; Schindler et al., 2014; Witzel et al., 2017). In line with this, disruption of the PCP pathway turns out into looping defects due to the disorganization of the SHF with an abnormal cell morphology, adhesion, polarity, defective actin organization and premature cell differentiation (Francou et al., 2017). Altogether, this suggests that coordination of asymmetric biomechanical forces mainly due to L/R asymmetric cell contribution and behaviour drive the displacement of the posterior pole of the heart and subsequent looping.

Asymmetric Nodal/*spaw* signalling directs cardiac jogging in zebrafish (Long et al., 2003; Noël et al., 2013). Nevertheless, a defective L/R Nodal/*spaw* signalling does not interfere with heart looping itself but rather with heart directionality in both mouse (Desgrange et al., 2020) and zebrafish (Grimes et al., 2020; Noël et al., 2013). In fact, asymmetries in cell proliferation, differentiation or in the composition of the ECM are downstream of Nodal signalling (Desgrange et al., 2020). This points out that: (i) jogging is a separate mechanism from looping which promotes a robust dextral looping in normal conditions (Grimes et al., 2020); (ii) Nodal acts as a modulator instead of a inducer amplifying L/R asymmetries at the HT poles for a correct laterality (Desgrange et al., 2020); (iii) a heart-specific random generator of asymmetry is functional in absence of Nodal (Desgrange et al., 2020).

Several studies had led to the conclusion that the intrinsic mechanisms are the major driver of the initial ventral bending while extrinsic mechanism can provide the directional information for driving the looping which is controlled by heart-intrinsic and extrinsic asymmetries in the actomyosin cytoskeleton and in the mechanical constraints essential in buckling mechanism (Desgrange et al., 2018; Grimes et al., 2020; Kawahira et al., 2020; Noël et al., 2013; Ocaña et al., 2017; Rago et al., 2019).

2.6. Heart laterality defects

Congenital heart defects (CHD) are the most common human defects in new-borns with an incidence of at least 1,8 % (Zimmerman et al., 2020). Further, CHD are the major cause of mortality as well as morbidity in children and adults (Triedman and Newburger, 2016), due to a defective determination of L/R axis or abnormal morphogenesis or maturation of the heart during early development (Pierpont et al., 2018; Ramsdell, 2005).

CHD are often associated with additional defects in other visceral organs. For instance, the correct orientation is called *situs solitus* (Figure 11a) and *situs inversus* (Figure 11d) is a condition where all visceral organs are a mirror-image of the former (Schweickert et al., 2017). Notably, complete inversion is not always pathological, and as such, this syndrome is associated with no CHD in 59 % of the cases and with simple or complex CHD in the 14,4 % and 26,6 % respectively (Lin et al., 2014). In the other extreme is heterotaxy or *situs ambiguous*, which implies the abnormal symmetry of the visceral organs (isomerism) and/or situs discordance of those organs which could be partial or complete (Schweickert et al., 2017). There are two types of abnormal symmetry of the organs: (i) right isomerism (Figure 11b) with bilateral trilobed lung,

Introduction

symmetric enlarged liver and absence of spleen; and (ii) left isomerism (**Figure 11c**) with multiple spleens and bilateral bilobed lung (Hamada, 2020). In any case, heterotaxy is associated with CHD in 82,8 %, as it is a heritable syndrome that has a prevalence of 1/10000 and includes cases with transposition of the great arteries or ventricular and atrial septal defects, among others (Lin et al., 2014). It is often associated with a randomization of the L/R cascade as this syndrome harbours mutations in genes implicated in the formation of the LRO or components of Nodal signalling pathway (Gabriel and Lo, 2020). Similarly, *situs inversus* is also related with mutations in primary cilia (Fliegauf et al., 2007). With respect the heart, dextrocardia implies that its apex points towards the right side rather than to the left (**Figure 11d**) and mesocardia occurs when the heart fails to be displaced from the midline, the initial position of the primary heart tube (Lin et al., 2014).

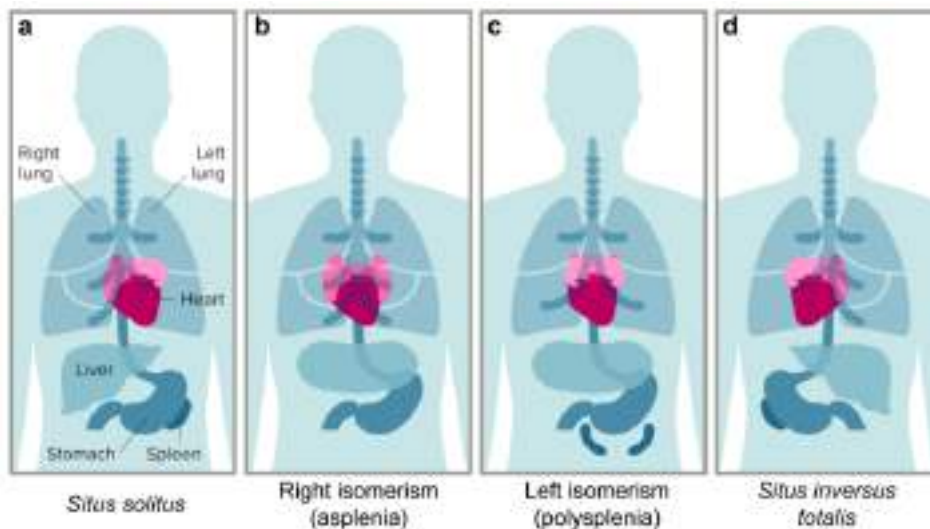


Figure 11| Organ laterality defects. (a) The normal disposition of internal organs, *situs solitus*. (b) In right isomerism there is an incorrect disposition of organs and absence of the spleen (asplenia). (c) In left isomerism there is also a disorganised location of organs and multiple spleens (polysplenia). (d) *Situs inversus totalis* is the mirror-image of *situs solitus*. For heart conditions see the text. Modified from <https://knowablemagazine.org/do/10.1146/knowable-012720-1/feature/media/G-confusing-left-right.svg>.

Defects in SHF development or their addition to the HT, derive in defective cardiac patterning and septation problems leading to incorrect oxygenation of the blood (Liu et al., 2015). Indeed, transcriptional regulation plays an important role in heart development as mutations in 25 TF have been identified in human patients with CHD (Hill et al., 2017; McCulley and Black, 2012). These include *Tbx5*, which mutation causes Holt–Oram syndrome (Basson et al., 1997; Bruneau et al., 2001) and *Nkx2.5*, which mutation causes tetralogy of Fallot and double outlet right ventricle (Benson et al., 1999; McElhinney et al., 2003). From a Genome-wide association

study (GWAS) and exome sequencing studies, cardiac TFs including TBX5, GATA4, NKX2-5, PITX2, ISL1 and PRRX1 (Aguirre et al., 2015; Lozano-Velasco et al., 2016, 2020; Nielsen et al., 2018; Van Ouwkerk et al., 2020; Roselli et al., 2020; Victorino et al., 2021) have been also associated with atrial fibrillation (AF), the most common cardiac arrhythmia (Nattel et al., 2020). As such, hearts from *tbx5a* zebrafish mutants *heartstring* (*hst*) exhibit severe bradycardia from the onset of contraction and mesocardia (Garrity et al., 2002; Gauvrit et al., 2022).

Although Nodal is not expressed in the HT (Collignon et al., 1996), mutant mice that express Nodal on both sides evidence left isomerism (Hamada, 2020). Likewise, *Pitx2c* loss in mouse embryos cause also laterality defects (Shiratori et al., 2006), while in zebrafish which presents a much less complicated vasculature connection does not affect organ asymmetry (Ji et al., 2016). Besides, L/R patterning mutants as *spaw* (Grimes et al., 2020) among others are fertile and they grow as controls in ample food and space facilities. Therefore, heart defects may not impinge survivability in zebrafish (Grant et al., 2017). Nevertheless, zebrafish mutants as *hst* which affect *tbx5a* recapitulate human cardiac syndromes, highlighting the importance of using zebrafish to associate human gene mutations with developmental CHD (Garrity et al., 2002; Kemmler et al., 2021).

3. Epithelial to Mesenchymal Transition in Development and Disease

Transition among cell states is defined by parameters as the promoter's accessibility, the transcriptome and proteome as well as the shape, behaviour and adhesion to their substrate (Mulas et al., 2021). During development of a multicellular organism, there are morphogenetic movements where cells acquire migratory properties and invasiveness to develop tissues and organs at the correct location (Scarpa and Mayor, 2016). As such, cells encompass dynamic changes between an epithelial to a mesenchymal phenotype through a cellular process called epithelial-mesenchymal transition (EMT) (Thiery et al., 2009). This programme would progressively transform epithelial cells through the modification of cell-cell adhesion complexes and cytoskeletal components, ECM remodelling and loss of apico-basal polarity into different morphologies depending on the final E-M state within the transition (Yang et al., 2020). EMT process takes place during development and in adulthood in physiological conditions such as wound healing (Nieto et al., 2016). Moreover, EMT can operate in pathological conditions such

Introduction

as fibrosis or cancer. In the latter, cells hijack this developmental programme to delaminate from the primary tumour and initiate the metastatic cascade (Nieto, 2013; Nieto et al., 2016).

The reverse process called mesenchymal-epithelial transition (MET), is linked with reciprocal changes in the cellular phenotype. Mesenchymal cells would reacquire the expression of cell-cell adhesion molecules, recover apico-basal polarity, reorganize the cytoskeleton and lose migratory properties, among others (Thiery et al., 2009). In fact, many cell populations undergo several rounds of EMT-MET during development, as it occurs during renal morphogenesis (Stark et al., 1994) or heart development (described further in the next section).

EMT triggered by signals in the microenvironment produce changes in gene expression that may be partially executed, leading to cells showing a diversity of intermediate stages that can be context-dependent (Nieto, 2017; Pastushenko and Blanpain, 2019). Embryonic and cancer cells are very plastic, having the ability to adopt different degrees of epithelial and mesenchymal traits (Yang et al., 2020). In fact, it is more likely to find cells in partial EMTs than undergoing a full EMT programme (Yang et al., 2020).

The cellular phenotypic changes are diverse and require the cooperation of different inducing signals (Yang et al., 2020), as the TGF- β family members (Katsuno and Derynck, 2021), activins or BMPs (McCormack and O’Dea, 2013), which are potent EMT-inducers. These signalling factors would activate the expression of different genes including EMT-TFs (members of the *Snail*, *Zeb*, *Twist*, or *Prrx* families among others) and miRNAs (Nieto et al., 2016).

The very first steps of EMT do not contribute directly to the acquisition of mesenchymal traits but rather prepare cells for the following phases such as remodelling of the BM (Mogi and Toyozumi, 2010), reduction of apical surface or relocation of nucleus to the basal side (Gelbart et al., 2012). Early EMT also implies progressive loss of the epithelial phenotype, including apical-basal polarity (Jung et al., 2019), which guides the remodelling of the cell-cell adhesion complexes (Figure 12) (Rodriguez-Boulan and Macara, 2014). A downregulation of adherens junctions is required for partial EMT while its complete loss would destroy epithelial integrity of a tissue and lead to a full EMT (Le Bras et al., 2012). Migratory cells that have switched the intermediate filaments from cytokeratin to vimentin and E-cadherin for N-cadherin (Cdh2) do not necessarily need to lose all epithelial traits (Yang et al., 2020).

Relaxation of cytoskeletal organization allows the formation of actin-based extensions at the cell front, such as lamellipodia, which are thin (≈ 200 nm height) sheet-like protrusions or filopodia, thin (≈ 200 nm diameter) tubular protrusions (te Boekhorst et al., 2016; Schaks et al., 2019). Lamellipodia promote the adhesion to cell substrate through cadherins and integrins, promoting an increase in cell motility (Bodor et al., 2020) while filopodia are more associated with sensing the environment and directing migration (te Boekhorst et al., 2016; Schaks et al., 2019).

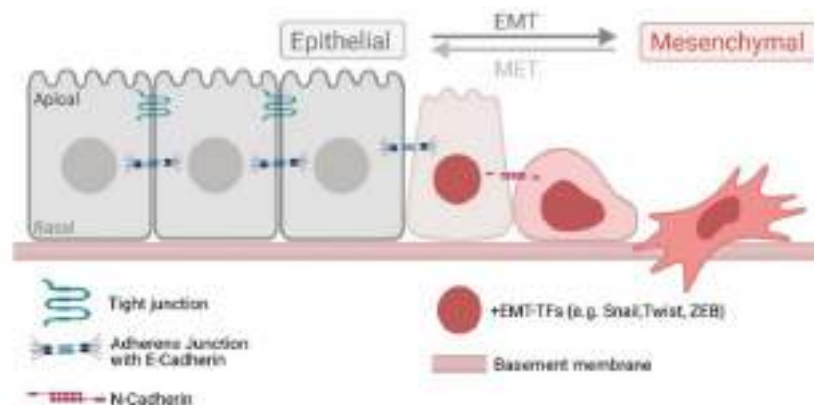


Figure 12 | Epithelial-to-mesenchymal transition (EMT) process. Overview of EMT, in which epithelial cells (grey cells) turn on EMT-TFs (red nucleus), disassemble cell–cell junctions (as E-cadherin), lose apico-basal polarity and can upregulate new cadherins such as N-cadherin. This leads to a change in cell shape (red cell) in a continuous spectrum while they acquire motility properties. The transition can be reversible through the mesenchymal-to-epithelial transition (MET). Image from Amack, 2021.

3.1. EMT during heart development

Heart development is a good example of an organ that undergoes several rounds of EMT/MET before its complete formation (Nieto et al., 2016). The first round occurs for the generation of the CPCs subpopulation of mesenchymal cells that migrate from the PS (Tam et al., 1997). These CPCs coalesce as bilateral sheets in the aLPM (Stalsberg and Dehaan, 1969), where the splanchnic layer organises as a bilayered epithelium via MET (Linask, 1992). A second round of EMT/MET occurs when the endothelial cell lining is formed from the two cardiogenic fields (Misfeldt et al., 2009). After HT formation, endothelial cells from the OFT and AVC undergo an endothelial-to-mesenchymal transition (EndMT) forming the endocardial cushions (Markwald et al., 1977).

In parallel with the EndMT of the AVC and OFT, epicardial progenitors arise from the PE, which derives from the pericardium adjacent to the VP of the heart (Cao et al., 2020; Garcia-Padilla et al., 2022; Maya-Ramos et al., 2013; Schulte et al., 2007) through an EMT-like process

Introduction

(Serluca, 2008; Wu et al., 2010). Particularly in zebrafish, the formation of the PE is mediated by BMP signalling to Tbx5a+ aLPM cells (Liu and Stainier, 2010). Heart beating enforces the floating into the pericardial cavity of this PE progenitors, which attach to the surface of the myocardium, covering it and forming the epicardial sheet (Peralta et al., 2013). Afterwards, the epicardium undergoes another EMT which never undergoes a full MET giving rise to interstitial fibroblasts in the myocardium, smooth muscle cells in the coronary arteries and part of the endothelium (Cano et al., 2016; Carmona et al., 2020; Dueñas et al., 2017).

In addition, in zebrafish, there is a *snail1b*-mediated EMT-like process in the ventricular myocardium during its trabeculation, as cells lose apicobasal polarity and delaminate towards the lumen (Gentile et al., 2021; Jiménez-Amilburu et al., 2016; Priya et al., 2020; Staudt et al., 2014).

3.2. EMT inducers

Unravelling the regulation of TFs which activate the expression of tissue specific genes leading to cell heterogeneity is key to understand normal development and disease (Boland et al., 2014; Reik, 2007). Activation of the classical EMT programme, including downregulation of both adhesion junctions and apico-basal polarity is mediated by core EMT-TFs. These master drivers of EMT are Snail1 (Nieto et al., 1992), Snail2 (also known as Slug) (Nieto et al., 1994), Twist-related protein 1 (Twist1) (Thisse et al., 1988), the zinc-finger E-box-binding homeobox proteins Zeb1 and Zeb2 (Funahashi et al., 1993; Verschuere et al., 1999) and Prrx1 (Ocaña et al., 2012).

The different EMT-TFs contain diverse protein domains that can lead to the induction of common and also non-redundant functions (Stemmler et al., 2019). EMT-TFs can cooperate in a dynamic and complex way to drive EMT (Yang et al., 2020). For instance, in response to TGF- β , SNAIL1 upregulates ZEB1 expression (Dave et al., 2011; Guaita et al., 2002), while it directly represses TWIST1 in breast cancer cells (Tran et al., 2011). High Snail1 expression is correlated with poor prognosis (Barrallo-Gimeno and Nieto, 2005) while high Prrx1 is associated with good prognosis in cancer (Ocaña et al., 2012). Prrx1 and Snail1 are expressed in a complementary manner, as they are mutual repressors (Fazilaty et al., 2019). On the other hand, Prrx1 expression cooperates with Twist1 (Ocaña et al., 2012). Therefore, studying commonalities and differences between these EMT-TFs besides their upstream signals and the post-transcriptional mechanisms that control their levels, can shed light into the cell plasticity required for the proper functioning of developmental processes, as well as their role in disease (Stemmler et al., 2019).

3.2.1. SNAIL

Identified for the first time in *Drosophila* (Boulay et al., 1987), Snail1 is involved in the migration of the mesoderm during gastrulation (Leptin, 1991; Nieto et al., 1992). In chick and mouse embryos, Snail family members and Sox2/3 are mutual repressors in the PS, with Snail favouring cell ingression and Sox preventing it (Acloque et al., 2011). During EMT, Snail1 represses *E-cadherin* transcription, leading to disassembly of adherens junctions, both in development and in cancer progression (Batlle et al., 2000; Cano et al., 2000). As such, *Snail1* mutant mouse embryos show defects during mesoderm formation and die shortly after E7.5 (Carver et al., 2001). Nonetheless, it is dispensable during neural crest (NC) delamination (Murray and Gridley, 2006) which is dependent on Twist (Soo et al., 2002) and Zeb2 (De Putte et al., 2003). In the chick embryo, Snail2 is required for gastrulation and NC formation (Nieto et al., 1994), while mouse mutants are viable and fertile (Jiang et al., 1998). This is due to the reshuffling of expression patterns in Snail family members during evolution (Locascio et al., 2002; Sefton et al., 1998).

The Snail genes are implicated in additional processes that involve cell movements, including the anterior migration of axial mesendoderm in the zebrafish (Blanco et al., 2007), while in the mouse, Snail1 is involved in an EMT process that occurs in a subset of axial progenitors in the epiblast to drive axial body elongation (Dias et al., 2020). Remarkably, Snail1 and/or Snail2 have additional morphogenetic functions, including the regulation of L/R asymmetry (Ocaña et al., 2017), bone morphogenesis (Chen and Gridley, 2013; De Frutos et al., 2009) and somitogenesis (Dale et al., 2006).

Snail1 has been considered a transcriptional repressor for decades, but in fact, when bound to Twist (Rembold et al., 2014) or CBP it can also act as an activator in development, cancer and fibrosis (Grande et al., 2015; Hsu et al., 2014; Lovisa et al., 2015; Rembold et al., 2014). Indeed, reactivation of Snail1 in renal epithelial cells induce renal fibrosis and failure (Boutet et al., 2006). Besides, Snail1/2 and Twist1 regulate cell survival and drug resistance (Dongre and Weinberg, 2019; Puisieux et al., 2014; Vega et al., 2004) and both are relevant for breast cancer progression (Tran et al., 2014; Xu et al., 2017), while dispensable for metastatic dissemination of pancreatic cancer (Zheng et al., 2015), which is mainly due to the reactivation of another EMT-TF, Zeb1 (Krebs et al., 2017).

Introduction

3.2.2. PRRX

The *Paired-related homeobox (Prrx)* gene family encodes TFs represented by *Prrx1* and *Prrx2* orthologues in tetrapods, while in zebrafish only *prrx1* has been maintained but represented by two paralogues, *prrx1a* and *prrx1b* (Braasch et al., 2014; Hernández-Vega and Minguillón, 2011). Their proteins present a paired-like domain in the N-terminus, a DNA-binding homeodomain and an OAR domain in the C-terminus (Leussink et al., 1995; Norris and Kern, 2001). The second DNA binding domain present in other paired-related homeobox genes that belong to the same family is absent in *Prrx1* (Galliot et al., 1999). *Prrx1* presents two isoforms due to alternative splicing: (i) a long isoform which contains paired-like, the OAR and the DNA-binding domain, being similar to the unique isoform of *Prrx2*; and (ii) a short isoform which lacks the OAR domain (Norris and Kern, 2001).

Prrx genes are important in morphogenetic processes, including the development of mesoderm and NC-derived mesenchyme (Cserjesi et al., 1992; Lu et al., 1999). In fact, it is expressed in a variety of mesenchymal tissues such as migratory NC, the LPM, branchial arches and limb buds (Beverdam and Meijlink, 2001; Kuratani et al., 1994; Leussink et al., 1995). It is not surprising then that mouse mutants for this EMT-TF present several malformations in jaws, craniofacial bone, limbs and vasculature (ten Berge et al., 1998; Ihida-Stansbury et al., 2004; Martin et al., 1995). In line with this, *prrx1a* and *prrx1b* zebrafish paralogues are involved in cartilage differentiation and their mutants form ectopic dorsal cartilages (Barske et al., 2016).

Importantly, PRRX1 induces EMT in a SNAIL1-independent manner during both embryonic development and disease, including cancer progression through the cooperation with TWIST1 (Ocaña et al., 2012). Basically, PRRX1 is important to confer migratory and invasive properties to cancer cells and needs to be downregulated to allow metastatic colonization, so that high levels of PRRX1 are correlated with good prognosis. This is due to the fact that PRRX1 represses stemness, which influences plasticity in embryonic development and cancer progression, as reversion to a more epithelial phenotype is required for the formation of tissues and metastases (Ocaña et al., 2012; Shi et al., 2018). Besides, *Prrx1* high levels activate members of the miR-15 family which attenuate Snail1 expression and consequently there is a decrease of stem cell properties and lower probability of developing metastases, increasing survival (Fazilaty et al., 2019). Both PRRX1 and TWIST1 are more potent mesenchymal inducers than epithelial repressors, while SNAIL1 and ZEB1 are strong epithelial repressors and weaker mesenchymal promoters (Nieto et al., 2016).

In addition, Prrx1 has also been involved in pancreas development and regeneration in the mouse (Reichert et al., 2013) and *prrx1b* in CM proliferation as it is key for balancing fibrosis and regeneration in the injured zebrafish heart (de Bakker et al., 2021). As a matter of fact, as Twist1 cooperates with Prrx1 in different contexts, a positive feedback loop is expected to occur between these EMT-TFs under pathologic conditions, which can lead to their irreversible activation (Lee et al., 2018). Prrx1 is related to AF, the most common arrhythmia, as there is a genetic variant in humans that leads to the alteration of this TF resulting in electrophysiological alterations in atrial myocytes (Bosada et al., 2021; Tucker et al., 2017; Wu et al., 2021). Besides, it is involved in the maintenance of adult neurogenesis in mammals (Shimozaki et al., 2013) and in the inhibition of adipogenesis through the activation of TGF- β signalling (Du et al., 2013). Therefore, the correct function of Prrx1 is crucial during embryonic development cancer progression and tissue homeostasis.

3.2.3. EMT-TFs and L/R asymmetry

EMT affects some aspects of cardiac morphogenesis as a conserved L/R asymmetric EMT programme in vertebrates gives rise to asymmetric cell movements of the aLPM towards the midline, higher from the right, leading to the leftward displacement of the posterior pole of the heart in a actomyosin-dependent manner (Ocaña et al., 2017). This asymmetric cell recruitment is compatible with the importance of extrinsic mechanisms driving heart laterality (Mao et al., 2021; Ocaña et al., 2017). On the other hand, *snail1b* has been implicated in the migration of CPCs through the modulation of fibronectin (Qiao et al., 2014), and also have a role in CM to maintain their wall integrity in an autonomous manner (Gentile et al., 2021).

On the right side of the node in the chick embryo, FGF8 antagonizes Sonic Hedgehog (SHH) and with BMP induces SNAIL1 in the right LPM, which in turn, represses PITX2 (Isaac et al., 1997). PRRX1 also shows a transient asymmetric expression with higher levels in the right LPM, being both EMT-TFs important for heart laterality (Ocaña et al., 2017). In fact, manipulating FGF8/SNAIL1 interferes with asymmetric expression (with higher right-hand levels) of the PE markers TBX18 and WT1 (Schlueter and Brand, 2013; Schlueter et al., 2006).

In mouse embryos, Prrx1/Prrx2 mutants show normal heart looping (Bergwerff et al., 2000; Martin et al., 1995), being Snail1 asymmetrically expressed and the one implicated in this process (Murray and Gridley, 2006; Ocaña et al., 2017; Sefton et al., 1998). Indeed, conditional disruption of Snail1 after E8 die at E9.5 due to cardiovascular defects, as there is bilateral

Introduction

expression of left-determinants, including *Nodal*, leading to defects in heart laterality (Murray and Gridley, 2006; Ocaña et al., 2017). In addition, *Snail1* in the mouse also plays a role in endocardial cushion development (Tao et al., 2011) which is regulated by *Hand2* expression (Laurent et al., 2017). *Wt1* is involved in the generation of mesenchymal cardiovascular progenitor cells in the mouse epicardium, where it transcriptionally regulates *Snail1* and *E-cadherin* expression (Martínez-Estrada et al., 2010).

Contrary to *Nodal* and *Pitx2*, which are exclusively expressed in the left LPM, *Prrx1* and *Snail1* are expressed on both sides, with a bilateral symmetry until they are transiently attenuated on the left LPM by *Nodal* downstream targets in a *Pitx2*-independent manner (Figure 5) (Patel et al., 1999; Rago et al., 2019). In fact, *Pitx2* mouse mutants do not display heart laterality defects, but rather cardiac right isomerism (Campione et al., 2001; Lin et al., 1999), which reinforces the concept of a prominence of the right-handed pathway in heart laterality (Ocaña et al., 2017). Therefore, asymmetric *Nodal*-*Pitx2* axis signalling on the left and *Bmp* signalling upstream of EMT-TFs on the right, act in parallel and mutually repress each other to establish cardiac laterality in zebrafish, chicken and mouse (Ocaña et al., 2017; Rago et al., 2019).

Nevertheless, Tessadori et al., 2020, reported that in zebrafish, the phenotype of two mutant alleles for *prrx1a* did not present morphological heart defects, while the combination with *prrx1b* mutants led to craniofacial defects (Barske et al., 2016). Therefore, as HT position in homozygous *prrx1a* mutants was unaffected, they raised concerns about the specificity of the described phenotype for defective *Prrx1* embryos. This work specifically addresses this issue and extends the analysis of EMT-driven heart laterality in zebrafish, through the results shown in the following chapters, part of them already published in Castroviejo et al., 2020.

OBJECTIVES |

Despite the external bilateral symmetry, most animals present internal L/R asymmetries evidenced by the morphology and position of several organs. Correct organ laterality is crucial for proper packaging and function. The incidence of L/R asymmetry defects is in 1/10,000 in humans, and the associated morbidity and mortality usually involve CHDs, which represent around 50 % of congenital malformations at birth (Lin et al., 2014; Triedman and Newburger, 2016). The L/R asymmetry of the vertebrate heart is evident by the displacement of the posterior pole to the left, despite like other individual organs, it initially appears as a midline structure (Desgrange et al., 2018). In the lab, we had previously shown that a differential L/R EMT generates more cells on the right-hand side of the embryo that, when migrating towards the developing heart at the midline, displace the posterior pole to the left in vertebrates (Ocaña et al., 2017). More precisely, in the zebrafish, whose heart is already displaced by a mechanism known as jogging, a similar process driven by the EMT-TF *prrx1a* maintains the displacement. As such, *prrx1a* morphant and crispant embryos showed mesocardia (Ocaña et al., 2017). Subsequent work by Tessadori et al., 2020 and our own data showed that *prrx1a* mutant embryos present normal heart laterality. Thus, two important questions arose: (i) whether the *prrx1a* knockdown (KD) mesocardia phenotypes were specific and (ii) whether *prrx1a* could be dispensable for heart laterality. If the latter was true, the next objective was to understand how heart laterality is regulated and, in particular, how the L/R differential EMT was implemented in the zebrafish during heart lateralization.

General Objective

Understanding the role of *prrx1a* and the EMT process in zebrafish heart laterality.

Specific Objectives

- **Objective 1:** Study the specificity and requirement of *prrx1a* in zebrafish heart laterality.
- **Objective 2:** Expression of other EMT-TFs in the cardiac progenitors of zebrafish embryos.
- **Objective 3:** Functional analysis of individual EMT-TFs in heart laterality.
- **Objective 4:** Regulatory relationship between EMT-TFs during the establishment of zebrafish heart laterality.

MATERIALS AND METHODS

1. Zebrafish Embryos

The different zebrafish strains described in **Table 1** and **Table 2** were maintained at 28°C under standard conditions, and the embryos were staged as described by Kimmel et al., 1995. When early stages were required, the embryos were maintained at 25°C to delay their development. No selection of sex of the animals was performed, as in all cases the zebrafish embryos analysed varied from 0 to 52 hpf, before sex is determined. Sample size of adult animals was not predefined as the number depends on the number of fertilized eggs obtained from the crosses.

All animal procedures were conducted in strict compliance with the European Community Council Directive (2010/63/EU) and Spanish legislation. The protocols were approved by the CSIC Ethical Committee and the Animal Welfare Committee at the Institute of Neurosciences.

<i>Danio rerio</i> reporters	Experimental Approach
<i>Tg(myI7:GFP)</i>	Zebrafish transgenic reporter line used to visualize CMs which generation is described in Geoffrey Burns et al., 2005.
<i>TgBAC(tbx5a:eGFP)</i>	Zebrafish transgenic reporter line used to visualize aLPM cells and HT which generation is described in Ocaña et al., 2017.
<i>TgBAC(prrx1a:dRFP)</i>	Zebrafish transgenic reporter line which recapitulates the expression pattern of <i>prrx1a</i> . A destabilized RFP-P2A cassette was introduced by homologous recombination (HR) (Suster et al., 2011) into a bacterial artificial chromosome (BAC) called DKEY-218H11 (Source BioScience) containing the zebrafish <i>prrx1a</i> gene. Those BACs were injected into 1-cell embryos, and RFP+ G ₁ embryos were raised to adulthood to generate the stable <i>TgBAC(prrx1a:dRFP)</i> transgenic line.

Table 1| Zebrafish (*Danio rerio*) transgenic lines.

Materials and Methods

<i>Danio rerio</i> mutants	Experimental Approach
Ab/Ab	Used as controls
<i>prrx1a</i> ⁱⁿ¹⁰	AB embryos were injected with CRISPR/Cas9 sgRNAs at 1-cell stage targeting AGCCACACTACCAAACCGAC and ACTGCGATCACCGCGAATC at exon 1 of <i>prrx1a</i> . <i>prrx1a</i> ⁱⁿ¹⁰ was identified as bearing a 10 nucleotide (nt) deletion in exon 1.
<i>prrx1a</i> ⁱⁿ⁶⁹	AB embryos were injected with CRISPR/Cas9 dgRNAs at 1-cell stage targeting the following genomic sequences GGACTCACCAGCGGGAGCGA at exon 1 and CACAGCAGGAGAGTAAG at intron 1 of <i>prrx1a</i> . <i>prrx1a</i> ⁱⁿ⁶⁹ was identified as bearing a 69 nt deletion that included the last 25 nt of exon1 and the first 44 nt of intron 1 (Castroviejo et al., 2020).
<i>prrx1a</i> ⁱⁿ⁷⁴	AB embryos were injected with CRISPR/Cas9 dgRNAs at 1-cell stage targeting TCATTCTTCACAACGACTCG in the promoter region and GGACTCACCAGCGGGAGCGA at exon 1 and CACAGCAGGAGAGTAAG at intron 1 of <i>prrx1a</i> . <i>prrx1a</i> ⁱⁿ⁷⁴ was identified as bearing a 2474 nt deletion from upstream of the 5'-UTR to intron 1.
<i>prrx1b</i> ⁱⁿ⁵	AB embryos were injected with CRISPR/Cas9 dgRNAs at 1-cell stage targeting GATGAAAGTGTGGCGAAAC at <i>prrx1b</i> exon 1. <i>prrx1b</i> ⁱⁿ⁵ was identified as bearing a 5 nt deletion in the exon 1.
<i>prrx1b</i> ⁱⁿ⁵¹	AB embryos were injected with CRISPR/Cas9 dgRNAs at 1-cell stage targeting TCGAAGAAGGAAGCTGTGAT and ACGTAATTACGAGAGCCTTTC upstream of 5'-UTR and GAAGAGCTGGACTGGTTTAG and GCGTTGTTGTCCCTCTCAAT in the 3'-UTR of <i>prrx1b</i> . <i>prrx1b</i> ⁱⁿ⁵¹ was identified as bearing an 8051 nt deletion from upstream of the 5'-UTR to 3'-UTR.
<i>snai1b</i> ^{bns351}	Mutant line for <i>snai1b</i> generated by CRISPR/Cas9 kindly provided by Dr. D. Stainier (Bad Neuheim, Germany). Generation of the line is published in Gentile et al., 2021.

Table 2| Zebrafish (*Danio rerio*) mutant lines and their generation.

1.1. Genotyping mutant lines

The genotyping of individual embryos used for experiments was performed using DNA extracted from the whole zebrafish embryo using the REExtract-N-Amp Tissue Polymerase chain reaction (PCR) Kit (Sigma, XNAT-10RXN), and the PCR was carried out using KAPA FAST 2x mix with the primers indicated in [Table 3](#).

Mutant Line	Primers - Forward (F) and Reverse (R) (5'→3')	Amplicon Length
<i>prrx1aⁱⁿ¹⁰</i>	WT Allele (F): CACCGCGAATCAGGATCA WT Allele (R): CTCCTCCAGATCCAACAGGT Mutant Allele (F): CTGGAGACTGCGATCAGGAT Mutant Allele (R): CTCCTCCAGATCCAACAGGT	WT Allele: 71 bp Mutant Allele: 74 bp
<i>prrx1aⁱⁿ⁶⁹</i>	WT Allele (F): GCCACACTACCAAACCGACT WT Allele (R): CCATTTTTCCCCTGTGTGAC Mutant Allele (F): GCCACACTACCAAACCGACT Mutant Allele (R): CCATTTTTCCCCTGTGTGAC	WT Allele: 350 bp Mutant Allele: 281 bp
<i>prrx1aⁱⁿ⁷⁴</i>	WT Allele (F): GCCACACTACCAAACCGACT WT Allele (R): CCATTTTTCCCCTGTGTGAC Mutant Allele (F): AAAAACGTTTCTTGTAGCCTATACA Mutant Allele (R): CCATTTTTCCCCTGTGTGAC	WT Allele: 350 bp Mutant Allele: 218 bp
<i>prrx1bⁱⁿ⁵</i>	WT Allele (F): GGATGAAAGTGTTGGCGAAAC WT Allele (R): AACACTTGTTGGTTTTTCTATGAGC Mutant Allele (F): GATGAAAGTGTTGGCGGG Mutant Allele (R): AACACTTGTTGGTTTTTCTATGAGC	WT Allele: 117 bp Mutant Allele: 118 bp
<i>prrx1bⁱⁿ⁵¹</i>	WT Allele (F): GGATGAAAGTGTTGGCGAAAC WT Allele (R): AACACTTGTTGGTTTTTCTATGAGC Mutant Allele (F): AGCTCTTTCGAAAACCCAAA Mutant Allele (R): CGTCTGCCACTTCTTTGTGA	WT Allele: 117 bp Mutant Allele: 392 bp
<i>snail1b^{bns351}</i>	WT Allele (F): CCTATAGCGCATGTGTTTGG WT Allele (R): GACCAATGACTTTAGTTCAAATCG Mutant Allele (F): TCACACACACATACACTATGGACA Mutant Allele (R): GACCAATGACTTTAGTTCAAATCG	WT Allele: 826 bp Mutant Allele: 315 bp

Table 3 | Primers used to genotype zebrafish mutant lines.

2. Injections in Zebrafish

2.1. CRISPR-Cas9 injections

Alt-R® S.r. Cas9 Nuclease V3 (IDT) enzyme and equimolar amounts of crRNA:tracrRNA (Alt-R® CRISPR-Cas9 crRNA and Alt-R® CRISPR-Cas9 tracrRNA IDT) were mixed and incubated 5 min at 37°C to form ribonucleoproteins (RNP) complexes. These complexes were injected into

Materials and Methods

the cytoplasm of 1-cell stage embryos and incubated at 28°C up to the indicated stage. 1 nL containing RNPs at 5 µM in 100 mM KCl was injected for targeting 1 gene, 1 nL at 10 µM RNP (5 µM each) to target two and 1 nL with 3,33 µM each when targeting three genes simultaneously.

Gene	dgRNA1	dgRNA2	dgRNA3
Ctrl	tccgtcccggcctgtgcatg	-	-
<i>prrx1a</i>	cacagcaggagagtaagtgc	tcgctcccgtggtgagtcc	-
<i>prrx1b</i>	gatgaaagtgttgcgaaac	aagagaaatggtcggttctc	aatgggactctccagtctgc
<i>snai1b</i>	cagtgatctctccccagac	acacgctggaggagaccca	-
<i>twist1a</i>	tgaggaagaggcgatgcacg	agactgtccaccggagactc	attccgacagtcccacgccc
<i>tbx5a</i>	gtatgtagtctcgatgacg	cgcgtcttacctccctgctt	
<i>tyr</i>	ggactggaggacttctgggg	-	-

Table 4| Sequence of the crRNA against the genes of interest to generate dgRNAs.

2.2. CRISPR-Cas13d injections

Unlike for CRISPR-Cas9 dgRNAs, there is not a systematic method or algorithm to design CRISPR-RfxCas13d gRNAs. The design was based on regions with a low probability of secondary structure according to the RNAfold programme (<http://rna.tbi.univie.ac.at/>). 4 different gRNAs were selected to target *prrx1a* mRNA sequences, with 50 nt of distance between them to avoid potential competition between gRNAs to access the target (Hernandez-Huertas et al., 2022; Kushawah et al., 2020). The DNA template to obtain gRNA was generated by fill-in PCR. A gRNA universal primer containing the T7 promoter and the processed direct repeat for Cas13d gRNAs (30 nt) preceded by 2GG were used in combination with a specific oligo of 42 nt adding the spacer (22 nt for target-binding) and part of the repeated sequence (reverse complement orientation).

PCR products were purified using PCR purification kit (ThermoFisher) and used as template (500 ng) for a T7 *in vitro* transcription reaction (AmpliScribe-T7-Flash transcription kit from Epicenter; 12-16 h of reaction). *In vitro* transcribed gRNAs were DNase-treated using TURBO-DNAs and RNA integrity and quantification was measured. gRNAs targeting *prrx1a* were individually transcribed *in vitro* and mixed at equal concentrations in pools after transcription. RfxCas13d was also transcribed *in vitro* from the pT3TS-RfxCas13d-HA plasmid (Addgene, plasmid #141320) using the mMESAGE mMACHINETM T3 transcription kit (AM1348, Thermofisher) following manufacturer's instructions and purified afterwards.

1-cell stage embryos were injected with 1 nL of mix of RfxCas13d purified mRNA (200–300 ng/mL) and 300–900 ng/mL (individual or mix gRNA final concentration) of gRNA using the microinjector stereomicroscope.

mRNA	<i>tyr</i>	<i>prrx1a</i>
gRNA1	ccggcgacggcuccgugugcgg	gauggugggagcucaagcggagg
gRNA2	aaaccugccagugcgccgaaa	gcuggagucuccgggacucacca
gRNA3	gugacgggucgcaguuugaugc	ggccuuagagagaguguuugaga
gRNA4	cuccuccucuucuuccucc	gaagcgggcagcugggcugucaa

Table 5 | Sequence of the gRNA against the mRNAs of interest.

3. Whole-mount *in situ* Hybridisation (Colorimetric and Fluorescent)

Whole mount *in situ* hybridisation (ISH) was carried out as described previously in Acloque et al., 2008 with minor modifications. Digoxigenin (DIG)-labelled probes (Roche) were synthesized from the full-length of zebrafish cDNAs and subcloned into the pGEMT-easy vector (Promega) with the primers included in Table 6. Probes for zebrafish *twist1a*, *myl7*, *snail1a*, *snail1b*, *spaw*, *amhc*, *prrx1a* and *prrx1b* were previously described (Fazilaty et al., 2019; Ocaña et al., 2012, 2017; Rago et al., 2019).

Zebrafish embryos were dechorionated and fixed or the other way around (if they were younger than 24-somite stage) with 4 % paraformaldehyde (PFA) in phosphate buffered saline (PBS) with diethylpyrocarbonate (DEPC) overnight (O/N).

Embryos were dehydrated and rehydrated through gradual series (0-25-50-75-100 %) of methanol diluted in PBS with 0.1 % of Triton X-100 (PBTx 0.1 %) (Sigma) and treated with 10 µg/mL proteinase K for 3 to 5 min (< 24 hpf to > 48 hpf). Afterwards, embryos were re-fixed with 4 % PFA in PBS-DEPC followed by PBTx 0.1 % washes. Samples were then incubated with hybridisation solution (50 % formamide (Sigma), 5x SSC, 2 % blocking powder (Roche), 0.1 % Triton X-100, 50 mg/mL yeast RNA (Sigma), 1 mM EDTA (Sigma), 0.1 % CHAPS (Sigma) in DEPC-treated distilled H₂O) at 60°C O/N. For hybridisation, embryos were incubated with denatured probes (3 min at 80°C) at 60°C O/N. Then, zebrafish embryos were washed at high stringency conditions (2 % and 0.2 % SSC washes at 60°C) and incubated with blocking solution (0.7 %

Materials and Methods

blocking powder and 20 % normal goat serum (NGS) (Invitrogen) in KTBT (50 mM Tris-HCl pH 7.5, 150 mM NaCl, 10 mM KCl diluted in PBTx 0.1 %). Subsequently, the samples were incubated with alkaline phosphatase-conjugated anti-DIG antibody (Roche, 1:1000) in blocking solution at 4°C O/N. For developing, embryos were incubated with alkaline phosphatase substrate (3 µL/mL NBT (Roche) and 2.6 µL/mL BCIP (Roche) in NTMT (100 mM Tris-HCl pH 9.5, 50 mM MgCl₂, 100 mM NaCl, 0.1 % Tween 20 (Sigma), 1 mM levamisol (Sigma) at room temperature (RT) until a blue precipitated was observed recapitulating the expression pattern. After hybridisation, the embryos were fixed in 4 % PFA in PBS-DEPC, washed and photographed.

For whole-mount fluorescent ISH, *amhc* and *prrx1b* were labelled using DIG. All the steps were the same as for the colorimetric ISH, except for the incubation with 1 % H₂O₂ for 20 min to inactivate endogenous peroxidase activity after the methanol series. Probes were detected with POD-conjugated anti-DIG (Roche, 1:500) antibody in blocking solution. The reaction was developed with a TSA-Plus Fluorescence Kit (Perkin Elmer), following manufacturer's instructions.

3.1. Design of probes for ISH

cDNA	Forward (F) primer (5'→3')	Reverse (R) primer (5'→3')
<i>snail2</i>	CATGCCTCGTTCATTCCTAGT	GTCTGAGATCAGTCTTCCCAATC
<i>snail3</i>	ACACAGCACATATCCCCTAAA	GTTTGTAGATGAGCCCGAAGA
<i>twist1b</i>	CCAGACTATAAGAGCTCCCTAAC	GCTCAGTTTATCGGAAGGTAAAG
<i>twist2</i>	AAACCGTGCCAAGCTCTAC	CTTCATGAGGATGCTCAAGTCC
<i>twist3</i>	CAGAGCTCGCTTCAGTGTTTA	TGCGAAGGCTTGATTTGGA
<i>zeb1a</i>	GCGACCTCAGATTCAGATGATG	CGGAGGCTTGTTGGTAATGT
<i>zeb1b</i>	CTACAGCACGAGTCCAAGTAAG	GACCATCAGCCGATAGGTTTAG
<i>zeb2a</i>	GCCATCTGACCCACTCTTATC	CAGCTCTGAAGAGGCATCAA
<i>zeb2b</i>	CACTTCCAGAACTCCTCCTTTAG	CCCTGGTTTCCGCTGATATT

Table 6 | Primers used to amplify zebrafish cDNA to generate ISH probes.

DNA extracted from 24 hpf Ab/Ab embryos was used to amplify fragments containing the sequences of EMT-TFs (which probes we did not have available in our laboratory) using Pwo DNA Polymerase (Roche) with the pair of primers of Table 6. Afterwards, PCR products were incubated with Taq DNA polymerase (Invitrogen), which adds a single deoxyadenosine (A) to the 3' ends. For vector cloning, PGEM®-T easy vector system (Promega) was used, which has overhanging 3'

deoxythymidine (T) residues when linearized. After ligation of the PCR product into the vector, transformation into bacteria was performed. Afterwards, vectors were purified using Plasmid DNA Mini Kit I Spin Protocol (Omega) and sequenced.

4. Whole-mount Immunofluorescence

Whole-mounted embryos were fixed with the chorion (if they were younger than 24-somite stage and dechorionated if they were older) in 4 % PFA O/N at 4°C. After fixation, embryos were dechorionated manually and dehydrated in a gradual series (0-25-50-75-100 %) of methanol diluted in PBS with 1 % Tween (PBTw 1 %), then kept in 100 % methanol O/N or at least 2 hours at -20°C. Embryos were then rehydrated in the reverse order of PBTw 1 %-methanol proportions.

Primary Antibodies	Host	Dilution	Source	Catalog nº
Prrx1	Rabbit	1:200	Tanaka Lab	-
Snail1	Rabbit	1:100	Cell Signalling	3879S
Acetylated α -tubulin	Mouse	1:600	Sigma	T6793
IgY anti-GFP	Chicken	1:500	Aveslab (2Bscientific)	AGFP-1020
anti-RFP	Rat	1:100	Chromotek	5F8
anti-BFP	Rabbit	1:200	BIO CAT	AB233-EV

Table 7 | List of primary antibodies used for immunofluorescence.

Secondary antibodies	Dilution	Source	Catalog nº
Alexa Fluor 488 goat anti-rabbit	1:500	Invitrogen	A11008
Alexa Fluor 488 goat anti-chicken IgG (H+L)	1:500	Life Technologies	A11039
Alexa Fluor 568 goat anti-rabbit	1:500	Invitrogen	A11011
Alexa Fluor 568 goat anti-mouse	1:500	Invitrogen	A11004
Alexa Fluor 568 goat anti-rat	1:500	Invitrogen	A11077

Table 8 | List of secondary antibodies used for immunofluorescence.

Antigen retrieval was performed by maintaining the embryos for 5 min at RT followed by 15 min at 70°C (or 20 min for Snail1 antibody) in 150 mM Tris-HCl buffer (pH 9.0). After cooling down the tubes for another 15 minutes, embryos were permeabilized with cold acetone for 20

Materials and Methods

min (or 30 min for Snail1 antibody) at -20°C followed by cold milliQ water quick washes. After washing with PBTw 1 % for 30 minutes, embryos were blocked with 5 % NGS 1 % Bovine Serum Albumin (BSA) 1 % Tx-100 for 3 h at RT and incubated with the primary antibodies from **Table 7** O/N or 48 hours for EMT-TFs at 4 °C. After washing for several hours in PBTw 1 %, the embryos were incubated with DAPI (4',6-diamidine-2'-phenylindole dihydrochloride) and the secondary antibodies from **Table 8** O/N at 4°C. After washing extensively with PBTw 1 %, embryos were imaged and analysed on microscopes.

5. *In silico* Analysis

Wagner and colleagues created a single cell level transcriptome lineage map for the developing zebrafish embryos (Wagner et al., 2018). They sequenced more than 90000 cells at different time points and annotated different cell types. We took advantage of this existing resource to check the expression of *prrx1a* during zebrafish heart development. We downloaded the pre-processed scRNA-Seq from their dedicated webserver (https://kleintools.hms.harvard.edu/paper_websites/wagner_zebrafish_timecourse2018/mainpage.html). We imported this data into python environment and extracted the expression matrix and metadata using scanpy package (Wolf et al., 2018). Expression analysis was performed in R3.6.0 statistical environment. Briefly, the cells belong to predefined heart development trajectories, specifically assigned to the population of mesoderm (lateral plate and heart field) and heart (heart field and heart mature) were subset and used for the downstream analysis. The expression of *prrx1a* was plotted as a heatmap using heatmap function and as violin plots. The individual gene expression was visualized on the pre-calculated cell embedding using the webserver (https://kleintools.hms.harvard.edu/tools/springViewer_1_6_dev.html?cgi-bin/client_datasets/fish_embryo_timecourse/full) developed by Wagner et al., 2018.

6. Fixed Sample – Image Acquisition and Processing

6.1. Microscopy image acquisition

Pictures of whole-mounted embryos subjected to ISH were taken with a Leica M125 stereoscope, using the Leica suite software with a Leica DFC 7000T digital camera.

Whole-mount immunofluorescence and fluorescence ISH were obtained with a Zeiss light-sheet Z.1 microscope using the following acquisition parameters: Dual side illumination with LSFM 5x/0.1 illumination optics and detection with a Papo 10x/0.5 (water immersion) or with

LSFM 10x/0.2 illumination optics and detection with 20x/1.0 (water immersion) objective with 2.5x system optical zoom. The excitation and collection of the light was performed as follows: DAPI was excited with laser line 405 nm and collected with a BP 420-470 filter; Alexa 488 was excited with laser line 488 nm and collected with a BP 505-545 filter; and Alexa 568 and Cy3 were excited with laser line 561 nm and collected with a BP575-615 filter. All images were acquired at 16-bit with sCMOS PCO.Edge cameras.

Immunofluorescence of **Figure 18a** and **Figure 25** were obtained with an Olympus FV1200 microscope with a 40x and 20x objective respectively. The fluorophore Alexa Fluor 568 was excited with a 559 nm laser line and was collected at 570– 620 nm.

6.2. Processing of image data

6.2.1. *spaw*, jogging and heart laterality

After taking pictures with a Leica DFC 7000T digital camera, for categoric quantification of phenotypes as *spaw*, jogging or heart laterality, embryos were assigned to one of the groups described in the figures which were more alike. For instance, left, middle or right jogging in **Figure 18c**.

6.2.2. Posterior pole displacement and looping angle

Raw data were analysed using ImageJ software in 2D. Scale bars were adjusted, and length was measured for the displacement of the posterior pole from the embryo midline and for the angle in heart looping.

6.2.3. Area of atrium and cilia length

Raw data were analysed using the Imaris software (Bitplane AG), to create 3D reconstructions of different views as well as for surface segmentation. Maximum intensity projection was used to generate images that were included in the figures.

6.2.4. Quantification of number of cells (L/R *Prrx1* in *TgBAC(tbx5a:eGFP)*)

Raw data were analysed using ARIVIS vision4D, to create 3D reconstructions of different views as well as for segmentation analysis. A pipeline was adjusted for each type of signal and segmentation was done through blob finder tool. After some filters, *Prrx1* segments were subdued to *TgBAC(tbx5a:eGFP)* segment through colocalization tools, to obtain only the

Materials and Methods

expression in the aLPM. The % of Prrx1a signal in *TgBAC(tbx5a:eGFP)* cells was calculated dividing the number of cells that express both by the total number of *TgBAC(tbx5a:eGFP)* cells in the region interest (ROI). The number of cells on the right versus left sides considered the anatomical position of cells in the *tbx5a*-ALPM in either side. Instead of a maximum intensity projection, 3D images were used to generate the pictures contained in the immunofluorescence figures as we could chose the orientation of the embryo.

7. *In vivo* Time Lapse

7.1. Acquisition

To measure heart beating, selective plane illumination microscopy (SPIM) of non-invasive imaging of live samples over short time was obtained with a Zeiss light-sheet Z.1 microscope using the following acquisition parameters: Dual side illumination with LSM 10x/0.2 illumination optics and detection with 20x/1.0 (water immersion) objective with 2.5x system optical zoom. The excitation and collection of the light was performed as follows: eGFP from endogenous reporter was excited with laser line 488 nm and collected with a BP 505-545 filter. All images were acquired at 16-bit with sCMOS PCO.Edge cameras.

TgBAC(tbx5a:eGFP) embryos at ≈ 48 hpf were dechorionated and mounted inside capillaries (size 4, ≈ 2.15 mm inner diameter, BRAND™ 701910) with their pistols (BRAND™ 701938) in 1 % low-melting-point agarose (Lonza, 50100) containing 200 mg/L tricaine (MS222; Sigma-Aldrich). This concentration of tricaine did not interfere with regular heart beating. The capillaries containing the embryos were suspended into egg water media containing 200 mg/L tricaine and maintained at 28.5°C. For 3 minutes, the camera acquired the image of only one optical section with one illumination side that gave us the best image quality taking in total 11486 snapshots. This was quick enough to resolve the dynamics of zebrafish heartbeat which is very speedy.

7.2. Processing of time-lapse data

For heart beating, beats were manually counted from time-lapse movies and the beats per minute were represented in **Figure 17b**.

8. Statistical Analysis and Figures Design

Statistical analysis was performed using the GraphPad Prism software version 7.0. Results were expressed as mean \pm SD (standard deviation), percentage mean \pm SD and in box plots (centre lines, medians; box limits, second and third quartiles; whiskers, first and fourth quartiles). Differences among groups were tested by two-tailed unpaired Student's t test, One-way ANOVA and Two-way ANOVA as indicated in the figure legends. Differences were considered statistically significant when P-values were * P < 0.05, ** P < 0.01, *** P < 0.001 and **** P < 0.0001. Statistics were applied to the number of independent experiments indicated in the standing figures.

Images and graphs were prepared using Adobe Photoshop, Adobe Illustrator from CS6 and some parts of the figures were created with Biorender (<https://biorender.com/>).

RESULTS |

1. *Prrx1a* in Heart Laterality

1.1. *prrx1a* is asymmetrically expressed in cardiac precursors

In zebrafish development, two parallel and mutually repressed pathways driven by Spaw (on the left) and BMP (on the right) in the LPM, lead to the asymmetric activation of the TFs *pitx2* and *prrx1*, respectively (Ocaña et al., 2017; Ryan et al., 1998). *prrx1a* is initially bilaterally symmetric and then is transiently attenuated by miRNAs activated by Spaw exclusively on the left LPM (Rago et al., 2019). Consequently, in embryos at the 20-somite stage when the cells of the FHF reach the midline to form the CD, the surrounding aLPM expresses higher levels of *prrx1a* on the right side (orange asterisk) as assessed by ISH (Figure 13a). At this same stage, it is also asymmetrically expressed in the pLPM (orange asterisk, Ocaña et al., 2017), and bilaterally symmetric in the NC, the tail bud and somites (Figure 13a). The latter territories were already described, but the expression in the aLPM was not characterized in depth.

As *tbx5a* is a TF expressed in the primary HT and in the surrounding aLPM that gives rise to the pericardium and the posterior pole, we had previously used a *tbx5a* reporter transgenic zebrafish line to follow the aLPM cells that contribute to the heart, showing its coexpression with *Prrx1a* in a subpopulation of this territory (Ocaña et al., 2017). Here we wanted to assess whether *tbx5a* was also L/R asymmetrically expressed in the LPM. Indeed, *tbx5a* is expressed at higher levels on the right-hand side in both the aLPM and pLPM (orange asterisk), in addition to the developing eyes at the 20-somite stage. At 28 hpf, after heart jogging, *prrx1a* expression is detected in the aLPM, pLPM, pectoral fin buds, branchial arches, hatching gland, somites and tailbud (Figure 13b). *prrx1a* is not expressed in the HT, indicating that it is downregulated when expressing cells join the heart, while *tbx5a* expression is maintained. In addition, *tbx5a* is also expressed in the pectoral fin, pLPM and eyes (Figure 13b) (See also Begemann and Ingham, 2000 and Ocaña et al., 2017). Thus, we confirmed that both *tbx5a* and *prrx1a* are L/R asymmetrically expressed in a transient manner in the aLPM that will contribute to the heart.

Results

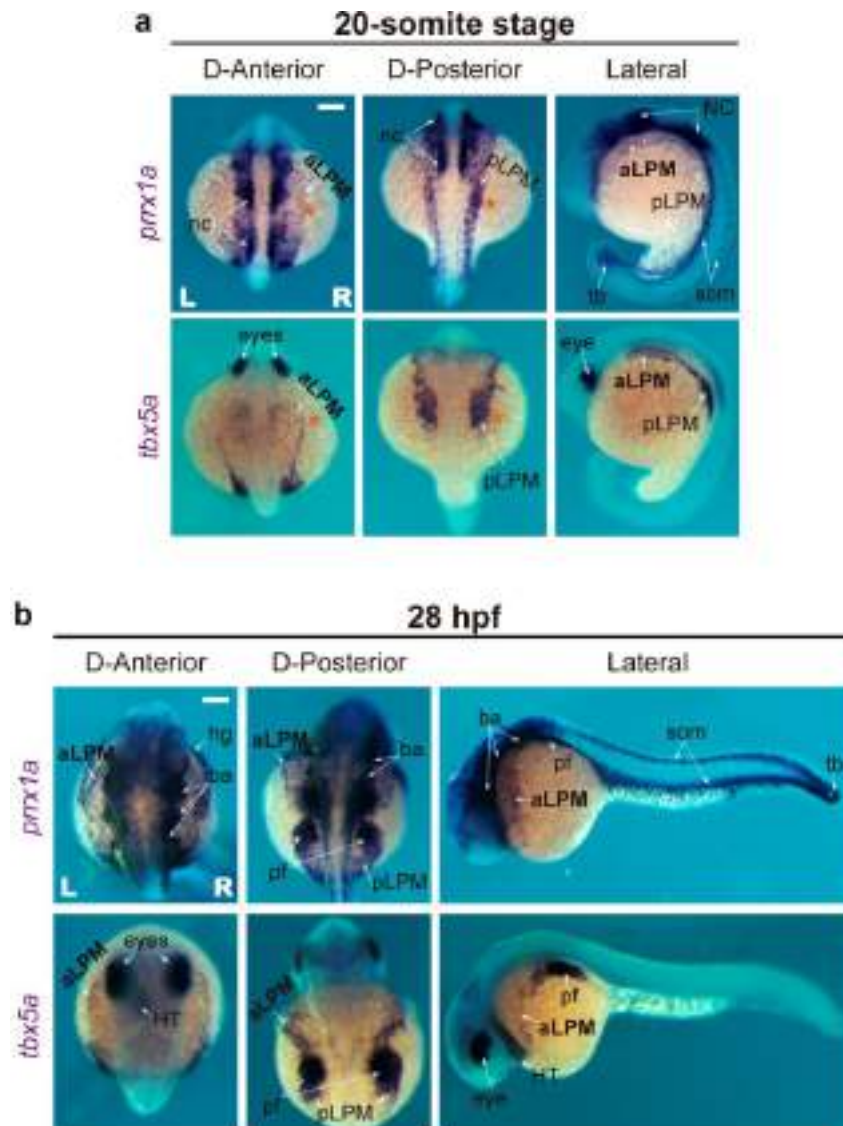


Figure 13 | *prrx1a* and *tbx5a* are asymmetrically expressed in the aLPM. **(a)** Dorsal and lateral views of 20-somite stage zebrafish embryos showing *prrx1a* and *tbx5a* expression by ISH. Both are expressed in the aLPM and pLPM. The orange asterisks denote the side of higher expression. The arrows indicate expression in the NC, somites (som) and tailbud (tb). *tbx5a* is also expressed in the eyes. Scale bar: 200 μ m. **(b)** Dorsal and lateral views of 28 hpf zebrafish embryos showing *prrx1a* and *tbx5a* expression by ISH. *prrx1a* is expressed in the aLPM, hatching gland (hg), branchial arches (ba), pLPM, pectoral fin (pf), somites and tailbud, while *tbx5a* is expressed in the aLPM, HT, eyes, pLPM and pectoral fin buds. Scale bar: 200 μ m.

To further study *prrx1a* expression in heart derivatives, we made use of a public scRNAseq of the first 24 hours of zebrafish embryonic development (Wagner et al., 2018). **Figure 14a** shows the projection of cell state trajectories during development, color-coded according to developmental stages. Our own analysis from this pre-processed scRNAseq data, confirms the expression sites for *prrx1a* and that in the developing heart, where it is only expressed in CPCs and downregulated once they join the heart to differentiate into CMs (**Figure 14**).

Consistent with our ISH data, *prrx1a* is expressed in somitic mesoderm, NC, pharyngeal arches, fin bud and heart trajectories. The majority of SHF cells at 18 hpf (orange circle) are *prrx1a*⁺ (orange square) (Figure 14b), where part of the aLPM at 10 hpf gives rise to the heart field (the rest of aLPM derivatives are not represented). Later, there are two branches, one towards differentiated CM (brown line) and another one for undifferentiated CPCs (dark blue line) (Figure 14c). Violin plots show *prrx1a* expression in heart precursors, a SHF population at 18 hpf and two branches either positive or negative for *hoxd9a* at 24 hpf. *Hoxd9a* controls cardiovascular system development and is not present in cells of the HT (18 hpf FHF and 24 hpf mature heart) (Figure 14c). In summary, *prrx1a* is expressed in most heart precursors (Figure 14d), confirming our ISH data and the conclusion that when *prrx1a*⁺ CM precursors enter the HT, it is downregulated.

Once we analysed the expression of both *prrx1a* and *tbx5a* and confirmed that both were expressed in a L/R asymmetric manner and in overlapping populations of cardiac precursors, we performed immunofluorescence studies for Prrx1 in the *tbx5a*-reporter line mentioned above, *TgBAC(tbx5a:eGFP)*, at the 20-somite stage and 28 hpf (Figure 15a). We found coexpression of both TFs in the aLPM in $\approx 60\%$ of the cells (Figure 15a), and the rest were *tbx5a*-GFP single-positive cells (asterisk). Next, we quantified the Prrx1⁺ cells contained in the *tbx5a*-GFP⁺ aLPM in both the right- and left-hand sides. At the 20-somite stage, we observed that Prrx1 is asymmetrically expressed with higher levels from the right-hand side, as previously described (Ocaña et al., 2017). Nevertheless, at the later stage 28 hpf this asymmetric expression is no longer detected, as cells have already started to be incorporated into the posterior pole of the heart (Figure 15b).

Cells from the most lateral part of the aLPM have higher degree of colocalization, while the more medial subpopulation have less Prrx1 expression. This suggests that some *tbx5a*⁺ cardiac progenitors including those that contribute to the FHF that are *prrx1a* independent and may rely on other EMT-TFs for migration.

Results

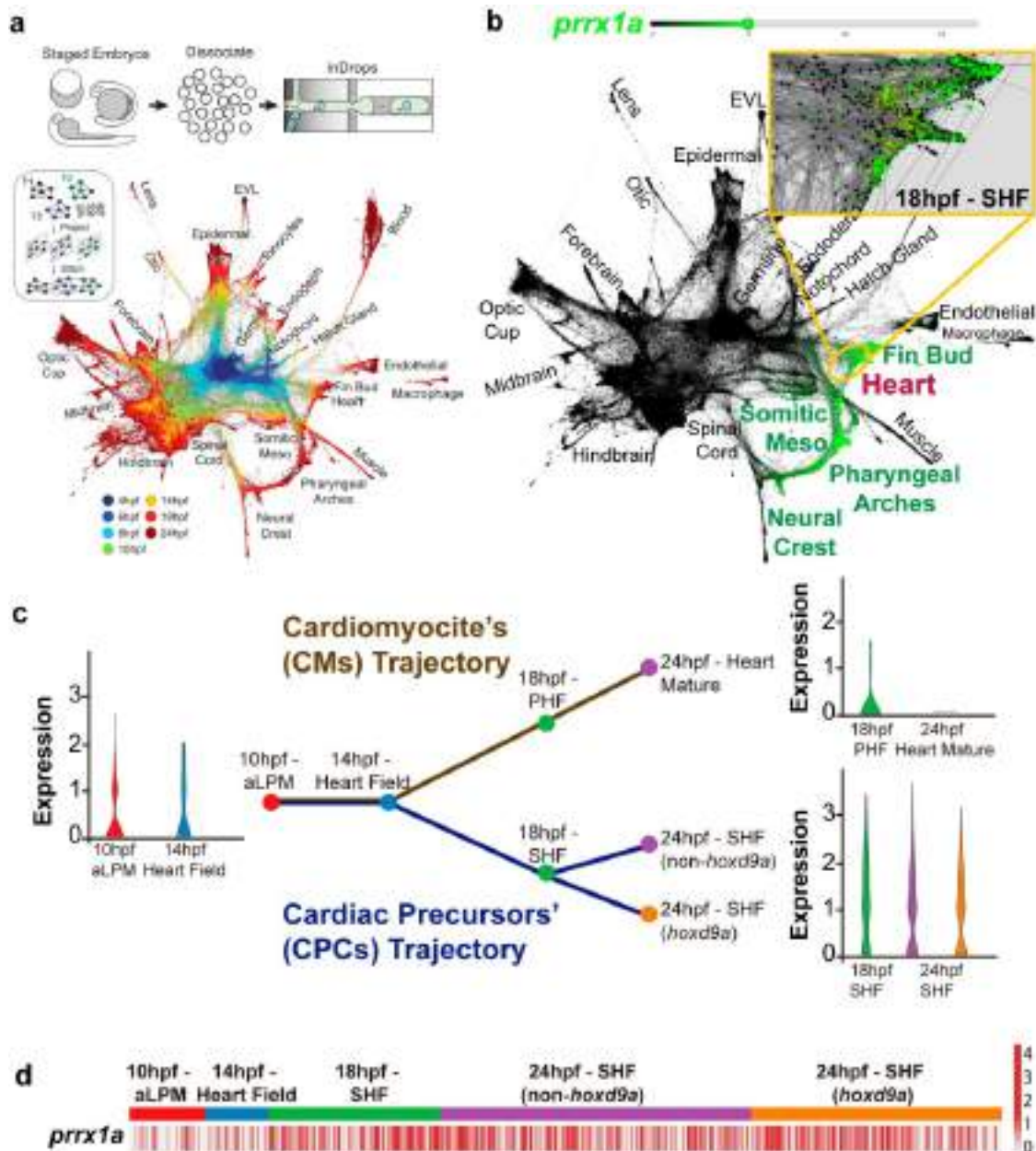


Figure 14 | *prrx1a* is expressed in cardiac precursors (CPCs) but not in cardiomyocytes (CMs). (a) Experimental workflow of public scRNAseq of zebrafish development, where single-cell suspensions were dissociated at different stages and introduced into the inDrops microfluidic device. Overview of graph construction strategy where nodes are coloured according to the developmental time of analysis, from 4 hpf to 24 hpf (Wagner et al., 2018). (b) Analysis of scRNAseq from (a) for *prrx1a* (highlighted in green) shows expression in the somitic mesoderm, neural crest, pharyngeal arches, fin bud and heart trajectories. A zoom-in of the heart trajectory for SHF at 18 hpf, shows that most of the cells are *prrx1a*⁺ (orange). (c) Schematic representation of the heart trajectory and violin plots showing the distribution of *prrx1a* expression. *prrx1a* is expressed as early as 10 hpf in the aLPM (red point). From 14 hpf (blue point), there are two branches in the heart lineage, one negative leading to CM differentiation (brown line) and one positive for *prrx1a* (dark blue line), corresponding to CPCs. (d) Heat map of *prrx1a* expression in the CPCs from (c) displaying high expression in most of SHF cells.

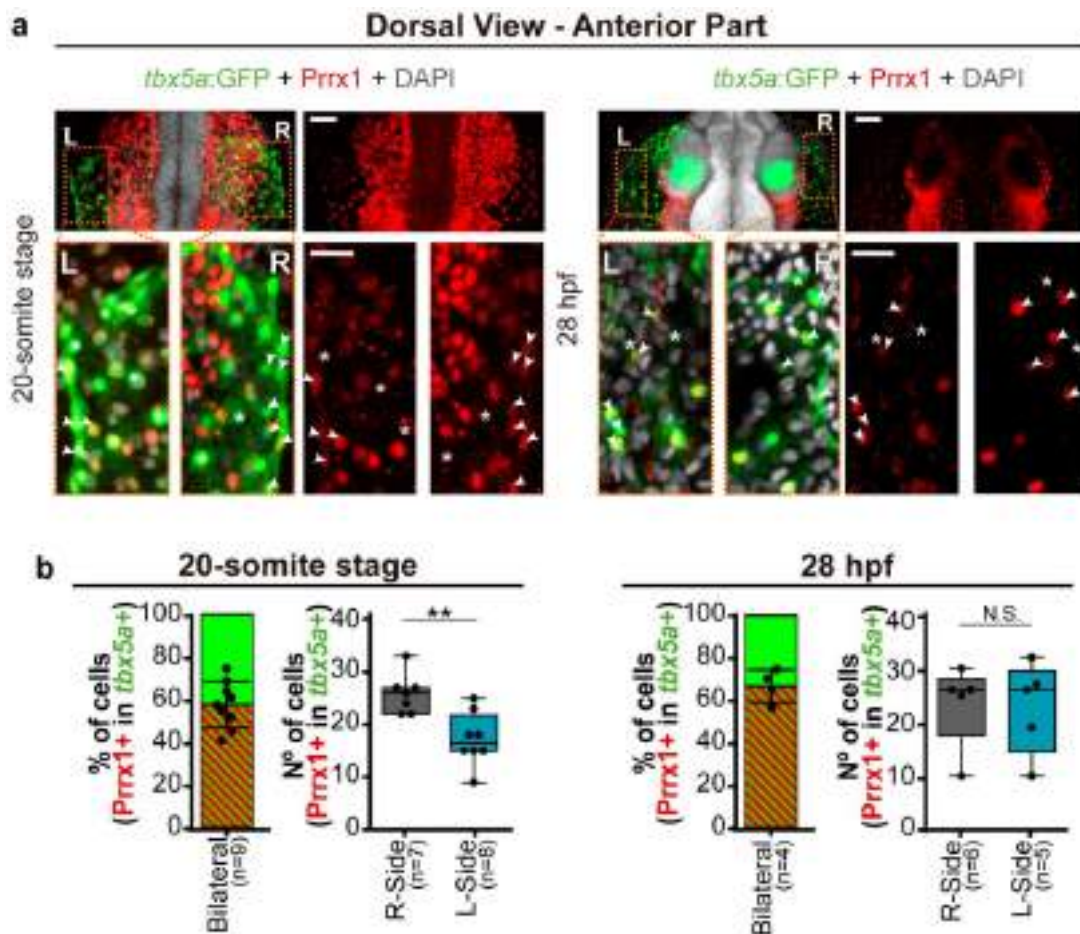


Figure 15 | *Prrx1* is asymmetrically expressed in *tbx5a*+ heart precursors. **(a)** Dorsal view of a 20-somite stage (left) and a 28 hpf (right) *TgBAC(tbx5a:eGFP)* zebrafish embryos showing *Prrx1* protein expression. Double positive *tbx5a*-GFP (green) and *Prrx1* (red) cells are denoted by arrowheads while *tbx5a*-GFP single positive cells are indicated by an asterisk. Scale bars: 100 μ m and 50 μ m. **(b)** Red dashed bars on the green background show the percentage of *Prrx1* positive cells within the *tbx5a*-GFP positive aLPM, both sides, quantified from embryos like those shown in (a). Data are represented as the mean percentage of *Prrx1*+ cells in *tbx5a*+ aLPM \pm s.d. $n = 9$ embryos at 20-somite stage and $n = 4$ embryos at 28 hpf. On the right panel for each developmental time, number of *Prrx1* positive cells contained either in the R or L-side of *tbx5a*-GFP+ aLPM. Data are represented in box plots: centre lines, medians; box limits, second and third quartiles; whiskers, first and fourth quartiles. $n = 7-8$ embryos at 20-somites and $n = 5-6$ embryos at 28 hpf. N.S., not significant and ** $p < 0.01$ by Unpaired Student t-test (two-tailed).

1.2. *G0-prrx1a* crispants show mesocardia and additional heart defects

Loss-of-function (LOF) in zebrafish embryos were initially obtained after the generation of “morphant” embryos, after injecting morpholino (MO) oligonucleotides in 1-cell stage embryos (Stainier et al., 2017). The advance in gene-editing technology thanks to the description of the CRISPR-Cas9 system (Clusters of Regularly Interspaced Short Palindromic Repeats - CRISPR-

Results

associated protein 9) (Hwang et al., 2013), has allowed to easily screen zygotic phenotypes in somatic cells. These embryos are called “crispants”, and result from the injection of RNA guides which efficiently generate biallelic editing. As with morphants, this also allows the assessment of phenotypes in the injected embryos, but with much reduced off-target effects (generation 0: G0 embryos, Wu et al., 2018).

We had previously generated both morphant and crispant *prrx1a* embryos and found a mesocardia phenotype, as a straight heart remained at the midline failing to maintain the left displacement of the posterior pole and to undergo dextral looping (D-Loop) (Ocaña et al., 2017). We also found a similar phenotype in chicken and mouse embryos when *Prrx1* and/or *Snail1* were downregulated/deleted by different means, including the generation of mouse mutants (Ocaña et al., 2017). As Tessadori and colleagues subsequently reported the absence of a heart phenotype in several *prrx1a* mutants (Tessadori et al., 2020), we decided to examine in depth the specificity of this phenotype. To do that, we injected at the 1-cell stage embryo, ribonucleoprotein (RNP) complexes consisting of synthetic crRNA:tracrRNA duplex guide RNAs (dgRNA) against *prrx1a* (Figure 16a) and Cas9 protein optimized to avoid off-target effects (Hoshijima et al., 2019; Vakulskas et al., 2018). The guides used for Figure 16 are more efficient producing double strand breaks (DSB) than those previously used in Ocaña et al., 2017, where RNPs were composed of canonical standard single guide RNA (sgRNA) and Cas9 was obtained after *in vitro* transcription (Li et al., 2016; Wu et al., 2018).

As mentioned above, these RNPs of dgRNAs are useful for rapid screens in G0-crispant embryos. As a control of gene editing efficiency, we also used dgRNA against the *tyrosinase* (*tyr*) gene, which encodes an enzyme that catalyses the production of melanin (Camp and Lardelli, 2001). As such, when we analysed zebrafish pigmentation at 52 hpf, we could appreciate that a high percentage of embryonic cells should harbour LOF mutations as the level of pigmentation is very low compared to G0-Ctrl crispant embryos (Figure 16b). As expected, heart position in G0-*tyr* crispants was normal, indicating that the DSB-repair-induced mutations by dgRNAs did not unspecifically interfere with the normal development of the heart (Figure 16c). After injecting embryos with RNPs against *prrx1a* we confirmed the defects that we described previously in morphant and crispant embryos obtained after injection with morpholinos or other guides as described above (Ocaña et al., 2017), namely mesocardia (No-Loop) in nearly 35 % of the embryos (Figure 16c).

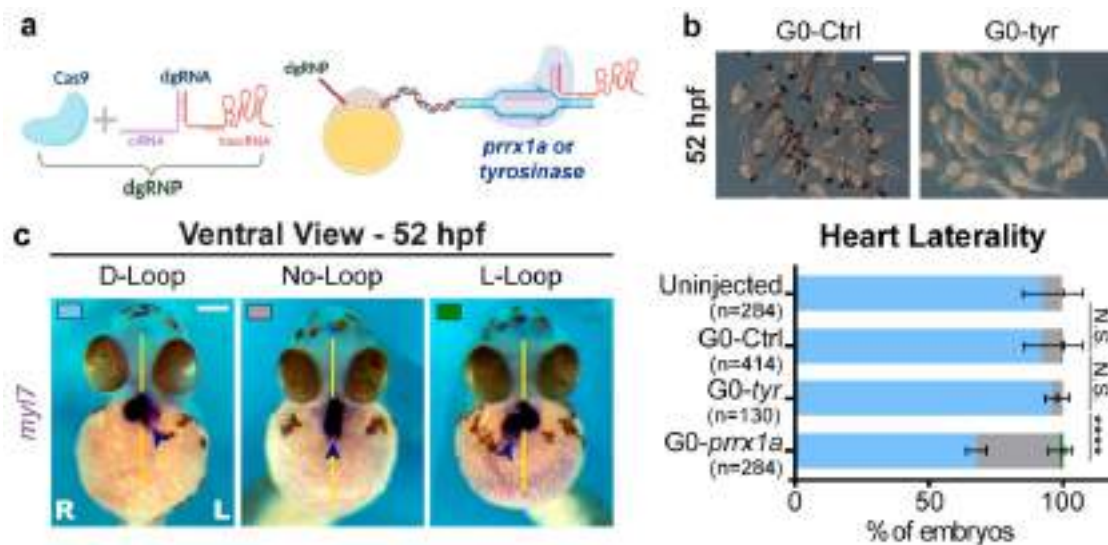


Figure 16 | G0-*prrx1a* crispants have mesocardia. (a) Schematic representation of the generation of G0-crispant embryos through the injection of duplex guide ribonucleoproteins (dgRNP) at the 1-cell stage. The dgRNP is composed by Cas9 protein and duplex guide RNAs (dgRNA) which contains a constant sequence (tracrRNA) and one specific against the gene of interest (crRNA). (b) Efficacy of CRISPR/Cas9 editing in the zebrafish embryo population, as assessed by the level of pigmentation in G0-*tyr* crispant embryos compared to controls at 52 hpf. Scale bar: 250 μ m. (c) Heart position at 52 hpf (ventral view) shows mesocardia: no loop and posterior pole (dark blue arrow) in the midline (highlighted by a yellow line) in a percentage of G0-*prrx1a* crispant embryos. G0-*tyr* crispants show the normal D-loop and posterior pole to the left as in control embryos. Data are represented as the mean percentage \pm s.d. n = number of embryos analysed pooling two (G0-*tyr*) or more than three independent experiments (for the rest of conditions). Statistical analysis (shown for the mesocardia phenotype in grey): two-way ANOVA. N.S., not significant, ****P < 0.0001. Scale bar: 200 μ m.

In addition to mesocardia, in the previous study from the lab, Ocaña and colleagues also described that *prrx1a* morphants had atrial and ventricular chambers specified, but the atrium was smaller (Ocaña et al., 2017). We decided to examine atrial size in our crispant embryos using a transgenic zebrafish line that expresses GFP under the control of the *myl7*, a marker of differentiating myocardium (Yelon et al., 1999). We injected dgRNA guides against *prrx1a* in *Tg(my17:GFP)* embryos, which were subsequently labelled with *atrial myosin heavy chain (amhc)* probe, to better see the atrium. We could confirm the mesocardia phenotype and a reduction in atrial size (Figure 17a). Furthermore, we assessed cardiac function in G0-*prrx1a* embryos measuring heartbeat rate. Using again the *TgBAC(tbx5a:eGFP)* fish line, we acquired time-lapse images during 3 minutes and the beats per minute were annotated in anesthetised zebrafish embryos at 52 hpf (Figure 17b). Heartbeat in crispants was compared to that in uninjected fish embryos and we found a significant decrease. As G0-*prrx1a* crispant embryos show mesocardia with a penetrance of around 35 %, we independently measured heart beating in embryos with

Results

normal heart laterality and in those with mesocardia and found that the bradycardia (slow heart beating) was associated with the mesocardia condition (No-loop) (Figure 17b).

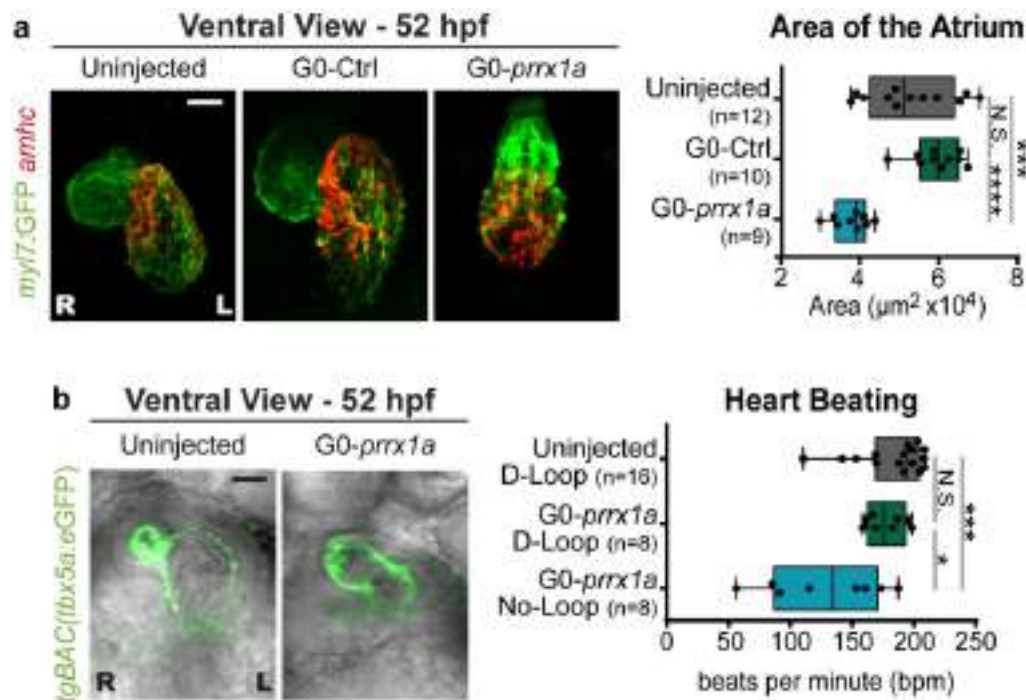


Figure 17 | G0-*prrx1a* crispants have a smaller atrium and bradycardia. (a) Whole-mount ISH for *amhc* (atrial marker) in *Tg(myl7:GFP)* fish embryos (*myl7* promoter drives GFP expression in CMs) at 52 hpf (ventral view of the heart). G0-*prrx1a* crispant embryos show a reduction in atrial size. Data represented in box plots: centre lines, medians; box limits, second and third quartiles; whiskers, first and fourth quartiles. n = number of embryos analysed. Statistical analysis: N.S., not significant, ***P < 0.001, ****P < 0.0001 by one-way ANOVA. Scale bar: 50 μm . **(b)** Snapshots taken from a 3 minute time-lapse movies (click the image to open) of 52 hpf *TgBAC(tbx5a:eGFP)* embryos showed from a ventral view. G0-*prrx1a* crispant embryos show a decrease in the rate of beats per minute (bradycardia) being significant in those with mesocardia (No-Loop). Thus, heart laterality defects are correlated with bradycardia. Data represented in box plots: centre lines, medians; box limits, second and third quartiles; whiskers, first and fourth quartiles. n = number of embryos analysed. Statistical analysis: N.S., not significant, *P < 0.05, ***P < 0.001 by one-way ANOVA. Scale bar: 50 μm .

The injection of dgRNA into zebrafish embryos is performed at the 1-cell stage. If the gene of interest is expressed at early stages it is important to examine whether it has an early role that, when defective, could influence later developmental processes. Thus, as the initial break of L/R symmetry occurs very early in embryonic development and requires the LRO (or KV), we investigated if G0-*prrx1a* crispant embryos had a defective LRO that could lead to an abnormal asymmetric L/R cascade and non-specifically influence heart laterality.

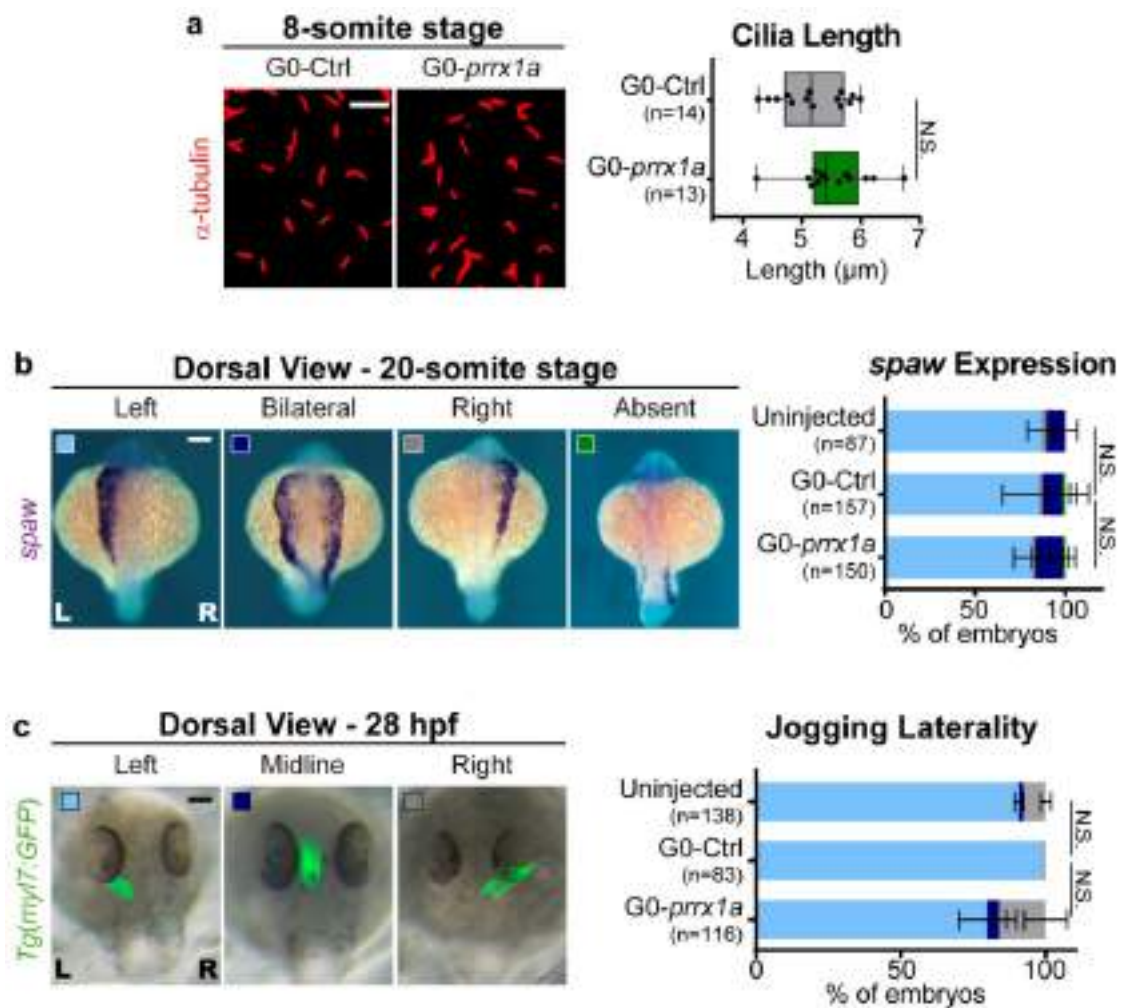


Figure 18| *G0-prrx1a* crispant embryos do not show early L/R phenotypes. **(a)** Cilia in the KV, observed after immunofluorescence for acetylated α -tubulin, are not affected in 8-somite stage *G0-prrx1a* crispant embryos. Data represented in box plots: centre lines, medians; box limits, second and third quartiles; whiskers, first and fourth quartiles. n = number of embryos analysed. Statistical analysis: N.S., not significant by unpaired Student's t-test (two-tailed). Scale bar: 40 μ m. **(b)** 20-somite stage *G0-prrx1a* crispant embryos (dorsal view) show normal left-sided *spaw* expression. Data are represented as mean percentage \pm s.d. n = number of embryos analysed pooling three independent experiments. Statistical analysis (shown for left-*spaw* expression; light blue): two-way ANOVA. N.S., not significant. Scale bar: 200 μ m. **(c)** 28 hpf *G0-prrx1a* crispant embryos (dorsal view) analysed do not show significant jogging defects. Data represented as mean percentage \pm s.d. n = number of embryos analysed from one (*G0-Ctrl*) or two independent experiments (uninjected and *G0-prrx1a*). Statistical analysis (shown for the left-jogging; light blue): two-way ANOVA. N.S., not significant. Scale bar: 250 μ m.

As a readout of LRO integrity, we examined the length and distribution of the cilia in the 8-somite stage embryos, as cilia produce a proper Nodal flow that induces L/R symmetry break (Leventea et al., 2016). We used immunofluorescence against acetylated α -tubulin, and we did not detect differences in cilia length between *G0-Ctrl* and *G0-prrx1a* crispants, indicating that the LRO was not defective (Figure 18a). Another readout of a proper establishment of a functional

Results

L/R cascade is the unilateral expression of *spaw* on the left side of the LPM (Brennan et al., 2002). Notably, G0-*prrx1a* crispants embryos had normal *spaw* expression (Figure 18b). As the initial leftward movement of the zebrafish heart posterior pole occurs through jogging (see introduction), we also examined jogging laterality in G0-*prrx1a* compared to G0-Ctrl crispants embryos and found no significant differences (Figure 18c). This is in agreement with the proposal that the final displacement of the posterior pole and heart looping are determined later and independent of the formation of the LRO and initial heart jogging (Grimes et al., 2020; Noël et al., 2013). All these data indicate that the mesocardia, the reduction in atrial size and the bradycardia observed in G0-*prrx1a* crispants are specific of a defective *prrx1a* function in the L/R asymmetric contribution of aLPM-cells to be incorporated into the posterior pole of the heart.

1.3. *Prrx1a* can be dispensable but plays a specific role in heart laterality

CRISPR-Cas9 technology grants a quick, accurate and unbiased way of manipulate the expression of any gene of interest unravelling its role during development through the screens of G0 embryos (Wu et al., 2018). But ideally, G0 crispant embryos should be used in combination with mutants that shelter heritable null mutations (Hoshijima et al., 2019). Thus, we generated an allelic series of *prrx1a* mutants through the injections of different combinations of RNPs against *prrx1a* into 1-cell stage WT zebrafish embryo as described above. In this case, the F0 crispants, which were mosaic, were bred until they were sexually mature to cross them with a WT fish to obtain a heterozygous F1 line. Adult F1 fishes carrying the same mutation were in-crossed to obtain the homozygous F2 used for subsequent analyses (Figure 19a).

We generated different *prrx1a* mutant lines following different strategies. The first *prrx1a*-mutant allele we generated was *prrx1aⁱⁿ¹⁰*. This allele bears a 10 nucleotide (nt)-deletion generated after the injection of sgRNA (pink, used in Ocaña et al., 2017) against *prrx1a* exon 1 with the aim of producing a frameshift mutation in its mRNA, leading to a premature termination codon (PTC) (Figure 19b). The second mutant line, *prrx1aⁱⁿ⁶⁹*, harbours a 69 nt deletion between exon 1 and intron 1, as the dgRNAs (orange guides, used in Castroviejo et al., 2020) were designed against the splice site to precisely impair the correct splicing of its mRNA (Figure 19b). This set of guides is the one used for the generation of G0-crispant embryos from previous experiments. The third line, *prrx1aⁱⁿ⁷⁴* carries a promoter-less allele avoiding the possibility of *prrx1a* transcription

(Jakutis and Stainier, 2021). The dgRNA (blue guides) were designed against the upstream promoter region of *prrx1a* and the end of exon 1, leading to a 2474 nt deletion (Figure 19b).

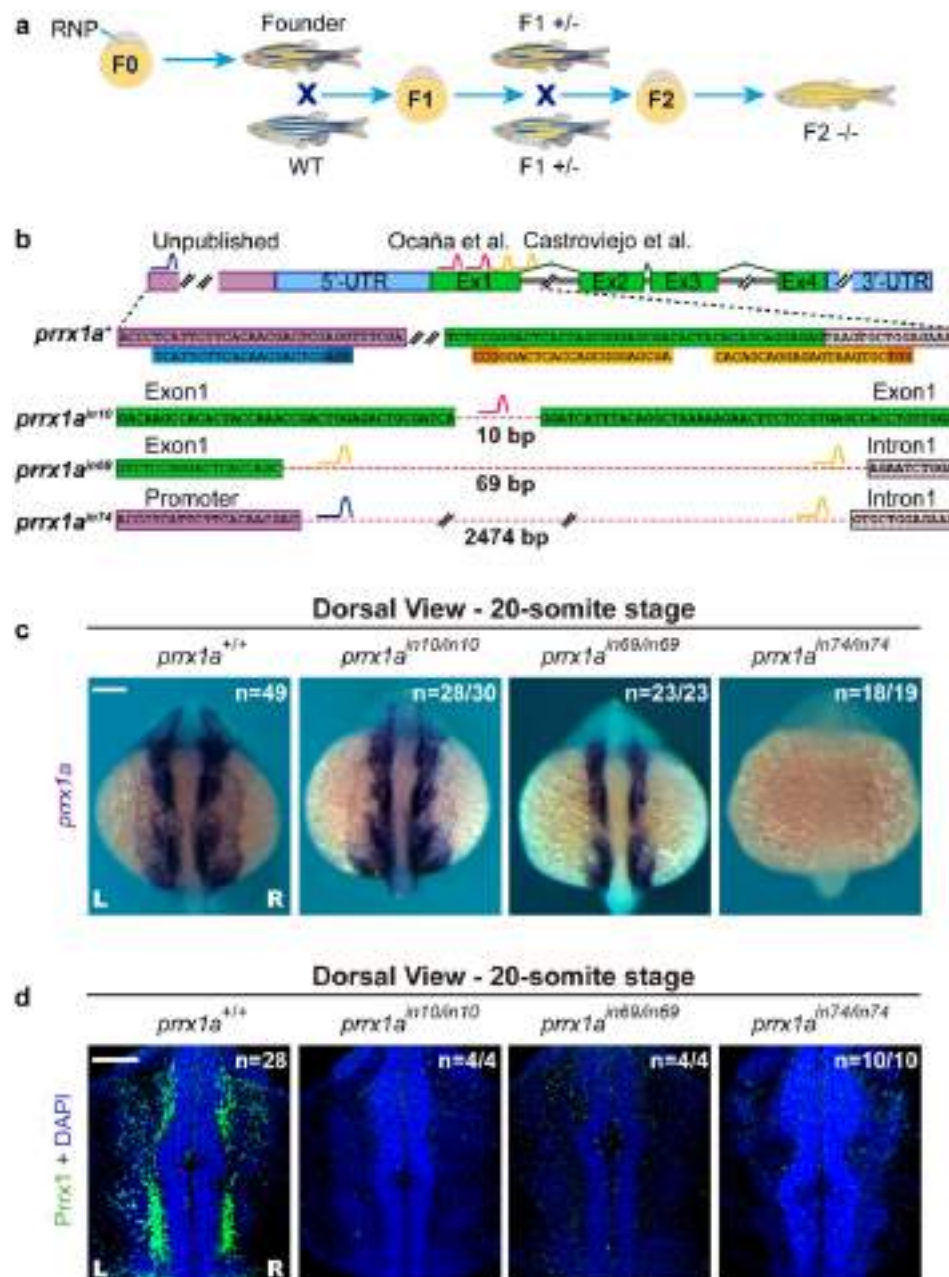


Figure 19| *prrx1a* mutants do not express Prrx1a protein. (a) Workflow for establishing zebrafish mutant lines with CRISPR/Cas9. WT embryos were injected with RNP at 1-cell stage. Founder fish (F0, mosaic with yellow stripes) is out-crossed with a WT giving rise to a heterozygous F1 (F1 +/-). Adult F1 fishes with the same mutation are then in-crossed to obtain homozygous F2 animals (F2 -/-). (b) Schematic representation of the *prrx1a* gene (purple: promoter region; light blue: untranslated region (UTR); green: open reading frame (ORF) and RNA guides (pink as in Ocaña et al., 2017; orange as in Castroviejo et al., 2020; dark blue, unpublished). (c) *prrx1a* mRNA is translated in *prrx1a*ⁱⁿ⁵ and *prrx1a*ⁱⁿ⁶⁹ mutants but not in the *prrx1a*ⁱⁿ⁷⁴ line as the edited allele does not contain the promoter region. n = number of embryos analysed. Scale bar: 200 μ m. (d) Absence of Prrx1a protein in the three *prrx1a* mutant alleles, as *prrx1a* transcripts do not encode a functional Prrx1a protein. n = number of embryos analysed. Scale bar: 100 μ m.

Results

We characterized the different allelic series for *prrx1a* mutant checking whether their mRNA was transcribed (Figure 19c). For *prrx1a*^{in10/in10} and *prrx1a*^{in69/in69} mutants, mRNA is detected although it seems to be expressed at lower levels, and asymmetry cannot be assessed. As expected, in the *prrx1a*^{in74/in74} mutant, there is a complete absence of mRNA due to the lack of promoter sequences, and therefore, of the transcription initiation start. Immunofluorescence against Prrx1 showed that, in the three cases, Prrx1a protein was not expressed (Figure 19d). Therefore, *in10*, *in69* and *in74* mutants are equivalent to *prrx1a* LOF.

We examined the mutants and found that unlike G0-crispant embryos, the three types of *prrx1a* mutant embryos, both heterozygous and homozygous, did not show mesocardia. As such, they all had normal heart position (D-Loop; light blue) (Figure 20), suggesting that *prrx1a* is dispensable for heart laterality (Castroviejo et al., 2020). However, this does not necessarily mean that Prrx1a is not involved in heart laterality.

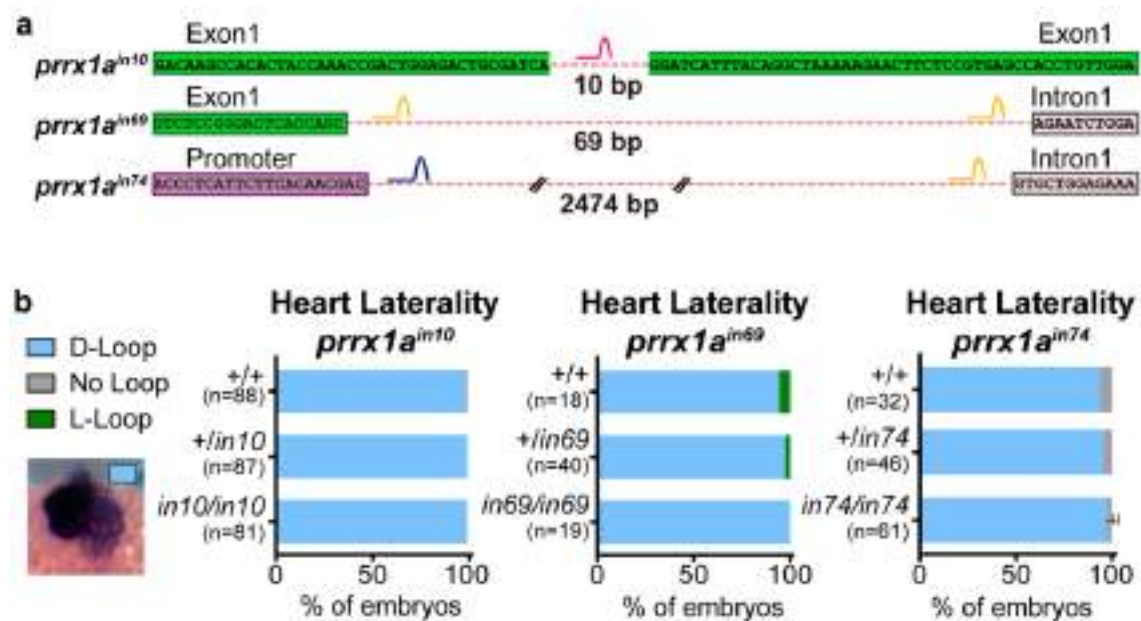


Figure 20| *prrx1a* mutants do not have mesocardia. (a) Schematic representation of the three *prrx1a* mutant alleles. (b) Heart position assessed at 52 hpf for the three *prrx1a* mutant alleles, all showing normal D-loop (posterior pole to the left and dextral loop). n = number of embryos analysed from one (all but *prrx1a*^{in74/in74}) or two independent experiments (*prrx1a*^{in74/in74}).

We also checked whether *prrx1a* mutations were harmful for the fitness of zebrafish embryos. If this were the case, there should be a reduction in survival and/or fertility of the zebrafish lines. Therefore, after in-crossing WTs and *prrx1a in10* and *in74* homozygous mutants we counted dead eggs and those that after 24 hpf did not develop (Figure 21a). After crossing,

most WT embryos were fertilised while around 50 % *prrx1a* mutants were already dead. After 24 hours of development, the number of embryos was reduced for both WT and *prrx1a* mutants, but it was more severe for the mutants (Figure 21b). Therefore, although *prrx1a* mutants have normal hearts, we are analysing the percentage of embryos that are escapers and most probably have compensatory mechanisms already operating.

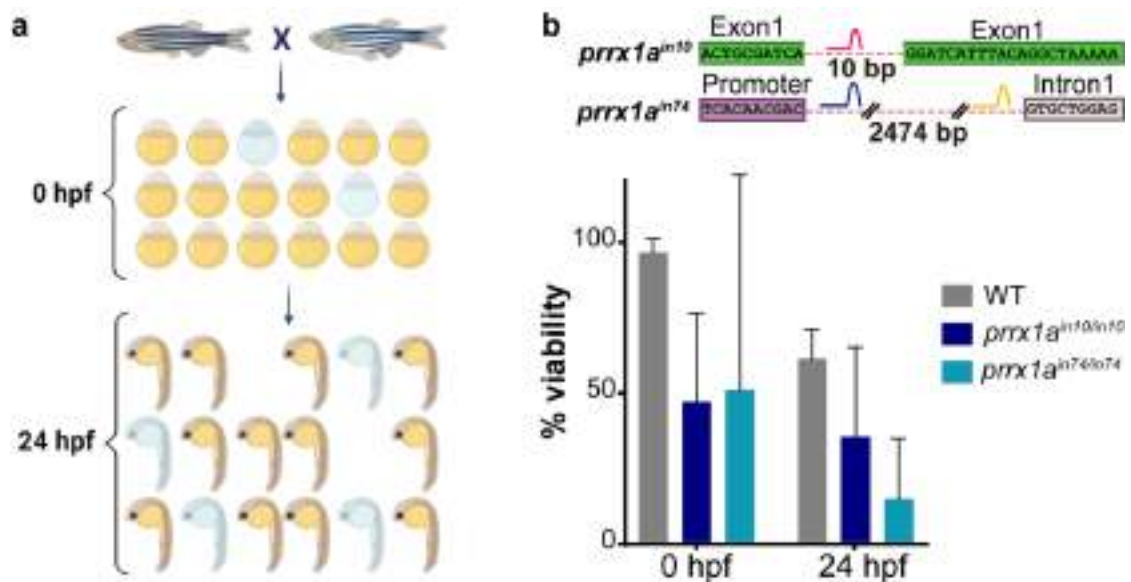


Figure 21 | *prrx1a* mutants have collateral fitness effects. (a) Schematic representation of viability test. After an in-cross of WT or mutant lines, viable eggs were counted. After 24 hpf, viability is counted again to check whether mutations have an effect in the correct development of the embryos. (b) Schematic representation of the deletion of the two *prrx1a* lines used (*in10* and *in74*). The graph shows the percentage of viable eggs. One half of the embryos from both *prrx1a* mutant lines were already dead. 24 hours later, some WT embryos did not develop, but the number was significantly higher in the *prrx1a* mutant lines.

Even though we had found a consistent phenotype using different dgRNA guides and CRISPR/Cas9 editing, with no early defects in L/R asymmetry, the absence of a phenotype in the different mutant lines prompted us to go a step further in assessing the specificity of the heart phenotype to be able to fully discard putative off-target effects. Thus, we further validated the reagent (dgRNAs) in a *prrx1a* null mutant background, as established in consensus guidelines in the field (Stainier et al., 2017).

We used the *prrx1aⁱⁿ⁶⁹* mutant allele, which allowed us to directly examine the specificity of the *prrx1a* dgRNAs, as the complementary sequences of the mentioned guides are missing (Figure 22a). Thus, if the guides are specific for *prrx1a*, the prediction is that injection of dgRNA in these mutants should not lead to any phenotypic defect. Indeed, the injection of *prrx1a* dgRNAs

Results

into *prrx1a*^{in69/in69} embryos did not have any impact in the position of the heart, whereas the injection of these same guides into WT sibling embryos led to mesocardia (Figure 22b). Thus, the mesocardia phenotype observed in the G0-*prrx1a* crispants embryos is a specific trait of targeting the *prrx1a* gene (Figure 16c and Figure 22b).

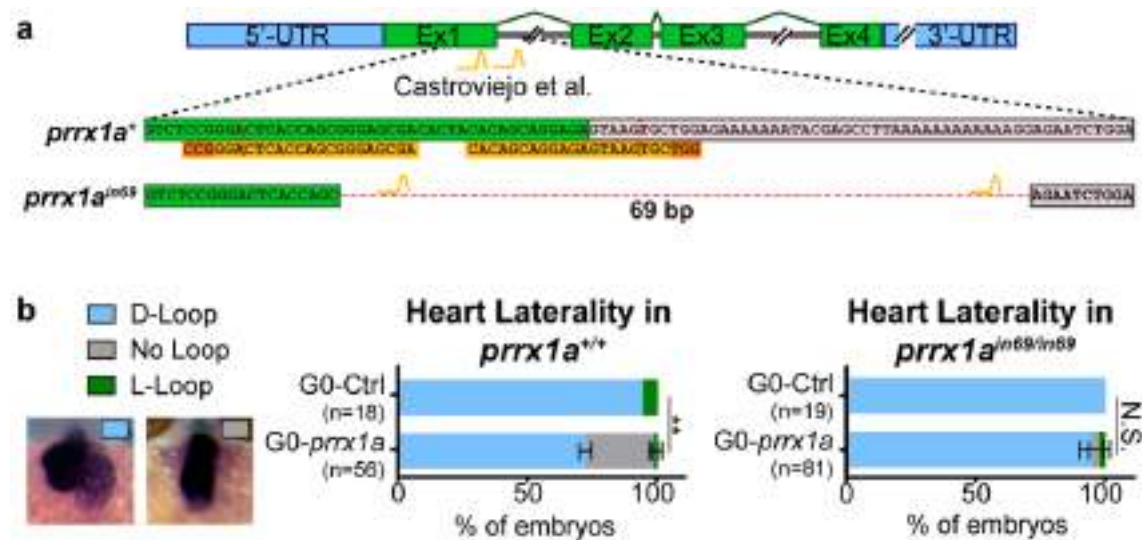


Figure 22 | CRISPR/Cas9 guides against *prrx1a* are specific and lead to mesocardia. (a) Scheme of the *prrx1a* gene, with coding sequences highlighted in green and intron sequences in grey. The *prrx1a*ⁱⁿ⁶⁹ allele contains a 69-nt deletion generated using the same CRISPR-*prrx1a* guides than the G0-crispant. The *in69* allele lacks the guide sequences (orange) at the *prrx1a* locus. **(b)** As expected from the lack of the guide sequences in the mutant, only the embryos with WT alleles present a mesocardia phenotype after injection of CRISPR-Cas9 *prrx1a* reagents. This is a proof of the specificity of both the guides and the mesocardia phenotype. Data are represented as mean percentage \pm s.d. n = number of embryos analysed at 52 hpf from one (G0-Ctrl) or two (G0-*prrx1a*) independent experiments. Statistical analysis (shown for the mesocardia phenotype; grey): two-way ANOVA. N.S., not significant, **P < 0.01.

Even though the previously discussed control experiment demonstrated that the dgRNAs used to impair *Prrx1a* function were specific and thus, also the mesocardia phenotype, we wanted to provide extra experimental evidence using a LOF strategy independent of DNA editing. We have used a novel CRISPR-RfxCas13d system, an endonuclease that specifically targets both zygotic and maternal mRNA, which would be degraded. This novel system provides a robust and straightforward method to target transcripts in zebrafish embryos (Kushawah et al., 2020). In addition, by targeting mRNA, it is possible to uncover phenotypes that may otherwise be compensated. This system has proven to not cause toxicity leading to developmental abnormalities or off-targets effects (Kushawah et al., 2020).

RfxCas13d mRNA and *prrx1a*-gRNA are also injected in the cell of 1-cell stage embryos. The RfxCas13d would be then translated and bound to gRNA, targeting the zygotic and maternal *prrx1a* mRNA and consequently, reducing its levels (Figure 23a). In those embryos injected with control reagents, we did not observe defects in heart laterality (D-Loop; light blue) (Figure 23b). However, when we assessed the heart position in embryos with targeted *prrx1a* mRNA we observed mesocardia with the same penetrance of that in crispant G0 embryos bearing *prrx1a* edited with Cas9 (Figure 16c). These data further demonstrate that *prrx1a* has a specific role in heart laterality. This also indicates that, if proper controls are used, KD experiments and mosaic gene editing (G0-crispant embryos) are useful and complementary tools to the generation of stable mutants. Furthermore, they can also reveal phenotypes than can be genetically compensated in the null mutant condition.

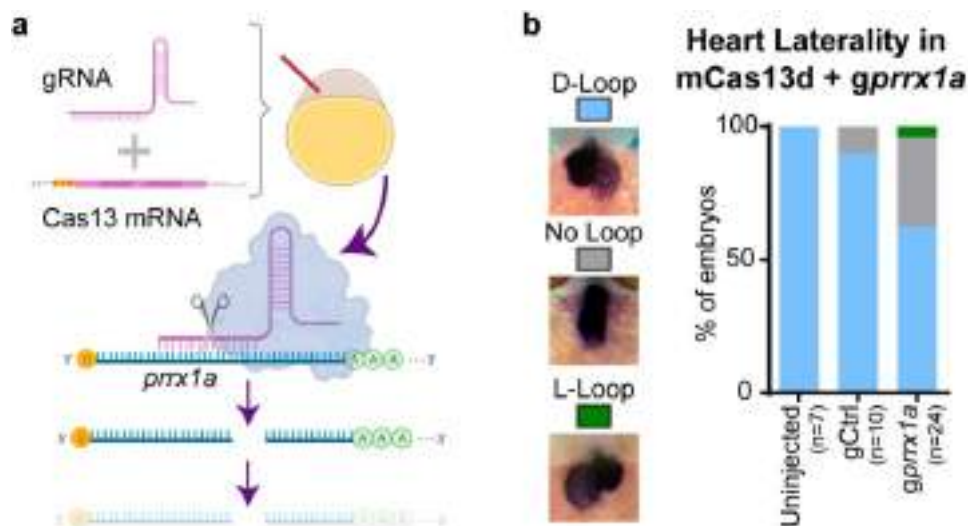


Figure 23| Cas13d-mediated degradation of *prrx1a* mRNA also leads to mesocardia. (a) Schematic representation of the generation of knockdown (KD) embryos through the co-injection at the 1-cell stage of RfxCas13d mRNA (mCas13d) with different sets of gRNAs against *prrx1a* mRNA. mCas13d is then translated and bound to gRNA, cutting, and triggering endogenous mRNA degradation. (b) Heart position at 52 hpf (ventral view) shows mesocardia (No-Loop) in *prrx1a*-Cas13 KD with the same penetrance than that found in G0-*prrx1a* Cas9 crispant embryos (Figure 16c). gCtrl-Cas13 injected embryos show the normal D-loop (posterior pole to the left as in WT embryos). These data provide additional proof of the specificity of the mesocardia phenotype observed after targeting the *prrx1a* gene. Data are represented as percentage. n = number of embryos analysed.

2. Genetic Cooperation of EMT-TFs in Zebrafish Heart Laterality

2.1. Other EMT-TFs, *prrx1b*, *snail1b* and *twist1a* are also asymmetrically expressed in heart precursors

Epithelial plasticity, and EMT in particular, is tightly regulated and it usually requires the cooperation of different signalling pathways and EMT-TFs (Katsuno and Derynck, 2021). During development, the most prominent EMT process occur during gastrulation and NC development. While in gastrulation the loss of individual genes usually causes strong phenotypes, the existence of multiple gene regulatory loops during NC development involves the cooperation of different EMT-TFs, with individual mutants showing much weaker phenotypes than those anticipated, and indicating the existence of compensatory mechanisms, making the process very robust (Thiery et al., 2009). Similarly, cancer cells activate several EMT inducing factors, and the lack of detectable effects on tumour progression after inactivation of a single factor, cannot be used to discard EMT as an important player in tumour progression, but rather a sign of both context-dependent EMT programmes and functional redundancy even between non-paralogous genes (Nieto et al., 2016).

After showing that *Prrx1a* plays an active role in heart laterality while seeming to be dispensable for the process, we wondered whether other EMT-TFs could be cooperating in this process and/or compensating for *prrx1a* loss. This was likely, as we and others have shown that in the mouse, *Snail1* is expressed in the heart precursors and its loss leads to heart laterality defects (Murray and Gridley, 2006; Ocaña et al., 2017). Thus, we examined the expression of different EMT-TFs, namely members of the *prrx*, *snail*, *twist* and *zeb* families in the aLPM.

Due to the teleost genome duplication (TGD) (Glasauer and Neuhauss, 2014), EMT-TFs families have more members in zebrafish than in other vertebrates. This also applies to the *Prrx* family as the *prrx1* gene is represented by two paralogues: *prrx1a* and *prrx1b* (Braasch et al., 2014). We began examining *prrx1b*, as paralogues are the most likely candidates for cooperation and/or compensation. At the 20-somite stage, *prrx1b* is absent from the aLPM but is detected in the pLPM in a L/R asymmetric manner with higher levels on the right-hand side. It is also expressed in the NC, the tail bud and the pronephric ducts (Figure 24a). At 28 hpf, *prrx1b* expression can be detected in the aLPM, the primordium of the caudal fin bud, the pectoral fin buds, in the tailbud and in the branchial arches (Figure 24b).

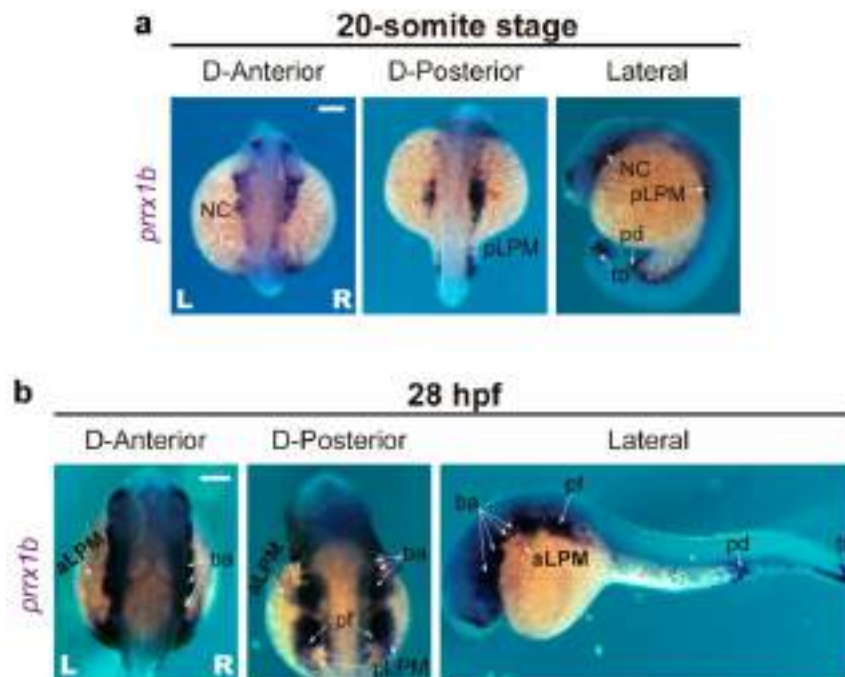


Figure 24 | *prrx1b* is expressed early and asymmetrically in the pLPM and in the aLPM at later stages. **(a)** Dorsal and lateral views of 20-somite stage zebrafish embryos showing *prrx1b* expression by ISH. The orange asterisk denotes the side of higher *prrx1b* expression in the pLPM and the arrows its expression in the NC, pronephric duct (pd) and tailbud (tb). Scale bar: 200 μ m. **(b)** Dorsal and lateral views of 28 hpf zebrafish embryos showing *prrx1b* expression in the aLPM, branchial arches (ba), pectoral fin (pf), pronephric duct and tailbud. Scale bar: 200 μ m.

prrx1b is not expressed in the aLPM at the same developmental stage than *prrx1a* is. Nevertheless, as it is expressed later, at 28 hpf, we used the *TgBAC(tbx5a:eGFP)* reporter line to see whether *prrx1b* was coexpressed with *tbx5a*. Instead of using Prrx1 antibody that recognises both *prrx1* paralogs, we performed a fluorescence ISH of *prrx1b* gene in the *tbx5a* reporter (**Figure 25**). We studied a developmental stage a little bit more advanced, 22-somite stage when the CD has been formed, where we could see colocalization in a small subpopulation of *tbx5a*⁺ cells of the most posterior part of the aLPM and in an asymmetric manner (arrowheads) (**Figure 25**). Therefore, as it is expressed later in some cells of the same territory, we decided to carry out LOF assays for this EMT-TF (see below).

Results

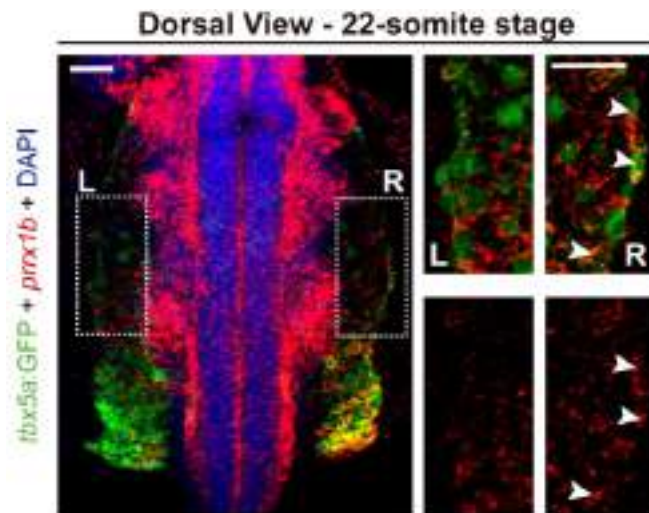


Figure 25 | *prrx1b* is coexpressed in *tbx5a+* cells located in the posterior region of the aLPM and in the pLPM. **(a)** Dorsal view of a 22-somite stage *TgBAC(tbx5a:eGFP)* zebrafish embryo showing *prrx1b* expression detected by fluorescence ISH. Asymmetric and double positive *tbx5a*-GFP (green) + *prrx1b* (red) signal in the aLPM is denoted by arrowheads. Scale bars: 100 μ m.

Zeb genes are represented in the zebrafish by *zeb1a*, *zeb1b*, *zeb2a* and *zeb2b*. At the 20-somite stage, *zeb1b* and *zeb2a* are expressed in the NC cells and somites (**Figure 26a**). In addition, *zeb1a* and *zeb2a* are expressed in the neural plate. None of the four family members is present in the aLPM (**Figure 26a**). We also checked their expression at 28 hpf (**Figure 26b**), finding *zeb2a* and *zeb2b* in cranial ganglia. Besides, *zeb1a* and *zeb2a* are still detected in the neural tube. As none of them were expressed in cardiac precursor territories, we decided not to perform functional assays for *zeb* genes.

With respect to the *twist* gene family, *twist1* is represented by two paralogues, *twist1a* and *twist1b*, and the family includes two more orthologues, *twist2* and *twist3*. As previously shown (Ocaña et al., 2012), *twist1a* is expressed in the LPM, the NC and somites. We paid particular attention to the aLPM where the CPCs reside, and found that *twist1a* is, as *prrx1a*, asymmetrically expressed with higher levels on the right-hand side (**Figure 27a**) (Castroviejo et al., 2020). In the case of *twist1b*, *twist2* and *twist3* we could detect them in NC and somites, but not in the aLPM (**Figure 27a**). At later time points, *twist1a* is maintained in the aLPM and pLPM, in addition to be expressed in the branchial arches and pectoral fins (**Figure 27b**). *twist1b* and *twist3* are also expressed in the brachial arches and the pectoral fin, but they are absent from the aLPM. *twist2* is only detected in the dorsal aorta (**Figure 27b**). Thus, we decided to continue our study only with *twist1a*.

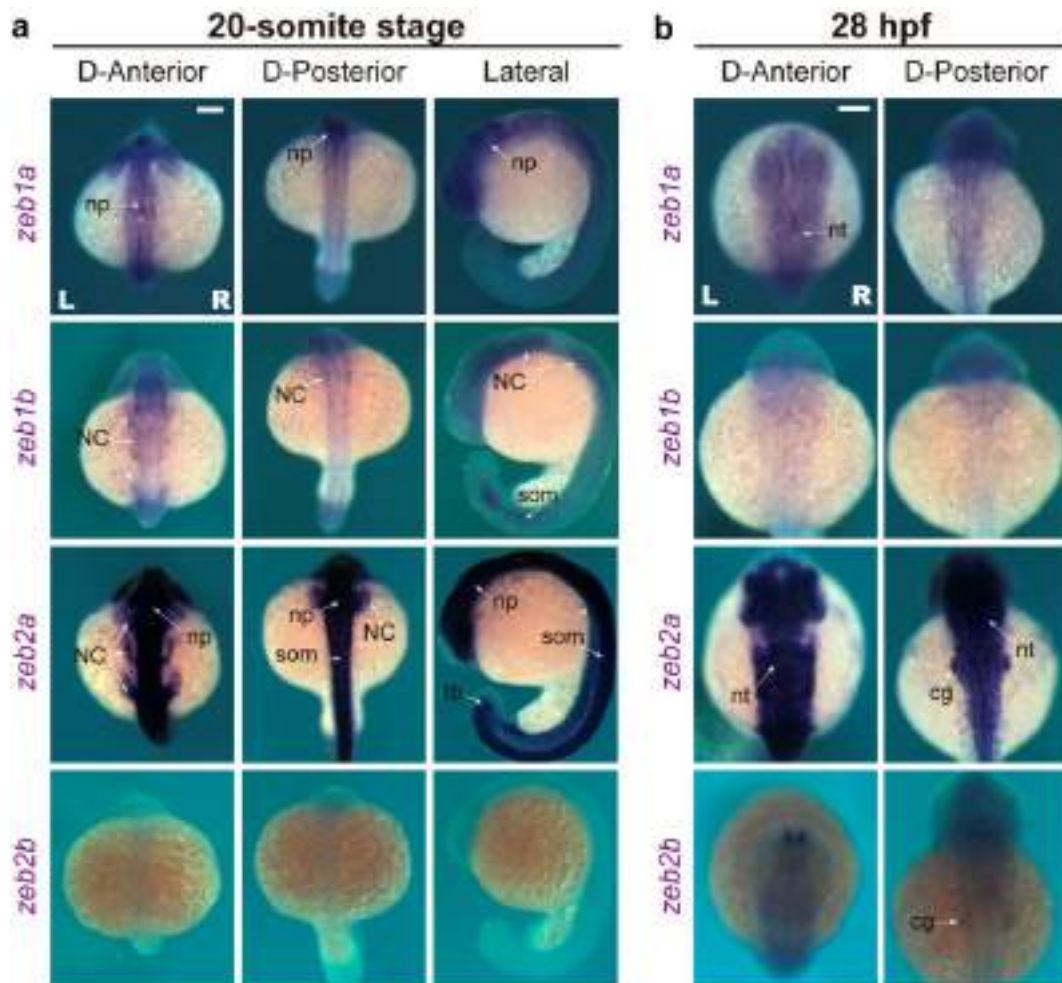


Figure 26 | zeb1s are not expressed in the aLPM. (a) Dorsal and lateral views of 20-somite stage zebrafish embryos showing *zeb1a*, *zeb1b*, *zeb2a* or *zeb2b* expression by ISH. *zeb1a* and *zeb2a* are expressed in the neural plate (np), *zeb1b* and *zeb2a* in the NC and somites, with additional sites for *zeb2a* in the tailbud. *zeb2b* could not be detected at this stage. Scale bar: 200 μ m. **(b)** Dorsal views of 28 hpf zebrafish embryos showing *zeb1a*, *zeb1b*, *zeb2a* and *zeb2b* expression by ISH. *zeb2a* and *zeb2b* are expressed in cranial ganglia (cg), and *zeb1a* and *zeb2a* continue to be expressed in the neural tube (nt). Scale bar: 200 μ m.

Finally, we characterized the expression of *snail* genes. Like *twist1*, *snail1* is represented by two paralogues, *snail1a* and *snail1b* and their two related orthologues *snail2* and *snail3*. *snail1a* was known to be expressed in the NC, somites, pronephric duct, and tailbud, and *snail1b* in the aLPM and pLPM, NC and somites (Figure 28a) (Ocaña et al., 2017). Importantly, the L/R asymmetric expression of *snail1b* in the aLPM was not described in previous studies (Ocaña et al., 2017; but see Castroviejo et al., 2020). *snail2* is also expressed in the NC, somites, the notochord and both aLPM and pLPM. Nevertheless, the expression in the aLPM does not seem to be asymmetric (Figure 28a). *snail3* is expressed only in the somite region and at very low levels at 20-somite stage (Figure 28a) (Manzanares et al., 2004).

Results

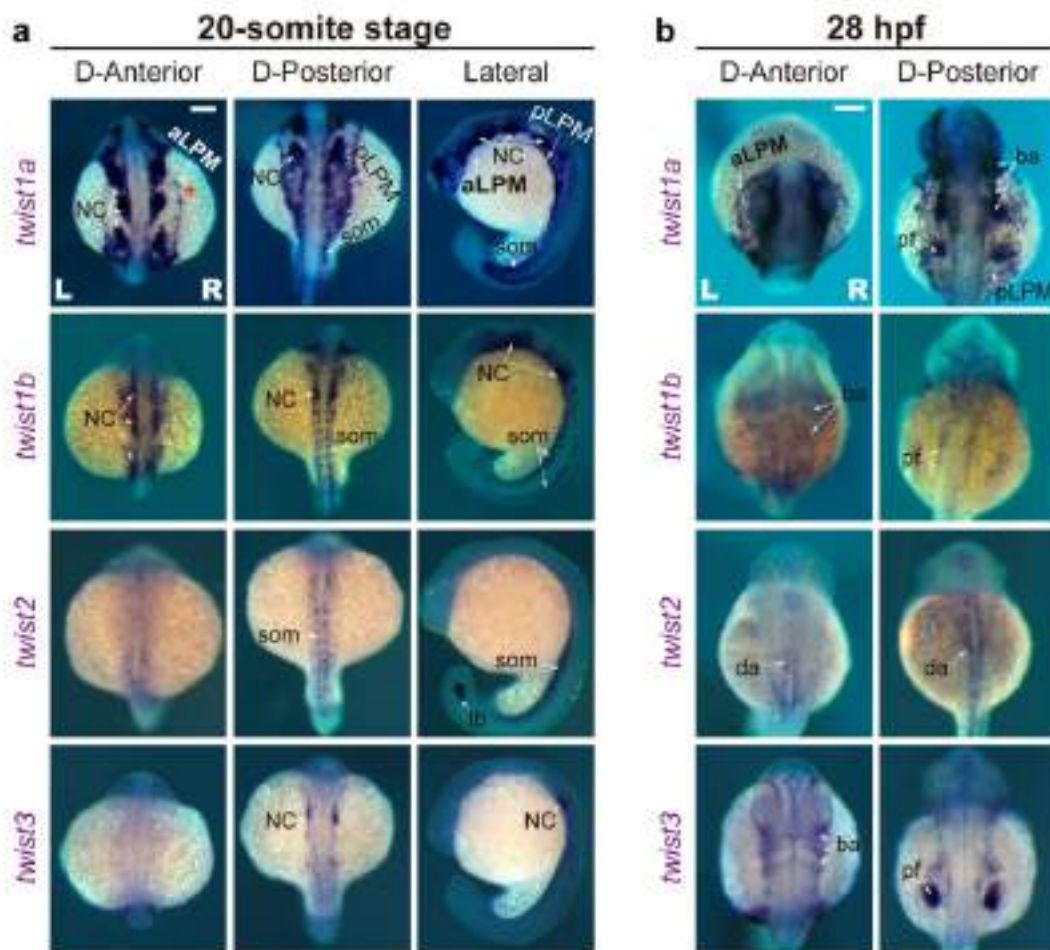


Figure 27 | *twist1a* is asymmetrically expressed in the aLPM. **(a)** Dorsal and lateral views of 20-somite stage zebrafish embryos showing *twist1a*, *twist1b*, *twist2* and *twist3* expression by ISH. The orange asterisk shows the right-hand side, with higher levels of *twist1a* expression in the aLPM. The arrows point to the NC, somites and pLPM. Its other paralogues are expressed in the NC, somites and tailbud. Scale bar: 200 μ m. **(b)** Dorsal views of 28 hpf zebrafish embryos showing *twist1a* expression in the aLPM, pLPM, branchial arches and pectoral fin. *twist1b* and *twist3* are also expressed in the branchial arches and pectoral fin while *twist2* is expressed in the dorsal aorta (da). Scale bar: 200 μ m.

At 28 hpf, *snail1a*, *snail1b* and *snail2* expression can be detected in the pectoral fin and branchial arches. In addition, *snail1b* and *snail2* continue to be expressed in the aLPM (Figure 28b). *snail3* expression is now detected only in the pectoral fin. As *snail1b* is L/R asymmetric in the aLPM, mouse *Snail1* mutants present mesocardia (Ocaña et al., 2017) and defects in heart laterality have been reported in *snail1b* morphants in zebrafish (Qiao et al., 2014), we decided to investigate the role of *snail1b* in heart laterality.

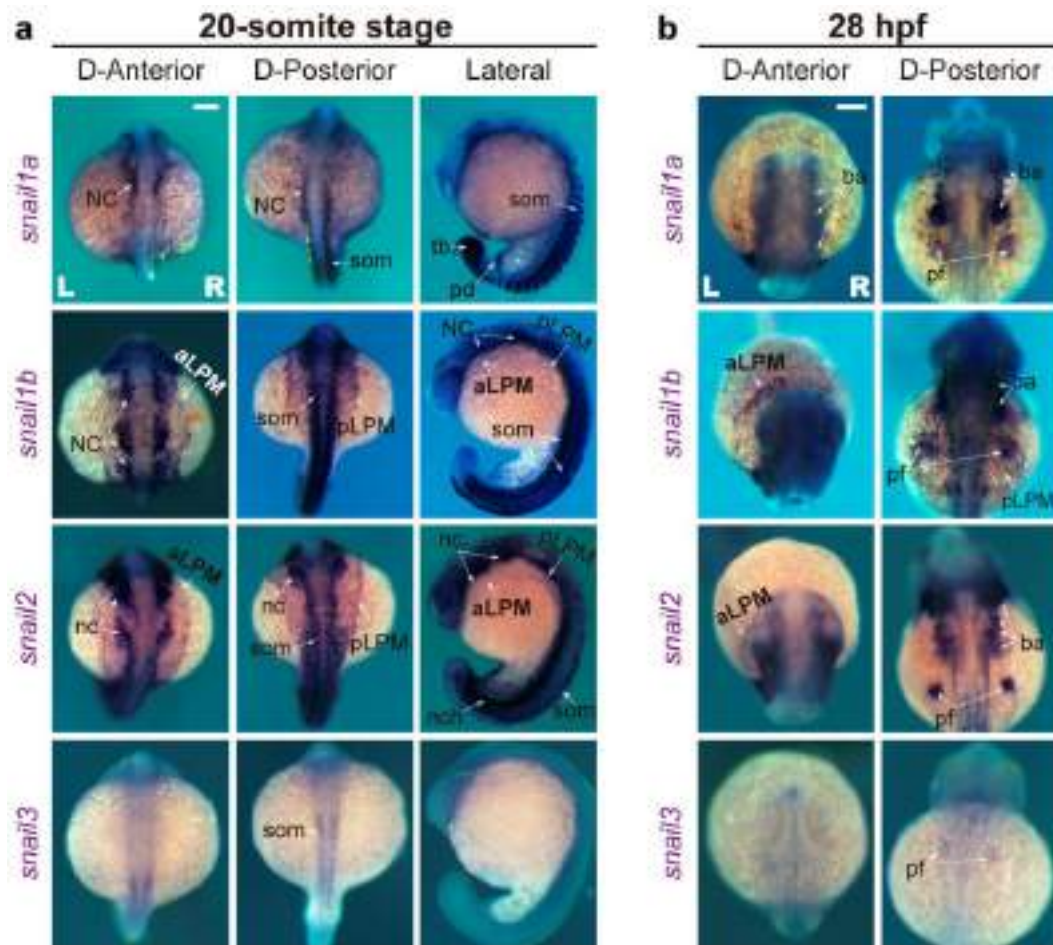


Figure 28 | *snail1b* is asymmetrically expressed in the aLPM. **(a)** Dorsal and lateral views of 20-somite stage zebrafish embryos showing *snail1a*, *snail1b*, *snail2* and *snail3* expression by ISH. The orange asterisk shows the right-hand side, with higher levels of *snail1b* in the aLPM. The arrows point to expression in the NC, somites and pLPM. The rest of the paralogues are expressed also in the NC and the somites. *snail1a* is also transcribed in the tailbud and pronephric duct. *snail2* is also expressed in the notochord (nch) and in the aLPM, but in a symmetric manner. Scale bar: 200 μm. **(b)** Dorsal views of 28 hpf zebrafish embryos showing *snail1b* expression in the aLPM, pLPM, branchial arches and pectoral fin. *snail1a*, *snail2* and *snail3* are also expressed in the branchial arches and pectoral fin. *snail2* expression is maintained in the aLPM and *snail3* is always expressed at very low levels. Scale bar: 200 μm.

Since *snail1b*, like *prrx1a*, is expressed in a L/R asymmetric manner in the aLPM, we used the *TgBAC(tbx5a:eGFP)* reporter line to see whether *snail1b* was also coexpressed with *tbx5a*. We studied the same developmental stages as before and found that, at both stages, we could appreciate colocalization (arrowheads) (Figure 29). Quantification of asymmetric cells could not be done as the *Snail1* protein expression was weak in many of the expressing cells, and the signal was not sufficient to run the image analysis programme. However, the colocalization occurs in many cells of the aLPM.

Results

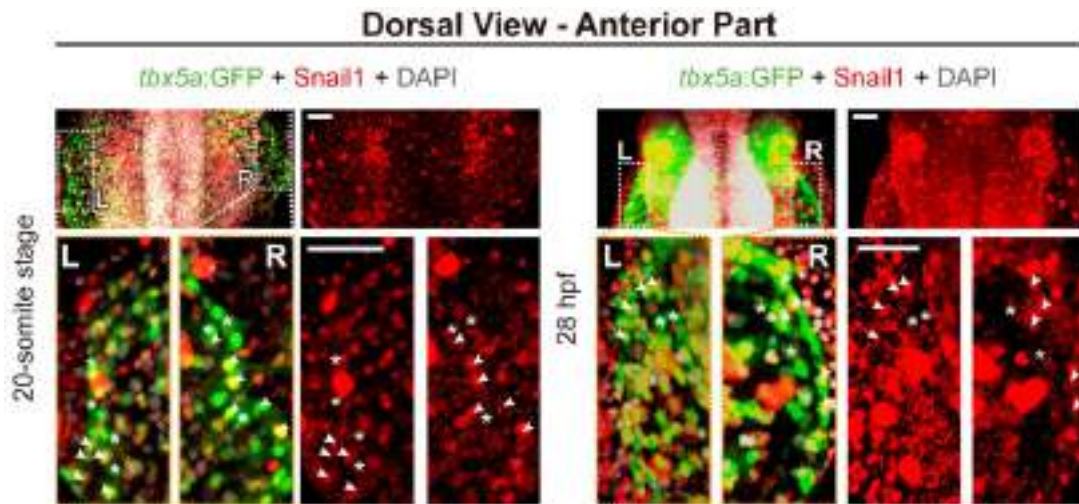


Figure 29 | *Snail1* is also expressed in *tbx5a+* heart precursors. Dorsal view of a 20-somite stage (left) and 28 hpf (right) *TgBAC(tb5a:eGFP)* zebrafish embryo showing *Snail1* expression detected by immunofluorescence. Double positive *tbx5a-GFP* (green) + *Snail1* (red) signal is denoted by arrowheads, and *tbx5a-GFP* alone by a white asterisk. Scale bars: 100 μ m.

2.2. Cooperation between EMT-TFs in heart laterality

2.2.1. Functional analysis of individual TFs

As we found that, in addition to *prrx1a*, several EMT-TFs are expressed in a L/R asymmetric manner in the aLPM, we decided to perform functional studies to investigate their putative role in heart laterality. We designed and injected dgRNAs + Cas9 into 1-cell stage embryos to generate individual *prrx1b*, *twist1a* and *snail1b* G0-crispant (Figure 30a) and found that all showed mesocardia but with a different penetrance ranging from 25 to 50 % (Figure 30b) (Castroviejo et al., 2020). Data for *prrx1a* crispants are included in the figure for comparison purposes. These data suggest that these EMT-TFs could be acting in parallel with *prrx1a* to regulate heart laterality and are compatible with a scenario in which EMT-TFs cooperate in the regulation of heart laterality, and where *Prrx1b*, *Snail1b* and/or *Twist1a* might compensate for the loss of *Prrx1a* (Castroviejo et al., 2020).

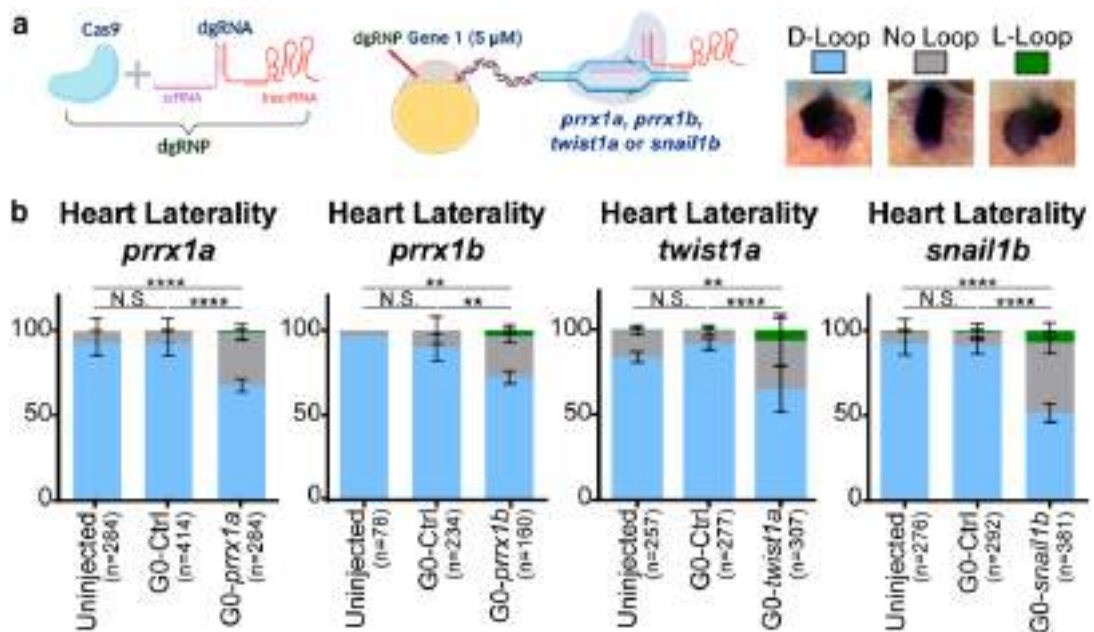


Figure 30 | *snail1b*, *twist1a* and *prx1b* G0-crippants present mesocardia. **(a)** Schematic representation of the generation of G0-crippant embryos through the injection of RNP at the 1-cell stage against the genes of interest. **(b)** Analysis of heart position at 52 hpf (ventral view) of the corresponding G0-crippant embryos. All show mesocardia with different penetrance. Data represents mean percentage \pm s.d. n = number of embryos analysed pooling three (G0-*prx1a*, G0-*twist1a*, G0-*prx1b*) or more independent experiments (G0-*snail1b*). Statistical analysis (shown for the mesocardia phenotype; grey): two-way ANOVA. N.S., not significant, **P < 0.01, ****P < 0.0001.

It is known that *tbx5a*^{-/-} mutants (*hst*) and morphants present heart laterality defects (Garrity et al., 2002), compatible with our finding that *tbx5a* also shows L/R asymmetric expression in the aLPM. We generated G0-*tbx5a* crispants and interestingly, we found that the percentage of embryos with mesocardia was around 70 %, higher than for the EMT-TFs (Figure 31), which may be due to the fact that *tbx5a* is expressed from very early in the FHF, the HT and in the SHF-derived aLPM (Figure 13).

We next measured the displacement of the posterior pole of the heart due the asymmetric integration of aLPM cells of the SHF (Ocaña et al., 2017) and also the angle of looping, which results from the twisting of the chambers around the AVC and it is supposed to be due to at least in part to cardiac intrinsic cues (Tessadori et al., 2021). Both, G0-*tbx5a* and G0-*prx1a* crispant embryos display a reduced displacement in the posterior pole when compared to controls and a reduced looping (Figure 32). Thus, both factors seem to contribute to both processes. The defect in looping is more pronounced in *tbx5a* crispants, likely reflecting its continuous expression in the HT and in the CM derived from the aLPM once they have been incorporated into the heart, and compatible with intrinsic mechanisms contributing to looping.

Results

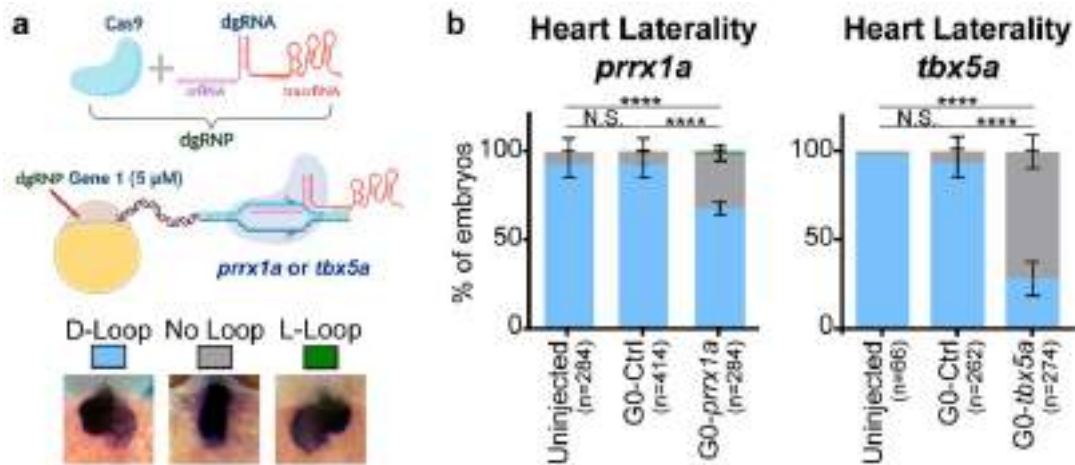


Figure 31 | G0-*tbx5a* crispants, as its mutant (*hst*), show mesocardia. (a) Schematic representation of the generation of G0-crippant embryos. (b) Analysis of heart position at 52 hpf (ventral view) of *tbx5a* compared with *prrx1a*. *tbx5a* crispant show mesocardia, as described for its mutant *hst*. Data are mean percentage \pm s.d. n = number of embryos analysed pooling three independent experiments. Statistical analysis (shown for the mesocardia phenotype; grey): two-way ANOVA. N.S., not significant, ****P < 0.0001.

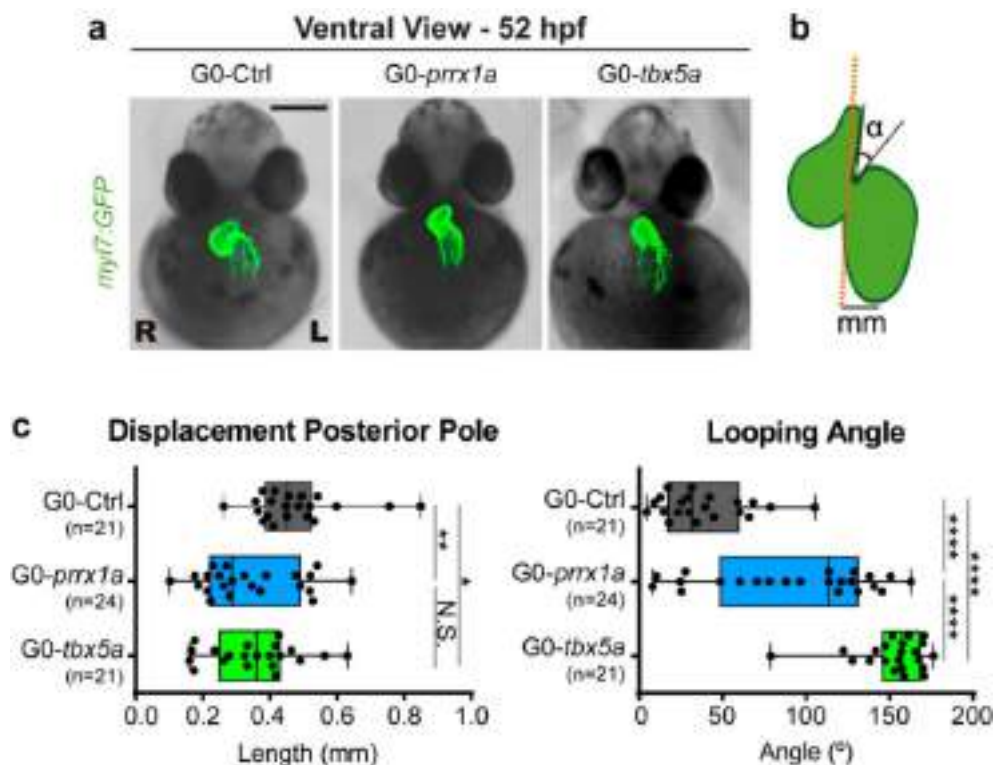


Figure 32 | Displacement of the posterior pole of the heart and angle of heart looping in *prrx1a* and *tbx5a* G0-crippant embryos. (a) Resulting heart phenotypes after injection of RNP at the 1-cell stage against *prrx1a* or *tbx5a*. Scale bar: 250 μ m. (b) Scheme showing the parameters measured for the quantification of the displacement of the posterior pole and the angle of looping. (c) Quantification of both processes. Data represented in box plots: centre lines, medians; box limits, second and third quartiles; whiskers, first and fourth quartiles. n = number of embryos analysed. Statistical analysis: N.S., not significant, *P < 0.05, **P < 0.01, ****P < 0.0001 by one-way ANOVA.

2.2.2. Functional analysis of combinations of EMT-TFs

After analysing the contribution to individual EMT-TFs to heart laterality, in the light of the observed mesocardia phenotypes and the different penetrance we decided to generate crispant embryos targeting combinations of the corresponding factors (Figure 33a).

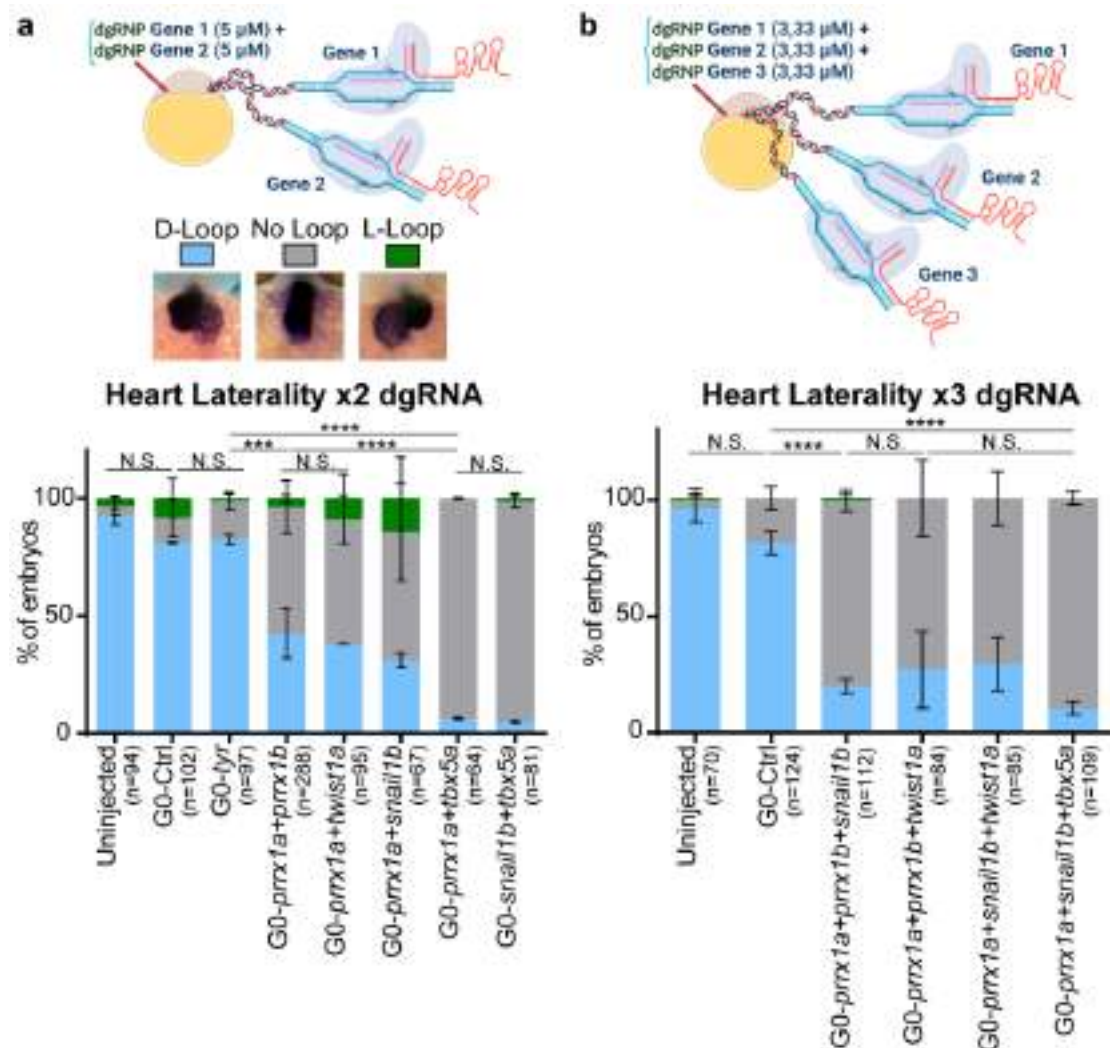


Figure 33| EMT-TFs cooperate in the process of heart laterality. (a) Schematic representation of the generation of double G0-crispant embryos through the injection at the 1-cell stage of RNPs designed to target two genes of interest (doubling the concentration of Cas9 and the guides), and analysis of heart position at 52 hpf (ventral view) of the different combinations of TFs (*prrx1a*, *prrx1b*, *twist1a*, *snail1b* and *tbx5a*). When *prrx1a* targeting is combined with that of another gene also expressed in the aLPM the penetrance increases. But when it is combined with *tbx5a* targeting, expressed in the aLPM and in the HT, mesocardia is observed in almost 100 % of the embryos. Data are mean percentage \pm s.d. n = number of embryos analysed pooling two (all but G0-*prrx1a+prrx1b*) or four (G0-*prrx1a+prrx1b*) independent experiments. Statistical analysis (shown for the mesocardia phenotype; grey): two-way ANOVA. N.S., not significant, ***P < 0.001, ****P < 0.0001. (b) Similar experiment to that in (a) but targeting three genes simultaneously. The penetrance is similar for all combinations. Data are mean percentage \pm s.d. n = number of embryos analysed pooling two independent experiments. Statistical analysis (shown for the mesocardia phenotype; grey): two-way ANOVA. N.S., not significant, ****P < 0.0001.

Results

dgRNPs are highly mutagenic, so they could be used in combination to effectively target several genes simultaneously. We injected two dgRNAs against two TF doubling the concentration of RNA and Cas9 protein, with the aim of maintaining the same efficiency of cutting as in the individual injected embryos (**Figure 33a**). As previously, we used *tyrosinase* crispant embryos (G0-*tyr*), where we observed normal heart laterality as in uninjected embryos. Interestingly, when we coinjected *dg-prrx1a* together with either *dg-prrx1b*, *dg-twist1a* or *dg-snai1b*, a clear increase in the penetrance of the mesocardia phenotype was observed, indicative of cooperation (**Figure 30b vs. Figure 33a**). When injection of *dg-prrx1a* or *dg-snai1b* was combined with that of *dg-tbx5a*, the percentage of mesocardia almost reached 100 % (**Figure 31b vs Figure 33a**).

To avoid toxicity when dgRNA against three genes were simultaneously injected, we used a maximum amount of 10 μ M in total (3.3 μ M each gene instead of 5 μ M) (**Figure 33b**). In this case, we have similar results independently of the three genes that were combined. These results again show the cooperative role of EMT-TFs in heart laterality.

2.3. Lack of heart laterality phenotype or low penetrance in individual EMT-TF stable mutants

After showing cooperation between EMT-TFs upon acute gene targeting, we generated stable mutants as we did for *prrx1a*. For *prrx1b*, we generated two different mutant lines. The *in5* mutant allele harbours a 5-nt deletion in *prrx1b* exon 1, leading to a PTC and consequently, a defective protein (**Figure 34a**). The *in51* mutant bears promoter-less alleles, as the guides were designed upstream of the promoter region and at the end of the open reading frame (ORF), generating an 8051-nt deletion and the absence of Prrx1b protein (**Figure 34a**). Both mutants showed normal hearts. (**Figure 34b**). Thus, as Prrx1a, Prrx1b also seems to play a role in heart laterality as assessed in the G0 crispants and be dispensable.

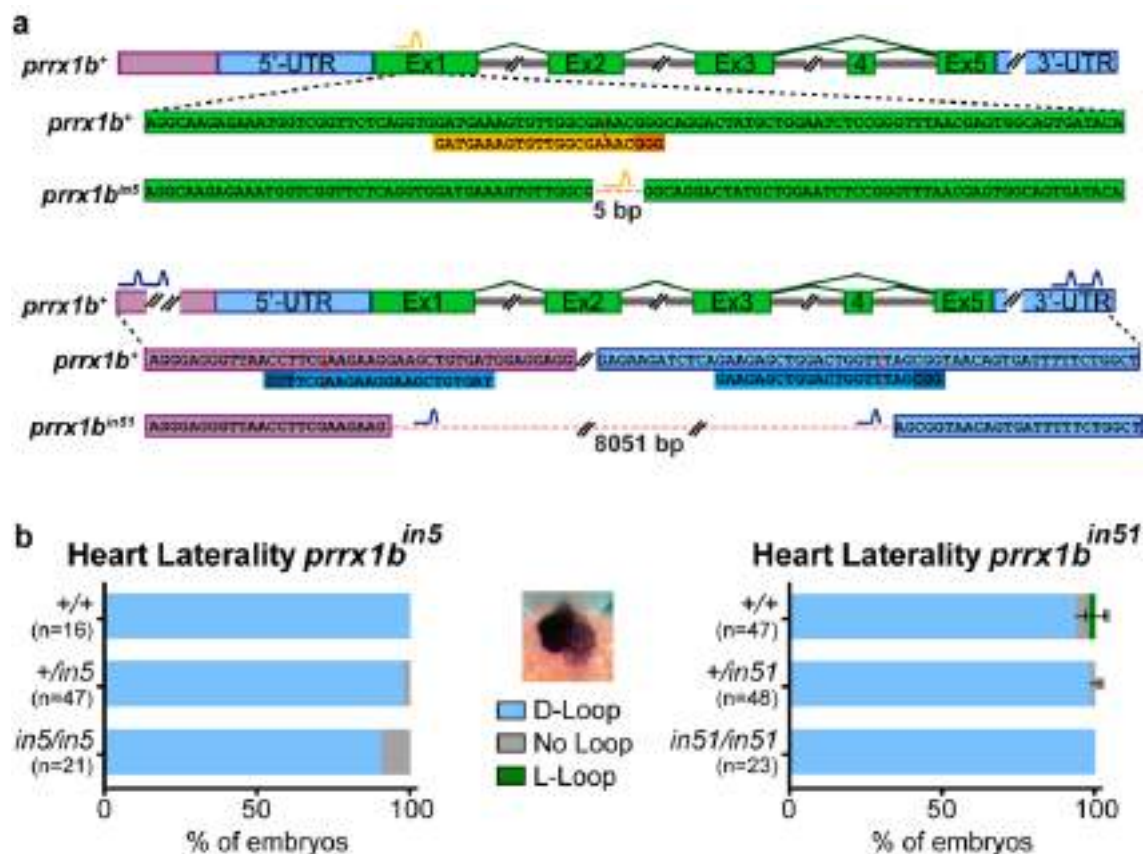


Figure 34 | *prrx1b* stable mutants do not have mesocardia. (a) Schematic representation of *prrx1b* gene (purple: promoter region; light blue: UTR; green: ORF). The *prrx1bⁱⁿ⁵* allele generates a PTC and the *prrx1bⁱⁿ⁵¹* mutant does not contain part of the promoter region. Guides were labelled in orange and blue, respectively. **(b)** Heart position assessed at 52 hpf for both *prrx1b* mutants, all showing normal D-loop (posterior pole to the left and dextral loop). Data are mean percentage \pm s.d. n = number of embryos analysed from one (*in5*) or two (*in51*) independent experiments.

We also examined *snail1b* mutant embryos (mutant line kindly provided by Didier Stainier, Bad Neuheim, Germany) carrying promoter-less alleles, similarly to *prrx1aⁱⁿ⁷⁴* (Figure 35a). As expected from an allele that lacks the transcription initiation start, Snail1b protein is not detected in *snail1b^{bns351/bns351}* mutant fish. Nevertheless, some positive cells are still detected due to the cross-reaction of the anti-Snail1 antibody with the Snail1a protein (Figure 35b). Heterozygous mutants showed normal hearts, but half of the population of homozygotes showed mesocardia (Figure 35c). Thus, although not fully penetrant, the loss of Snail1b induces mesocardia, indicating that Snail1b is required for the correct position of the heart in zebrafish.

Results

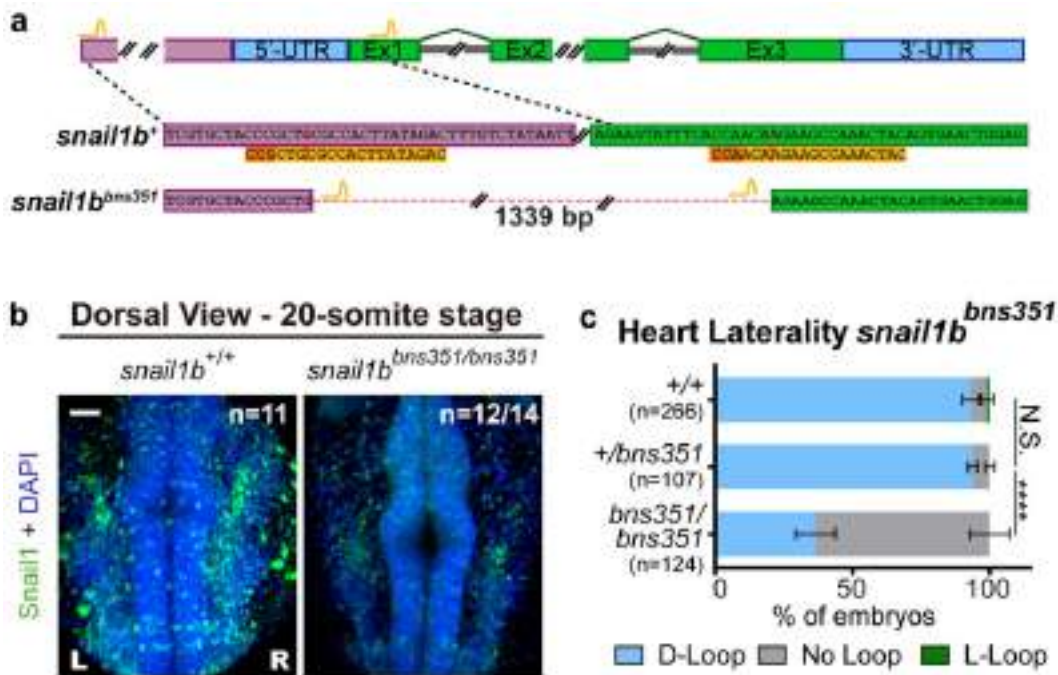


Figure 35 | *snail1b* stable mutant present mesocardia. (a) Schematic representation of the *snail1b* gene (purple: promoter region; light blue: UTR; green: ORF). The *snail1b*^{bns351} allele contains a 1339-nt deletion generated using the orange CRISPR-*snail1b* guides. (b) Snail1 immunofluorescence at 20-somite stage shows the absence of the Snail1 protein in the *snail1b* homozygous mutant. Images are shown in dorsal view. n = number of embryos analysed. Scale bar: 50 μm. (c) Analysis of heart position at 52 hpf (ventral view) shows D-Loop in heterozygous and mesocardia (No-Loop) in homozygous *snail1b*^{bns351} mutants. Data are mean percentage ± s.d. n = number of embryos analysed from two (*snail1b*^{+/bns351}) or three independent experiments (WT and *snail1b*^{bns351/bns351}). Statistical analysis (shown for the mesocardia phenotype; grey): two-way ANOVA. N.S., not significant, ****P < 0.0001.

2.4. Cooperation explains the lack or incomplete penetrance of heart laterality phenotype in individual EMT-TF stable mutants

snail1b, like *prrx1a*, is expressed in the aLPM, compatible with the observed cooperation, as both can provide SHF cells to the developing heart, but as homozygous animals had defective heart laterality only in *snail1b* mutants, we also wanted to know if their expression overlapped in space and time, so that it could explain a compensatory mechanism for Prrx1a loss by Snail1b.

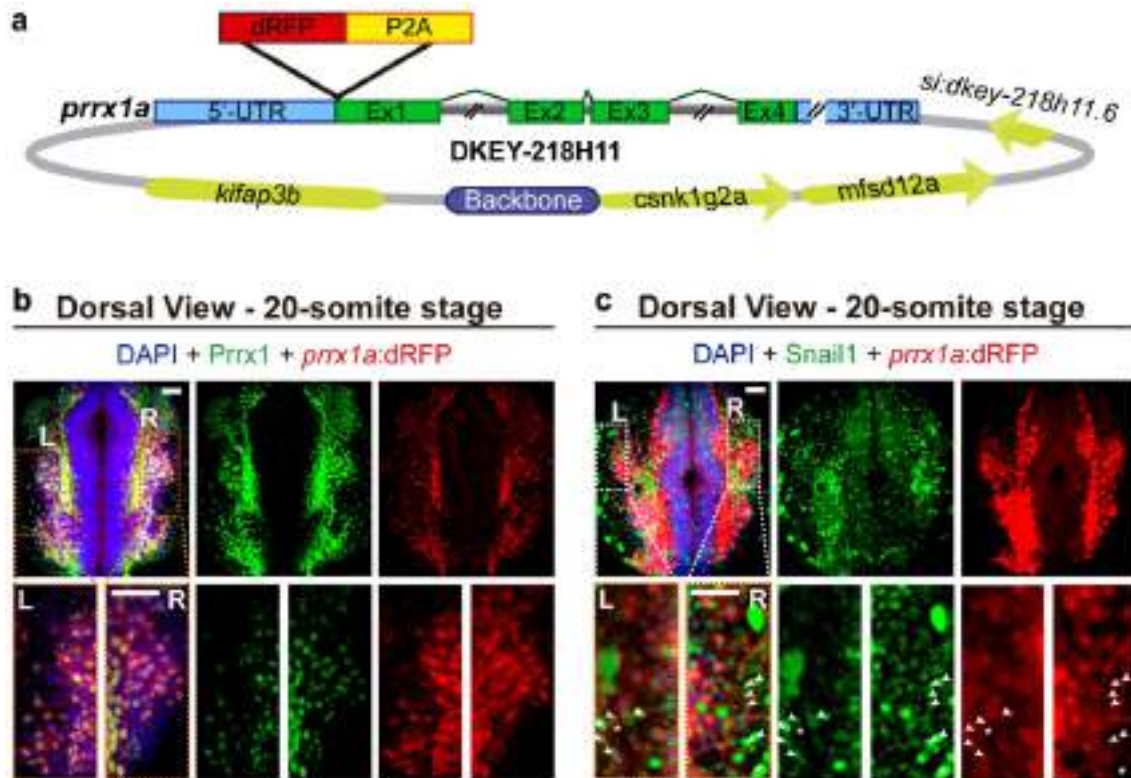


Figure 36 | Prrx1a and Snail1 are coexpressed in aLPM cells. (a) Schematic representation of the BAC used for the generation of the *TgBAC(prrx1a:dRFP)* line, including the genes present in the construct and a detailed view of the *prrx1a* gene with the insertion of the P2A cassette in the ATG of its exon 1. **(b)** Prrx1 immunofluorescence at 20-somite stage (dorsal view) in *TgBAC(prrx1a:dRFP)* shows that the transgenic reporter line reproduces the endogenous expression pattern of Prrx1a, as there are not RFP+ cells that do not express Prrx1. Scale bars: 50 μ m. **(c)** Snail1 immunofluorescence at 20-somite stage (dorsal view) in *TgBAC(prrx1a:dRFP)* shows that a great percentage of Snail1+ cells colocalize with RFP+ (*prrx1a*+) cells in the aLPM which explains the cooperation among these EMT-TFs in heart laterality and the putative compensation of Prrx1a loss by Snail1b. Scale bars: 50 μ m.

As both antibodies against Snail1 and Prrx1 were raised in rabbit (see materials and methods), we generated a *prrx1a* reporter zebrafish line to search for double-positive cells. We injected bacterial artificial chromosomes (BAC) containing a *prrx1a* gene whose ATG translation initiation codon was recombined with the sequence of a destabilized red fluorescence protein (dRFP) followed by a P2A cassette (Figure 36a). This construct was injected into 1-cell stage embryos and red fishes were raised to generate a stable reporter line. Prrx1 immunofluorescence in the *TgBAC(dprrx1a:dRFP)* line showed that this reporter recapitulates the endogenous pattern of Prrx1a expression. As the RFP protein is a destabilized form and thus, rapidly degraded, we could not detect RFP+/Prrx1- cells (Figure 36b). Snail1 immunofluorescence in *TgBAC(dprrx1a:dRFP)* line allowed the visualization of Prrx1/Snail1 double positive cells (yellow) (Figure 36c).

Results

After confirming the coexpression of *Prrx1* and *Snail1* in cells of the aLPM, we crossed heterozygous animals from the two promoter-less *prrx1a* and *snail1b* mutants and examined the position of the heart (**Figure 37a**). Interestingly, while in single heterozygous mutants, heart laterality is not affected, double heterozygous mutants showed mesocardia in almost half of the population (**Figure 37b**). Thus, there is a genetic interaction between *prrx1a* and *snail1b*, which cooperate in the establishment of heart laterality, in the L/R asymmetric contribution of SHF-derived aLPM cells, higher from the right, that displaces the posterior pole of the heart to the left.

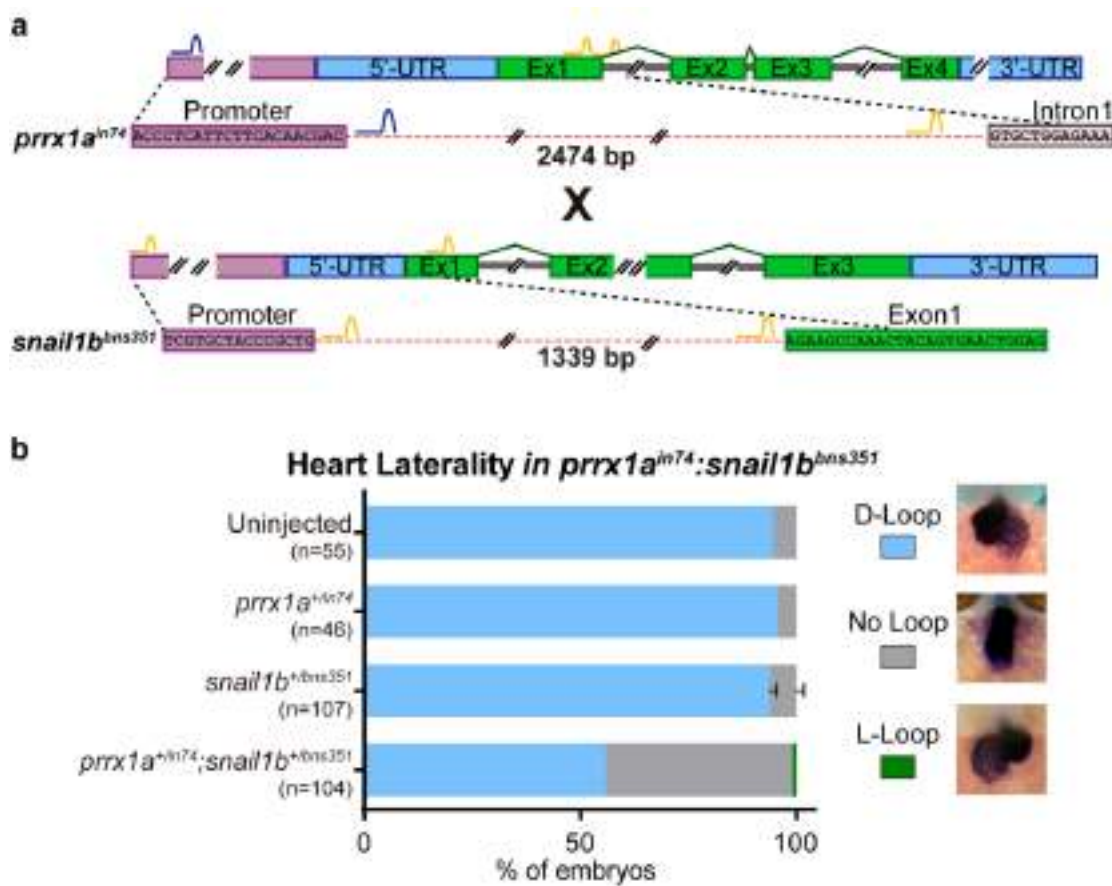


Figure 37 | Genetic interaction between *prrx1a* and *snail1b* and cooperation in heart laterality. (a) Schematic representation of the *prrx1a*ⁱⁿ⁷⁴ and *snail1b*^{bns351} alleles used alone or to generate double heterozygotes. **(b)** Analysis of heart position at 52 hpf (ventral view) shows D-Loop in single *prrx1a*ⁱⁿ⁷⁴ or *snail1b*^{bns351} heterozygous mutants. Mesocardia (No-Loop) is observed in the double heterozygous. Data represents the mean percentage \pm s.d. n = number of embryos analysed from one or two (only *snail1b*^{bns351}) independent experiments.

DISCUSSION |

The EMT is a fundamental process during embryonic development that endows epithelial cells with migratory properties to travel long distances. Once they reach their final destination they undergo the reverse process, MET, and form different tissues and organs (Nieto et al., 2016). Furthermore, EMT is also involved in L/R asymmetry, including heart positioning, required to be correct for its optimal function (Kemmler et al., 2021; Ocaña et al., 2017). As such, BMP-induced EMT in the LPM and subsequent attenuation on the left, triggers transient L/R asymmetric cell movements and forces toward the midline, higher from the right, which are crucial for heart laterality in vertebrates (Ocaña et al., 2017; Rago et al., 2019). In zebrafish, downregulation of *prrx1a* prevents heart laterality and leads to mesocardia. This mechanism is conserved in the chicken embryo where *PRRX1* and *SNAIL1* are involved, while in mouse it is *Snail1* which instructs those L/R asymmetric cell movements (Ocaña et al., 2017). Therefore, there is an evolutionarily conserved role of EMT in the regulation of heart laterality.

In Ocaña et al., 2017 *Prrx1a* function in zebrafish was investigated by two different approaches affecting this EMT-TF at the level of mRNA splicing with the use of morpholino oligonucleotides and at the level of genomic DNA with sgRNAs (CRISPR-Cas9 technology). These methods allowed assessing *prrx1a* contribution to heart laterality and showed the impact of acute gene losses. Nevertheless, knockdown and G0 screens should be complemented with the generation of transgenic lines with heritable mutations (Hoshijima et al., 2019; Stainier et al., 2017). In the case of *prrx1a*, mutants presented normal heart laterality (Tessadori et al., 2020 and part of this work, already published in Castroviejo et al., 2020).

In the zebrafish genetic field, there are multiple examples in which embryos with targeted gene knockdowns exhibit stronger phenotypes than those from established knockout mutants (Kok et al., 2015). For instance, *klf2a*-morpholino injected embryos present cardiovascular defects (Nicoli et al., 2010) while mutants generated by Transcription Activator-Like Effector Nucleases (TALEN) are unaffected (Novodvorsky et al., 2015). Although in some cases, the phenotype of defective embryos obtained with nucleases and particularly with morpholinos have been proven to be due to unspecific off-target effects, phenotypic discrepancy between knockdown and knockout can be due to compensatory mechanisms (Jakutis and Stainier, 2021). Therefore, in this work, after showing the *Prrx1a* could be dispensable, we wanted to assess whether the mesocardia phenotype observed after acute *prrx1a* loss in zebrafish was specific and revealed its role in heart laterality, and if so, what could be the compensatory mechanism observed in the mutants.

1. *prrx1a*-LOF reagents specifically impair heart laterality in zebrafish

One of the main aims of this work was to get further insight into the process of heart laterality in zebrafish. As mentioned, we generated null mutants for *prrx1a* and we found that they had normal hearts, in agreement with similar findings from Jeroen Bakker's lab (Tessadori et al., 2020). Altogether, these data indicated that Prrx1a was dispensable for heart laterality in zebrafish, or that the phenotype we had previously observed after acute loss of function (Ocaña et al., 2017) was non-specific. Although the latter seemed unlikely due to the specificity checks and quality control experiments, we had already performed, we needed to examine both possibilities very carefully.

We used different means that could conclusively proof or disproof the specificity of the phenotype, and with that, getting further inside into the endogenous role of Prrx1a in heart laterality in the zebrafish. Some of the required controls had been described in a very useful review by leaders in the zebrafish field (Stainier et al., 2017). We first used a new and even more efficient set of RNA guides to target *prrx1a* sequences through the CRISPR/Cas9 system (Hoshijima et al., 2019). In addition, we used the new CRISPR/Cas13d system (Cox et al., 2017; Kushawah et al., 2020), which rather than targeting DNA, it targets the transcripts. Morpholinos also target the transcripts, but they may have toxicity, off-target effects and even trigger the innate immunity response (Lai et al., 2019; Stainier et al., 2017). As a matter of fact, we and others could detect some early laterality problems with the use of morpholinos to knockdown *prrx1a* (Tessadori et al., 2020; Castroviejo et al., 2020), which we avoided using CRISPR-mediated DNA editing or RNA targeting with CRISPR-Cas13d. After targeting *prrx1a* with the latter, we observed the exact same penetrance of the mesocardia phenotype than in gene-mutated *G0-prrx1a* crispants. Thus, both with the optimized guides and the Cas13d system, we could reproduce the phenotype that we had observed previously (Castroviejo et al., 2020; Ocaña et al., 2017).

In addition to target *prrx1a* by different means, we also performed additional controls that could directly proof the specificity of our loss of function reagents. We included another control experiment, challenging our dgRNA guides. One of our deletion mutants, bearing the *in69* mutant allele, which do not contain the complementary sequence to these guides that we had used to generate it (and also to induce acute loss of function). The prediction is that in this genetic background, the guides could not work and thus, the result of the experiment should be the absence of DNA editing and therefore, no phenotype. This is what we observed, indicating that

the mesocardia phenotype was due to the targeting of *prrx1a* sequences, which are the only sequences missing in the mutant. It also immediately indicates that the guides cannot induce mesocardia as an off-target effect.

As developmental defects could be the result of having affected earlier developmental pathways (Grimes and Burdine, 2017), we also examined early embryonic laterality pathway. We assessed whether in our acute loss of function experiments there was a correct establishment of the early L/R cascade in the embryo which, if affected, could indirectly lead to heart defects including laterality. We confirmed that in G0-*prrx1a* crispant embryos, the cilia in the KV had a correct morphology and function, as the left-specific expression of *spaw* was observed. Together with the left-sided jogging observed, we confirmed that the early asymmetric cascade was correct and transmitted to the LPM. This confirms that the phenotype we observed arise from a later defective *prrx1a* function in SHF-derived aLPM cells and not from the induction of off-target laterality phenotypes at early time points.

Our data are compatible with the described uncoupling between jogging and looping (Grimes et al., 2020; Noël et al., 2013). It is worth noting here that jogging and looping in zebrafish are processes prone to errors, as 2 – 10 % of the embryos present defects (Chen et al., 1997). However, in chicken, heart looping is correct in 97 % of the embryos (Hoyle et al., 1992), and in mouse embryos there is a size checkpoint control at gastrulation stages (Lewis and Rossant, 1982; Snow and Tam, 1979). Zebrafish embryos use the so-called *r* strategy for reproduction, as opposed to the alternative *K* strategy (MacArthur and Wilson, 1967). They have evolved to maximize the speed of development, securing their offspring through the layoff of hundreds of eggs, even though they may present defects. This explains the percentage of uninjected embryos with phenotype, that include laterality defects due to an incorrect establishment of the L/R cascade but not those related to heart laterality itself (further explained in section 3) (Moreno-Ayala et al., 2021).

At this point it is worth discussing the origin of the phenotype we have observed and the relationship between the different traits, namely mesocardia, smaller atrium and bradycardia (slow heartbeat rate). Mesocardia arises from the lack of L/R asymmetric contribution of EMT and cells of the right aLPM migrating towards the posterior pole in higher numbers than the population migrating from the left side (Ocaña et al., 2017 and this work). The poles of the heart are hotspots for cardiac heart diseases in humans' patients, highlighting the importance of

Discussion

studying their morphogenesis and its associated genetic networks (Francou, A. and Kelly, 2016). At 30 hpf, the heart tube is not free at its ends, as SHF cells joining the poles are integrated into the developing heart. Those being incorporated to the posterior (venous) pole contribute to the atrium, and as they are more abundant from the right hand side, promote the leftward displacement of the pole and can also contribute to looping (Kemmler et al., 2021). Thus, as expected, G0-*prrx1a* crispants show mesocardia and a reduction in atrial size. In addition, we checked heart function through the monitoring of heart beating in G0-*prrx1a* crispants and found that mesocardia correlated with bradycardia. This is somehow expected considering that the pacemaker develops from the posterior pole of the heart (Martin and Waxman, 2021). This is also compatible with the finding that LOF mutations in *Prrx1* cause atrial fibrillation in humans (Bosada et al., 2021; Tucker et al., 2017; Wu et al., 2021), suggesting that this EMT-TF is involved in the correct electrical activation of the atria in vertebrates and the development of the pacemaker. Interestingly, in this work, we describe a similar L/R asymmetric expression with higher levels on the right for *tbx5a*, a TF expressed in heart precursors, in the primary heart tube and in the surrounding aLPM coexpressed with *prrx1a* (Ocaña et al., 2017). The L/R asymmetric expression of both genes and our findings in the crispant embryos is compatible with the finding that there are more cardiac precursor cells on the right hand side (Mao et al., 2021). Remarkably, *hst* and *oug* zebrafish mutants, defective for *tbx5a* function, also present laterality defects and reduced heartbeating (Garrity et al., 2002; Tessadori et al., 2021). Holt-Oram syndrome patients, which have *TBX5* disrupted, have upper limb defects where the left arm is shorter than the right one (Newbury-Ecob et al., 1996). Interestingly, in *Tbx5* mouse hypomorphs, limb patterning genes are L/R asymmetrically expressed, leading to left-sided defects, and indicating that a threshold level of *Tbx5* is required to buffer L/R asymmetries, ensuring bilaterally symmetric forelimb formation (Sulaiman et al., 2016).

In summary, altogether, our data indicate that the phenotype we had observed after the induction of *prrx1a* acute loss of function was specific. Nevertheless, as mentioned, we and Tessadori et al., 2020 characterized different allelic series of *prrx1a* mutants with premature termination codons expected to produce simple LOF alleles (Popp and Maquat, 2016), and found hearts with correct laterality. Thus, we examined whether new splicing variants or compensatory mechanisms could arise due to this type of CRISPR-induced mutations (Anderson et al., 2017; Lalonde et al., 2017; Mou et al., 2017; Wilkinson, 2019). For instance, *egfl7* zebrafish mutants do not display the vascular phenotype than morphants do, but rather than being due to off-targets effects of the morpholino, there was a compensatory mechanism through the upregulation of

emilin genes which did not occur in morphants or G0 crispants (Parker et al., 2004; Rossi et al., 2015). This phenomenon is called transcriptional adaptation (TA), an upregulation of related genes not triggered by the loss of the protein but rather by mRNA degradation due to premature termination codon-mutations (El-Brolosy et al., 2019; Ma et al., 2019). Thus, to further clarify the situation for *Prrx1a*, as *in10* and *in69* alleles generate mRNA transcripts, we generated a *prrx1a* promoter-less allele (*in74*) which could not induce TA as mRNA is not produced. In parallel, Tessadori et al., 2020 also generated different *prrx1a* alleles which could not produce mRNA, *hu13685*, *hu13762* and *el803*. All these promoter-less alleles also had a correct position of the heart.

With all the data discussed above, the conclusion is that *Prrx1a* seems to be dispensable for heart laterality in zebrafish. Nevertheless, it is worth pointing out that the fitness of *prrx1a* mutants, including the viability of their offspring, is significantly reduced when compared to WT embryos, suggesting that we recover the embryos able to overcome *prrx1a* loss through unknown compensatory mechanisms. In addition, the fact that a gene can be dispensable, does not necessarily mean that it does not play a role in the corresponding process. As such, *spaw* is crucial for the establishment of the L/R cascade and nevertheless, *spaw* mutants can be viable and fertile (Grimes et al., 2020). As a matter of fact, acute losses can reveal gene functions that are obscured in mutants, providing valuable information about their contribution to gene regulatory networks in crucial developmental processes such as heart laterality, as it seems to be the case for *prrx1a* in the zebrafish. Since *Prrx1* is not expressed in the territories relevant for heart looping in mouse embryos (Ocaña et al., 2017), it may not be involved in this process in mammals. Nevertheless, as *Prrx1* mouse mutants cause atrial fibrillation (Bosada et al., 2021; Tucker et al., 2017) and defects in the development of vascular and perivascular matrix (Bergwerff et al., 2000), other genes may compensate for the loss of *Prrx* during heart development.

2. Additional TFs expressed in the aLPM are also involved in driving heart laterality in zebrafish

When the phenotype of null mutants is milder than that observed after acute losses due to somatic mutations in G0-crispant or knockdowns not due to off-targets effects, genetic robustness could be the reason behind (Jakutis and Stainier, 2021; Zimmer et al., 2019). Genetic robustness refers to the ability of tolerating genetic perturbations without changing its

Discussion

phenotype through: (i) dosage compensation (Brockdorff and Turner, 2015); (ii) redundancy with paralogues (Dean et al., 2008; Masel and Siegal, 2009); (iii) redundant wiring of TFs (MacNeil and Walhout, 2011); (iv) or regulatory compensation by genes from the same network (Peng et al., 2016). Due to the teleost genome duplication (Braasch et al., 2014; Glasauer and Neuhauss, 2014), zebrafish genes are less likely to be essential than singleton genes due to functional redundancy (Gu et al., 2003; White et al., 2013). As such, mutations in one particular gene in teleosts can be compensated by its/their orthologues or paralogues (Kemmler et al., 2021).

Following the argument mentioned above, we studied *prrx1b*, the *prrx1a* paralogue. We found that it is asymmetrically expressed in the pLPM compatible with the fact that it may also be subjected to the same post-transcriptional regulation than *prrx1a* (Rago et al., 2019). But in the aLPM, it is only expressed in a subpopulation of *tbx5a+* cells and much later than *prrx1a*. *prrx1b* shows a conserved synteny with mouse *Prrx1*, and the mouse gene seems to have lost all expression in sites relevant for heart laterality. As the chicken embryo maintains *Prrx1* expression in relevant territories, the situation in both zebrafish *prrx1b* and mouse *Prrx1* genes is very likely due to the loss (albeit to different degree) of tissue-specific enhancers (Leussink et al., 1995). In fact, *prrx1b* does not seem to be able to compensate for *prrx1a* loss, as double mutants do not show heart laterality defects (Tessadori et al., 2020). However, although *prrx1b* has a more limited and late expression than *prrx1a* in the relevant territories, it seems to also play a role in heart laterality as crispant embryos also show mesocardia and the penetrance significantly increases in double crispants.

All the above suggests that factors other than *prrx* paralogues, can be at play to account for the loss of overt phenotype in the null mutants. Interestingly, robustness does not necessarily involve gene duplicates, but it could also be the result of the function of other TFs associated with the same gene regulatory network (MacNeil and Walhout, 2011). Therefore, we examined the expression of additional EMT-TFs. This was supported by the fact that both embryonic and cancer mesenchymal cells express different combinations of EMT-TFs (Nieto, 2013 and unpublished) and because we and others previously found that *Snail1* is involved in chicken and mouse heart laterality (Isaac et al., 1997; Murray and Gridley, 2006; Ocaña et al., 2017).

The analysis of the expression pattern for all the members of EMT-TF families *zeb*, *twist* and *snail* in the aLPM confirmed that three out of the twelve genes analysed, *prrx1b*, *twist1a* and *snail1b*, had L/R asymmetric expression in the aLPM at the time relevant to be also involved in

heart laterality during zebrafish development. In the case of *twist* genes, it was already known that *twist1a* and *prrx1a* were coexpressed in LPM with a similar expression to those of Prrx1 and Twist1 in chick embryos (Ocaña et al., 2012). Nonetheless, *twist1a* asymmetric expression in the aLPM, as that of *tbx5a*, was previously neglected in the numerous studies for these genes, as well as it was initially the case of the L/R asymmetric expression for *snail1b* (Ocaña et al., 2017). Again, the same miRNAs that regulate *prrx1a* post-transcriptionally and attenuate their levels on the left LPM are predicted to also bind the 3'-UTR of *snail1b* (Rago et al., 2019).

After describing the asymmetric patterns of expression for additional EMT-TFs from different families, we generated CRISPR/Cas9 G0 embryos to assess whether their acute loss of function had an impact in heart laterality. We found that *twist1a* and *snail1b* crispants showed mesocardia albeit with a different penetrance, thus providing evidence of their contribution to the gene regulatory network driving heart laterality. Importantly, there is a temporal hierarchy of EMT-TF, as Snail expression normally precedes the expression of other EMT-TFs, and clearly that of *prrx1* (Fazilaty et al., 2019; Nieto, 2013; Youssef et al., unpublished), which could explain its higher penetrance compared to the rest. The penetrance of the mesocardia phenotype in G0-*tbx5a* crispants was higher than that of any individual EMT-TF, compatible with heart laterality defects described in previous studies (Garrity et al., 2002; Pi-Roig et al., 2014; Tessadori et al., 2021).

It is believed that heart looping evolves from being mostly intrinsic in fish to mostly extrinsic in amniotes as it is required a more efficient buckling mechanism for the proper establishment of a double circulation instead of the simpler from zebrafish (Desgrange et al., 2018). Extrinsic forces displace the posterior pole of the heart in all vertebrates (Domínguez et al., 2012; Le Garrec et al., 2017; Ocaña et al., 2017). Thus, as expected, both G0-*tbx5a* and G0-*prrx1a* crispants have a defective displacement of the posterior pole (Ocaña et al., 2017 and this work for *tbx5a*). Subsequent looping depends on the twisting of the chambers around the AVC, believed to be mostly intrinsic and recently described to be Tbx5a-dependent (Tessadori et al., 2021). Interestingly, the angle of looping is also defective in both *tbx5a* and *prrx1a* crispants, indicating that both contribute to looping as well. It is worth noting here that Prrx1 can only contribute to extrinsic forces and their consequences, as once the cells of the SHF are incorporated into the heart, they immediately lose *prrx1a* expression to differentiate into CMs. This is reminiscent of Prrx1 downregulation when cells reach their destinations in other embryonic structures as well as in cancer cells, as they revert to a non-migratory and more

Discussion

epithelial phenotype (Ocaña et al., 2012). Altogether this explains why *tbx5a* mutants show a stronger phenotype and higher penetrance, but also confirms that extrinsic cues also contribute to the laterality of the heart in zebrafish.

3. Heart laterality is a robust process supported by the cooperation of EMT-TFs in the aLPM

The existence of multiple EMT-TF expressed within the same territory and the phenotype observed after individual acute loss of function experiments immediately pointed to their cooperation in driving heart laterality. To directly examine whether that was the case, and to reveal putative epistatic relationships that could unveil cooperation or redundant functions (Adamson et al., 2016; Hoshijima et al., 2019), we injected combinations of dgRNAs to induce mutations by CRISPR/Cas9 editing in several EMT-TFs simultaneously. We already mentioned that concurrent editing of *prrx1a* and *prrx1b* led to mesocardia with higher penetrance than when both were targeted individually. This higher penetrance is also observed in *prrx1a/twist1a* crispants, compatible with our previous findings that both factors cooperate in zebrafish development and in cancer cells (Ocaña et al., 2012). As such, individual knockdown of PRRX1 or TWIST1 by RNAi decreased the ability of BT-549 cancer cells to degrade collagen, but invasiveness was fully abolished only when both were downregulated (Ocaña et al., 2012). In addition, *Prrx1a* overexpression induced a dramatic invasive phenotype in LPM cells, that broke the normal tissue boundaries in a Twist-dependent manner (Ocaña et al., 2012). It is also well known that Snail factors cooperate during zebrafish development. As such, *snail1a* and *snail1b* cooperate in the anterior migration of the axial mesendoderm (Blanco et al., 2007). Here we find that *snail1b* cooperates with *prrx1a*, and finally, that when dg-*tbx5a* is combined with dg-*snail1b* or dg-*prrx1a*, almost all embryos show mesocardia, showing the requirement of EMT-TFs in driving the migration of SHF-derived Tbx5a+ cells to the posterior (venous) pole of the heart. A similar scenario has been described in the specification of the neural crest. As such, G0 crispants with edited genes involved in the specification of the neural crest as *foxd3* or *tfap2a*, only have a mild reduction in melanophore numbers, but embryos are fully devoid of them when both genes are simultaneously disrupted (Hoshijima et al., 2019). The neural crest is a developmental innovation known to be crucial for the appearance of the vertebrate head (Gans and Northcutt, 1983; Manzanares and Nieto, 2003), and it is known to constitute a very robust system with multiple gene regulatory loops, cooperation, and compensatory mechanisms (Martik and Bronner, 2017).

Similarly, in the context of EMT-TFs in cancer, it has been shown that the deletion of individual factors are frequently not sufficient to abrogate EMT (Nieto, 2017).

After testing asymmetrically expressed EMT-TFs and examining the phenotypes of their acute losses either individually or in combination, we decided to generate and analyse germline mutants. Firstly, we generated *prrx1b* mutants and found that, as *Prrx1a*, *Prrx1b* also seemed to be dispensable for heart laterality. However, promoter-less *snail1b* mutants (Gentile et al., 2021) exhibit cardiac laterality defects in half of their homozygous mutants. Importantly, mutations associated to cardiac heart diseases in humans are normally found in heterozygosity but often their orthologues in zebrafish and mouse models behave as recessive mutants (Kemmler et al., 2021; Lieschke and Currie, 2007; Macrae and Seidman, 2017). Interestingly, we have found that while single heterozygous for either *prrx1a* or *snail1b* do not show heart laterality defects, double heterozygous mutants did. This indicates that (i) *prrx1a* is a *bona fide* player in heart laterality in zebrafish; (ii) that *prrx1a* and *snail1b* cooperate in the process. Similar scenarios have been observed during heart development in the mouse, as the cardiac TF TBX5, NKX2-5, and GATA4, known to interact with each other, present more severe heart defects in double heterozygosity than in individual null mutants (Maitra et al., 2009; Moskowitz et al., 2007).

Embryonic development is a complex process that requires the activation of genes at the proper place and at the correct time. Hence, organisms have developed mechanisms to secure the accomplishment of the different genetic programmes and overcome perturbations that threaten the system, endowing the individual with genetic robustness (Jakutis and Stainier, 2021). Evolution favours genetic robustness, but the systems are fragile in acute situations as in zebrafish G0 crispants (Akinci et al., 2021; Hwang et al., 2013). In the mouse, acute loss of function of Rb1 allows cell cycle re-entry of quiescent embryonic fibroblast (MEFs), while the MEFs derived from Rb1 mutant animals are unable to re-enter the cell cycle (Sage et al., 2003). Chronic deficiency of β -Actin in mice causes the upregulation of other actins and compensation (Tondeleir et al., 2012). However, when the loss of function of β -Actin is restored in mutant MEFs, the upregulation of the other actins does not occur (Tondeleir et al., 2012). Thus, the use of G0 CRISPR/Cas9-induced mutations allows getting further insight into endogenous gene functions, as we show here for different EMT-TFs in heart laterality.

In summary, robustness of heart laterality has just started to be understood (Meilhac and Buckingham, 2018) and our own data indicate that several EMT-TFs cooperate and may even

Discussion

have a redundant role in this process, providing an explanation as to why the absence of one of the players may be compensated by others. This cooperative behaviour enhances robustness of the system and secures the proper position of the heart, fundamental for its correct function and coordination with other organs.

CONCLUSIONS |

1. The heart laterality phenotype observed after acute loss or knockdown of *prrx1a* is specific, and includes mesocardia, small atrial size and bradycardia. The same defects were observed after editing the gene with new sets of dgRNA guides in the CRISPR/Cas9 system and after targeting the transcripts with the new CRISPR/Cas13d system. Additional quality controls, including the absence of DNA editing in individuals devoid of *prrx1a* target sequences and the analysis of early embryonic laterality pathways, also confirmed the specificity of the phenotype.
2. Different allelic series for mutant *prrx1a*, including those lacking promoter sequences, have normal hearts, indicating that Prrx1a can be dispensable for heart laterality in zebrafish.
3. We have revealed the L/R asymmetric expression of a series of TFs previously believed to be expressed in a bilaterally symmetric manner. These include the cardiac factor *tbx5a* and the EMT inducers *prrx1b*, *twist1a* and *snail1b*.
4. CRISPR/Cas9-mediated gene editing of *tbx5a*, *prrx1b*, *twist1a* or *snail1b* in acute loss of function experiments also led to mesocardia phenotypes.
5. Different combinations of acute loss for several of the mentioned factors and some double heterozygous mutants for different EMT-TF, lead to mesocardia with increased penetrance, highlighting the genetic interaction and cooperation between these TFs in driving the laterality of the heart.
6. Cooperation between different EMT-TFs provides robustness to the system, capable of overcoming the loss of individual players, and still achieving proper heart laterality.

1. El fenotipo de lateralidad del corazón que se observa tras la pérdida aguda de *prrx1a* en el pez cebra es específico e incluye mesocardia, una aurícula reducida y bradicardia. Hemos observado estos mismos defectos tras la edición del gen con un nuevo conjunto de guías de dgRNA mediante el sistema CRISPR/Cas9 y tras la utilización de un sistema CRISPR novedoso basado en Cas13d, que degrada los transcritos del gen correspondiente en lugar de editar el genoma. Controles de calidad adicionales, incluyendo la ausencia de edición genómica en individuos desprovistos de secuencias complementarias de las dgRNA de *prrx1a* y el análisis temprano de la cascada de señalización que inicia el proceso de lateralidad en vertebrados, también confirmaron la especificidad del fenotipo.
2. Distintos mutantes de *prrx1a*, incluidos aquellos que carecen de secuencias promotoras, y por tanto de transcripción, presentan corazones normales, lo que indica que *Prrx1a* puede ser prescindible para la lateralidad del corazón en el pez cebra.
3. Hemos encontrado expresión asimétrica I/D de una serie de FTs que se pensaba que se expresaban de forma bilateral. Estos incluyen el FT cardíaco *tbx5a* y los inductores de EMT *prrx1b*, *twist1a* y *snail1b*.
4. La pérdida de función aguda de *tbx5a*, *prrx1b*, *twist1a* o *snail1b* mediada por CRISPR/Cas9 también condujo a fenotipos de mesocardia.
5. Distintas combinaciones de pérdida aguda de varios de los factores mencionados y algunos dobles mutantes heterocigóticos conducen a una mayor penetrancia del fenotipo de mesocardia en pez cebra, poniendo de manifiesto la interacción y cooperación genética entre estos factores en la determinación de la lateralidad del corazón.
6. La cooperación entre los diferentes factores inductores de EMT proporciona robustez al sistema, siendo de esta forma capaz de superar la pérdida de uno de ellos y aun así lograr una correcta lateralidad cardíaca.

BIBLIOGRAPHY |

- Acloque, H., Wilkinson, D.G., and Nieto, M.A. (2008). Chapter 9 - In Situ Hybridization Analysis of Chick Embryos in Whole-Mount and Tissue Sections. *Methods Cell Biol.* *87*, 169–185.
- Acloque, H., Ocaña, O.H., Matheu, A., Rizzoti, K., Wise, C., Lovell-Badge, R., and Nieto, M.A. (2011). Reciprocal repression between Sox3 and Snail transcription factors defines embryonic territories at gastrulation. *Dev. Cell* *21*, 546–558.
- Adams, D.S., Robinson, K.R., Fukumoto, T., Yuan, S., Albertson, R.C., Yelick, P., Kuo, L., McSweeney, M., and Levin, M. (2006). Early, H⁺-V-ATPase-dependent proton flux is necessary for consistent left-right patterning of non-mammalian vertebrates. *Development* *133*, 1657–1671.
- Adamson, B., Norman, T.M., Jost, M., Cho, M.Y., Nuñez, J.K., Chen, Y., Villalta, J.E., Gilbert, L.A., Horlbeck, M.A., Hein, M.Y., et al. (2016). A Multiplexed Single-Cell CRISPR Screening Platform Enables Systematic Dissection of the Unfolded Protein Response. *Cell* *167*, 1867–1882.
- Aguirre, L.A., Alonso, M.E., Badía-Careaga, C., Rollán, I., Arias, C., Fernández-Miñán, A., López-Jiménez, E., Aránega, A., Gómez-Skarmeta, J.L., Franco, D., et al. (2015). Long-range regulatory interactions at the 4q25 atrial fibrillation risk locus involve PITX2c and ENPEP. *BMC Biol.* *13*, 1–13.
- Akinci, E., Hamilton, M.C., Khowpinitchai, B., and Sherwood, R.I. (2021). Using CRISPR to understand and manipulate gene regulation. *Dev.* *148*, 1–16.
- Alzein, M., Lozano-Velasco, E., Hernández-Torres, F., García-Padilla, C., Domínguez, J.N., Aránega, A., and Franco, D. (2021). Differential Spatio-Temporal Regulation of T-Box Gene Expression by microRNAs during Cardiac Development. *J. Cardiovasc. Dev. Dis.* *8*, 1–14.
- Amack, J.D. (2014). Salient features of the ciliated organ of asymmetry. *Bioarchitecture* *4*, 6–15.
- Amack, J.D. (2021). Cellular dynamics of EMT: lessons from live in vivo imaging of embryonic development. *Cell Commun. Signal.* *19*, 1–16.
- Anderson, J.L., Mulligan, T.S., Shen, M.C., Wang, H., Scahill, C.M., Tan, F.J., Du, S.J., Busch-Nentwich, E.M., and Farber, S.A. (2017). mRNA processing in mutant zebrafish lines generated by chemical and CRISPR-mediated mutagenesis produces unexpected transcripts that escape nonsense-mediated decay. *PLoS Genet.* *13*, 1–18.
- Andrés-Delgado, L., Ernst, A., Galardi-Castilla, M., Bazaga, D., Peralta, M., Münch, J.,

Bibliography

- González-Rosa, J.M., Marques, I., Tessadori, F., de la Pompa, J.L., et al. (2019). Actin dynamics and the Bmp pathway drive apical extrusion of proepicardial cells.
- Arceci, R.J., King, A.A., Simon, M.C., Orkin, S.H., and Wilson, D.B. (1993). Mouse GATA-4: a Retinoic Acid-Inducible GATA-Binding Transcription Factor Expressed in Endodermally Derived Tissues and Heart. *Mol. Cell. Biol.* *13*, 2235–2246.
 - Arnold, S.J., and Robertson, E.J. (2009). Making a commitment: Cell lineage allocation and axis patterning in the early mouse embryo. *Nat. Rev. Mol. Cell Biol.* *10*, 91–103.
 - Auman, H.J., Coleman, H., Riley, H.E., Olale, F., Tsai, H.J., and Yelon, D. (2007). Functional Modulation of Cardiac Form through Regionally Confined Cell Shape Changes. *PLoS Biol.* *5*, 0604–0615.
 - Aw, S., Adams, D.S., Qiu, D., and Levin, M. (2008). H,K-ATPase protein localization and Kir4.1 function reveal concordance of three axes during early determination of left-right asymmetry. *Mech. Dev.* *125*, 353–372.
 - Baker, K., Holtzman, N.G., and Burdine, R.D. (2008). Direct and indirect roles for Nodal signaling in two axis conversions during asymmetric morphogenesis of the zebrafish heart. *Proc. Natl. Acad. Sci. U. S. A.* *105*, 13924–13929.
 - de Bakker, D.E.M., Bouwman, M., Dronkers, E., Simões, F.C., Riley, P.R., Goumans, M.-J., Smits, A.M., and Bakkers, J. (2021). *Prrx1b* restricts fibrosis and promotes *Nrg1*-dependent cardiomyocyte proliferation during zebrafish heart regeneration. *Development* *148*, 1–13.
 - Bakkers, J. (2011). Zebrafish as a model to study cardiac development and human cardiac disease. *Cardiovasc. Res.* *91*, 279–288.
 - Barrallo-Gimeno, A., and Nieto, M.A. (2005). The Snail genes as inducers of cell movement and survival: Implications in development and cancer. *Development* *132*, 3151–3161.
 - Barske, L., Askary, A., Zuniga, E., Balczerski, B., Bump, P., Nichols, J.T., and Crump, J.G. (2016). Competition between Jagged-Notch and Endothelin1 Signaling Selectively Restricts Cartilage Formation in the Zebrafish Upper Face. *PLoS Genet.* *12*, 1–33.
 - Basson, C.T., Bachinsky, D.R., Lin, R.C., Levi, T., Elkins, J.A., Soultz, J., Grayzel, D., Kroumpouzou, E., Trai, T.A., Leblanc-straceski, J., et al. (1997). Mutations in human cause limb and cardiac malformation in Holt-Oram syndrome. *Nat. Genet.* *15*, 30–35.
 - Batlle, E., Sancho, E., Francí, C., Domínguez, D., Monfar, M., Baulida, J., and De Herreros, A.G. (2000). The transcription factor Snail is a repressor of E-cadherin gene expression in

- epithelial tumour cells. *Nat. Cell Biol.* 2, 84–89.
- Bayraktar, M., and Männer, J. (2014). Cardiac looping may be driven by compressive loads resulting from unequal growth of the heart and pericardial cavity. Observations on a physical simulation model. *Front. Physiol.* 5, 1–15.
 - Begemann, G., and Ingham, P.W. (2000). Developmental regulation of *Tbx5* in zebrafish embryogenesis. *Mech. Dev.* 90, 299–304.
 - Beis, D., Bartman, T., Jin, S.W., Scott, I.C., D’Amico, L.A., Ober, E.A., Verkade, H., Frantsve, J., Field, H.A., Wehman, A., et al. (2005). Genetic and cellular analyses of zebrafish atrioventricular cushion and valve development. *Development* 132, 4193–4204.
 - Benson, D.W., Silberbach, G.M., Kavanaugh-McHugh, A., Cottrill, C., Zhang, Y., Riggs, S., Smalls, O., Johnson, M.C., Watson, M.S., Seidman, J.G., et al. (1999). Mutations in the cardiac transcription factor *NKX2.5* affect diverse cardiac developmental pathways. *J. Clin. Invest.* 104, 1567–1573.
 - ten Berge, D., Brouwer, A., Korving, J., Martin, J.F., and Meijlink, F. (1998). *Prx1* and *Prx2* in skeletogenesis: roles in the craniofacial region, inner ear and limbs. *Development* 125, 3831–3842.
 - Bergwerff, M., Gittenberger-de Groot, A.C., Wisse, L.J., DeRuiter, M.C., Wessels, A., Martin, J.F., Olson, E.N., and Kern, M.J. (2000). Loss of function of the *Prx1* and *Prx2* homeobox genes alters architecture of the great elastic arteries and ductus arteriosus. *Virchows Arch.* 436, 12–19.
 - Beverdam, A., and Meijlink, F. (2001). Expression patterns of group-I *aristaless*-related genes during craniofacial and limb development. *Mech. Dev.* 107, 163–167.
 - Beyer, T., Thumberger, T., Schweickert, A., and Blum, M. (2012). Connexin26-mediated transfer of laterality cues in *Xenopus*. *Biol. Open* 1, 473–481.
 - Bisgrove, B.W., Essner, J.J., and Yost, H.J. (1999). Regulation of midline development by antagonism of lefty and nodal signaling. *Development* 126, 3253–3262.
 - Blanco, M.J., Barrallo-Gimeno, A., Acloque, H., Reyes, A.E., Tada, M., Allende, M.L., Mayor, R., and Nieto, M.A. (2007). *Snail1a* and *Snail1b* cooperate in the anterior migration of the axial mesendoderm in the zebrafish embryo. *Development* 134, 4073–4081.
 - Blum, M., and Ott, T. (2018). Animal left–right asymmetry. *Curr. Biol.* 28, R301–R304.
 - Blum, M., Schweickert, A., Vick, P., Wright, C.V.E., and Danilchik, M. V. (2014). Symmetry breakage in the vertebrate embryo: When does it happen and how does it work? *Dev.*

Bibliography

- Biol. 393, 109–123.
- Bodor, D.L., Pönisch, W., Endres, R.G., and Paluch, E.K. (2020). Of Cell Shapes and Motion: The Physical Basis of Animal Cell Migration. *Dev. Cell* 52, 550–562.
 - te Boekhorst, V., Preziosi, L., and Friedl, P. (2016). Plasticity of Cell Migration In Vivo and In Silico. *Annu. Rev. Cell Dev. Biol.* 32, 491–526.
 - Boland, M.J., Nazor, K.L., and Loring, J.F. (2014). Epigenetic regulation of pluripotency and differentiation. *Circ. Res.* 115, 311–324.
 - Bosada, F.M., Rivaud, M.R., Uhm, J.S., Verheule, S., Van Duijvenboden, K., Verkerk, A.O., Christoffels, V.M., and Boukens, B.J. (2021). A Variant Noncoding Region Regulates Prrx1 and Predisposes to Atrial Arrhythmias. *Circ. Res.* 129, 420–434.
 - Boulay, J.L., Dennefeld, C., and Alberga, A. (1987). The Drosophila developmental gene snail encodes a protein with nucleic acid binding fingers. *Nature* 330, 395–398.
 - Boutet, A., De Frutos, C.A., Maxwell, P.H., Mayol, M.J., Romero, J., and Nieto, M.A. (2006). Snail activation disrupts tissue homeostasis and induces fibrosis in the adult kidney. *EMBO J.* 25, 5603–5613.
 - Braasch, I., Guiguen, Y., Loker, R., Letaw, J.H., Ferrara, A., Bobe, J., and Postlethwait, J.H. (2014). Connectivity of vertebrate genomes: Paired-related homeobox (Prrx) genes in spotted gar, basal teleosts, and tetrapods. *Comp. Biochem. Physiol. Part - C Toxicol. Pharmacol.* 163, 24–36.
 - Brade, T., Pane, L.S., Moretti, A., Chien, K.R., and Laugwitz, K.L. (2013). Embryonic heart progenitors and cardiogenesis. *Cold Spring Harb. Perspect. Med.* 3, 1–17.
 - Le Bras, G.F., Taubenslag, K.J., and Andl, C.D. (2012). The regulation of cell-cell adhesion during epithelial-mesenchymal transition, motility and tumor progression. *Cell Adhes. Migr.* 6, 365–373.
 - Brennan, J., Norris, D.P., and Robertson, E.J. (2002). Nodal activity in the node governs left-right asymmetry. *Genes Dev.* 16, 2339–2344.
 - Brockdorff, N., and Turner, B.M. (2015). Dosage compensation in mammals. *Cold Spring Harb. Perspect. Biol.* 7, 1–25.
 - Bruneau, B.G., Logan, M., Davis, N., Levi, T., Tabin, C.J., Seidman, J.G., and Seidman, C.E. (1999). Chamber-specific cardiac expression of Tbx5 and heart defects in Holt-Oram syndrome. *Dev. Biol.* 211, 100–108.
 - Bruneau, B.G., Nemer, G., Schmitt, J.P., Charron, F., Robitaille, L., Caron, S., Conner, D.A., Gessler, M., Nemer, M., Seidman, C.E., et al. (2001). A murine model of Holt-Oram

syndrome defines roles of the T-Box transcription factor Tbx5 in cardiogenesis and disease. *Cell* 106, 709–721.

- Burns, C.G., Milan, D.J., Grande, E.J., Rottbauer, W., Macrae, C.A., and Fishman, M.C. (2005). High-Throughput Assay for Small Molecules That Modulate Zebrafish Embryonic Heart Rate. *Nat. Chem. Biol.* 1, 263–264.
- Cai, C.L., Liang, X., Shi, Y., Chu, P.H., Pfaff, S.L., Chen, J., and Evans, S. (2003). *Isl1* identifies a cardiac progenitor population that proliferates prior to differentiation and contributes a majority of cells to the heart. *Dev. Cell* 5, 877–889.
- Camenisch, T.D., Spicer, A.P., Brehm-Gibson, T., Biesterfeldt, J., Augustine, M. Lou, Calabro, A., Kubalak, S., Klewer, S.E., and McDonald, J.A. (2000). Disruption of hyaluronan synthase-2 abrogates normal cardiac morphogenesis and hyaluronan-mediated transformation of epithelium to mesenchyme. *J. Clin. Invest.* 106, 349–360.
- Camp, E., and Lardelli, M. (2001). Tyrosinase gene expression in zebrafish embryos. *Dev. Genes Evol.* 211, 150–153.
- Campione, M., and Franco, D. (2016). Current Perspectives in Cardiac Laterality. *J. Cardiovasc. Dev. Dis.* 3, 34.
- Campione, M., Ros, M.A., Icardo, J.M., Piedra, E., Christoffels, V.M., Schweickert, A., Blum, M., Franco, D., and Moorman, A.F.M. (2001). *Pitx2* expression defines a left cardiac lineage of cells: Evidence for atrial and ventricular molecular isomerism in the *iv/iv* mice. *Dev. Biol.* 231, 252–264.
- Campos-Baptista M., M.I., Holtzman, N.G., Yelon, D., and Schier, A.F. (2008). Nodal signaling promotes the speed and directional movement of cardiomyocytes in zebrafish. *Dev. Dyn.* 237, 3624–3633.
- Cano, A., Pérez-Moreno, M.A., Rodrigo, I., Locascio, A., Blanco, M.J., Del Barrio, M.G., Portillo, F., and Nieto, M.A. (2000). The transcription factor Snail controls epithelial-mesenchymal transitions by repressing E-cadherin expression. *Nat. Cell Biol.* 2, 76–83.
- Cano, E., Carmona, R., Ruiz-Villalba, A., Rojas, A., Chau, Y.Y., Wagner, K.D., Wagner, N., Hastie, N.D., Muñoz-Chápuli, R., and Pérez-Pomares, J.M. (2016). Extracardiac septum transversum/proepicardial endothelial cells pattern embryonic coronary arterio-venous connections. *Proc. Natl. Acad. Sci. U. S. A.* 113, 656–661.
- Cao, Y., Duca, S., and Cao, J. (2020). Epicardium in heart development. *Cold Spring Harb. Perspect. Biol.* 12, 1–18.
- Carmona, R., Barrena, S., López Gambero, A.J., Rojas, A., and Muñoz-Chápuli, R. (2020).

Bibliography

- Epicardial cell lineages and the origin of the coronary endothelium. *FASEB J.* *34*, 5223–5239.
- Carver, E.A., Jiang, R., Lan, Y., Oram, K.F., and Gridley, T. (2001). The Mouse Snail Gene Encodes a Key Regulator of the Epithelial-Mesenchymal Transition. *Mol. Cell. Biol.* *21*, 8184–8188.
 - Castroviejo, N., Ocaña, O.H., Rago, L., Coskun, H., Arcas, A., Galcerán, J., and Nieto, M.A. (2020). Reply to: Zebrafish *prrx1a* mutants have normal hearts. *Nature* *585*, E17–E19.
 - Chen, J.N., and Fishman, M.C. (1996). Zebrafish tinman homolog demarcates the heart field and initiates myocardial differentiation. *Development* *122*, 3809–3816.
 - Chen, Y., and Gridley, T. (2013). The SNAI1 and SNAI2 proteins occupy their own and each other's promoter during chondrogenesis. *Biochem. Biophys. Res. Commun.* *435*, 356–360.
 - Chen, J.N., Van Eeden, F.J.M., Warren, K.S., Chin, A., Nüsslein-Volhard, C., Haffter, P., and Fishman, M.C. (1997). Left-right pattern of cardiac BMP4 may drive asymmetry of the heart in zebrafish. *Dev.* *124*, 4373–4382.
 - Chocron, S., Verhoeven, M.C., Rentzsch, F., Hammerschmidt, M., and Bakkers, J. (2007). Zebrafish *Bmp4* regulates left-right asymmetry at two distinct developmental time points. *Dev. Biol.* *305*, 577–588.
 - Christoffels, V.M., Habets, P.E.M.H., Franco, D., Campione, M., De Jong, F., Lamers, W.H., Bao, Z.Z., Palmer, S., Biben, C., Harvey, R.P., et al. (2000). Chamber formation and morphogenesis in the developing mammalian heart. *Dev. Biol.* *223*, 266–278.
 - Collignon, J., Varlet, I., and Robertson, E.J. (1996). Relationship between asymmetric nodal expression and the direction of embryonic turning. *Nature* *381*, 155–158.
 - Colombo, S., De Sena-Tomás, C., George, V., Werdich, A.A., Kapur, S., Macrae, C.A., and Targoff, K.L. (2018). *Nkx* genes establish second heart field cardiomyocyte progenitors at the arterial pole and pattern the venous pole through *isl1* repression. *Dev.* *145*, 1–13.
 - Compagnon, J., Barone, V., Rajshekar, S., Kottmeier, R., Pranjic-Ferscha, K., Behrndt, M., and Heisenberg, C.P. (2014). The notochord breaks bilateral symmetry by controlling cell shapes in the Zebrafish laterality organ. *Dev. Cell* *31*, 774–783.
 - Cox, D.B.T., Gootenberg, J.S., Abudayyeh, O.O., Franklin, B., Kellner, M.J., Joung, J., and Zhang, F. (2017). RNA editing with CRISPR-Cas13. *Sci. (New York)* *358*, 1019–1027.
 - Cserjesi, P., Lilly, B., Bryson, L., Wang, Y., Sassoon, D.A., and Olson, E.N. (1992). *MHox*: A mesodermally restricted homeodomain protein that binds an essential site in the muscle

- creatine kinase enhancer. *Development* *115*, 1087–1101.
- Cui, C., Little, C.D., and Rongish, B.J. (2009). Rotation of organizer tissue contributes to left-right asymmetry. *Anat. Rec.* *292*, 557–561.
 - Dale, J.K., Malapert, P., Chal, J., Vilhais-Neto, G., Maroto, M., Johnson, T., Jayasinghe, S., Trainor, P., Herrmann, B., and Pourquié, O. (2006). Oscillations of the snail genes in the presomitic mesoderm coordinate segmental patterning and morphogenesis in vertebrate somitogenesis. *Dev. Cell* *10*, 355–366.
 - Danilchik, M. V., Brown, E.E., and Riegert, K. (2006). Intrinsic chiral properties of the *Xenopus* egg cortex: An early indicator of left-right asymmetry. *Dev.* *133*, 4517–4526.
 - Dasgupta, A., and Amack, J.D. (2016). Cilia in vertebrate left-right patterning. *Philos. Trans. R. Soc. B Biol. Sci.* *371*, 1–9.
 - Dave, N., Guaita-Esteruelas, S., Gutarra, S., Frias, À., Beltran, M., Peiró, S., and García De Herreros, A. (2011). Functional cooperation between snail1 and twist in the regulation of ZEB1 expression during epithelial to mesenchymal transition. *J. Biol. Chem.* *286*, 12024–12032.
 - Dean, E.J., Davis, J.C., Davis, R.W., and Petrov, D.A. (2008). Pervasive and persistent redundancy among duplicated genes in yeast. *PLoS Genet.* *4*, 1–11.
 - Delling, M., Indzhukulian, A.A., Liu, X., Li, Y., Xie, T., Corey, D.P., and Clapham, D.E. (2016). Primary cilia are not calcium-responsive mechanosensors. *Nature* *531*, 656–660.
 - Derrick, C.J., Pollitt, E.J.G., Sevilla Uruchurtu, A.S., Hussein, F., Grierson, A.J., and Noël, E.S. (2021a). Lamb1a regulates atrial growth by limiting second heart field addition during zebrafish heart development. *Dev.* *148*, 1–15.
 - Derrick, C.J., Sánchez-Posada, J., Hussein, F., Tessadori, F., Pollitt, E.J.G., Savage, A.M., Wilkinson, R.N., Chico, T.J., van Eeden, F.J., Bakkers, J., et al. (2021b). Asymmetric Hapln1a drives regionalized cardiac ECM expansion and promotes heart morphogenesis in zebrafish development. *Cardiovasc. Res.* *118*, 226–240.
 - Desgrange, A., Garrec, J.F. Le, and Meilhac, S.M. (2018). Left-right asymmetry in heart development and disease: Forming the right loop. *Dev.* *145*, 1–19.
 - Desgrange, A., Le Garrec, J.F., Bernheim, S., Bønnelykke, T.H., and Meilhac, S.M. (2020). Transient Nodal Signaling in Left Precursors Coordinates Opposed Asymmetries Shaping the Heart Loop. *Dev. Cell* *55*, 1–19.
 - Devine, W.P., Wythe, J.D., George, M., Koshiba-Takeuchi, K., and Bruneau, B.G. (2014). Early patterning and specification of cardiac progenitors in gastrulating mesoderm. *Elife*

Bibliography

3, 1–23.

- Dias, A., Lozovska, A., Wymeersch, F.J., Nóvoa, A., Binagui-Casas, A., Sobral, D., Martins, G.G., Wilson, V., and Mallo, M. (2020). A Tgf β RI/Snai1-dependent developmental module at the core of vertebrate axial elongation. *Elife* 9, 1–28.
- Diogo, R., Kelly, R.G., Christiaen, L., Levine, M., Ziermann, J.M., Molnar, J.L., Noden, D.M., and Tzahor, E. (2015). A new heart for a new head in vertebrate cardiopharyngeal evolution. *Nature* 520, 466–473.
- Domínguez, J.N., Meilhac, S.M., Bland, Y.S., Buckingham, M.E., and Brown, N.A. (2012). Asymmetric fate of the posterior part of the second heart field results in unexpected left/right contributions to both poles of the heart. *Circ. Res.* 111, 1323–1335.
- Dongre, A., and Weinberg, R.A. (2019). New insights into the mechanisms of epithelial–mesenchymal transition and implications for cancer. *Nat. Rev. Mol. Cell Biol.* 20, 69–84.
- Du, B., Cawthorn, W.P., Su, A., Doucette, C.R., Yao, Y., Hemati, N., Kampert, S., McCoin, C., Broome, D.T., Rosen, C.J., et al. (2013). The transcription factor paired-related homeobox 1 (Prrx1) inhibits adipogenesis by activating transforming growth factor- β (TGF β) signaling. *J. Biol. Chem.* 288, 3036–3047.
- Dueñas, A., Aranega, A.E., and Franco, D. (2017). More than just a simple cardiac envelope; cellular contributions of the epicardium. *Front. Cell Dev. Biol.* 5, 1–11.
- Duong, T.B., Holowiecki, A., and Waxman, J.S. (2021). Retinoic acid signaling restricts the size of the first heart field within the anterior lateral plate mesoderm. *Dev. Biol.* 473, 119–129.
- El-Brolosy, M.A., Kontarakis, Z., Rossi, A., Kuenne, C., Günther, S., Fukuda, N., Kikhi, K., Boezio, G.L.M., Takacs, C.M., Lai, S.L., et al. (2019). Genetic compensation triggered by mutant mRNA degradation. *Nature* 568, 193–197.
- Essner, J.J., Amack, J.D., Nyholm, M.K., Harris, E.B., and Yost, H.J. (2005). Kupffer’s vesicle is a ciliated organ of asymmetry in the zebrafish embryo that initiates left-right development of the brain, heart and gut. *Dev.* 132, 1247–1260.
- Esteban, I., Schmidt, P., Temiño, S., Kobbelt, L., and Torres, M. (2021). Pseudo-dynamic analysis of heart tube formation in the mouse reveals strong regional variability and early left-right asymmetry (<https://doi.org/10.1101/2021.10.07.463475>). *BioRxiv* 1–23.
- Fazilaty, H., Rago, L., Kass Youssef, K., Ocaña, O.H., Garcia-Asencio, F., Arcas, A., Galceran, J., and Nieto, M.A. (2019). A gene regulatory network to control EMT programs in development and disease. *Nat. Commun.* 10, 1–16.

- Felker, A., Prummel, K.D., Merks, A.M., Mickoleit, M., Brombacher, E.C., Huisken, J., Panáková, D., and Mosimann, C. (2018). Continuous addition of progenitors forms the cardiac ventricle in zebrafish. *Nat. Commun.* *9*, 1–14.
- Ferreira, R.R., and Vermot, J. (2017). The balancing roles of mechanical forces during left-right patterning and asymmetric morphogenesis. *Mech. Dev.* *144*, 71–80.
- Field, S., Riley, K.L., Grimes, D.T., Hilton, H., Simon, M., Powles-Glover, N., Siggers, P., Bogani, D., Greenfield, A., and Norris, D.P. (2011). Pkd11l1 establishes left-right asymmetry and physically interacts with Pkd2. *Development* *138*, 1131–1142.
- Fliegauf, M., Benzing, T., and Omran, H. (2007). When cilia go bad: Cilia defects and ciliopathies. *Nat. Rev. Mol. Cell Biol.* *8*, 880–893.
- Francou, A. and Kelly, R.G. (2016). Properties of Cardiac Progenitor Cells in the Second Heart Field. *Etiol. Morphog. Congenit. Hear. Dis. From Gene Funct. Cell. Interact. to Morphol. Chapter 23*, 1–383.
- Francou, A., De Bono, C., and Kelly, R.G. (2017). Epithelial tension in the second heart field promotes mouse heart tube elongation. *Nat. Commun.* *8*, 1–14.
- De Frutos, C.A., Dacquin, R., Vega, S., Jurdic, P., Machuca-Gayet, I., and Nieto, M.A. (2009). Snail1 controls bone mass by regulating Runx2 and VDR expression during osteoblast differentiation. *EMBO J.* *28*, 686–696.
- Fukui, H., Miyazaki, T., Chow, R.W.Y., Ishikawa, H., Nakajima, H., Vermot, J., and Mochizuki, N. (2018). Hippo signaling determines the number of venous pole cells that originate from the anterior lateral plate mesoderm in zebrafish. *Elife* *7*, 1–24.
- Funahashi, J.I., Sekido, R., Murai, K., Kamachi, Y., and Kondoh, H. (1993). δ -crystallin enhancer binding protein δ EF1 is a zinc finger-homeodomain protein implicated in postgastrulation embryogenesis. *Dev.* *119*, 433–446.
- Gabriel, G.C., and Lo, C.W. (2020). Left–right patterning in congenital heart disease beyond heterotaxy. *Am. J. Med. Genet. Part C Semin. Med. Genet.* *184*, 90–96.
- Galli, D., Domínguez, J.N., Zaffran, S., Munk, A., Brown, N.A., and Buckingham, M.E. (2008). Atrial myocardium derives from the posterior region of the second heart field, which acquires left-right identity as Pitx2c is expressed. *Dev.* *135*, 1157–1167.
- Galliot, B., De Vargas, C., and Miller, D. (1999). Evolution of homeobox genes: Q50 Paired-like genes founded the Paired class. *Dev. Genes Evol.* *209*, 186–197.
- Gans, C., and Northcutt, R.G. (1983). Neural crest and the origin of vertebrates: A new head. *Sci. (New York)* *220*, 268–274.

Bibliography

- Garcia-Padilla, C., Hernandez-Torres, F., Lozano-Velasco, E., Dueñas, A., Muñoz-Gallardo, M. del M., Garcia-Valencia, I.S., Palencia-Vincent, L., Aranega, A., and Franco, D. (2022). The Role of Bmp- and Fgf Signaling Modulating Mouse Proepicardium Cell Fate. *Front. Cell Dev. Biol.* *9*, 1–18.
- Le Garrec, J.F., Domínguez, J.N., Desgrange, A., Ivanovitch, K.D., Raphaël, E., Bangham, J.A., Torres, M., Coen, E., Mohun, T.J., and Meilhac, S.M. (2017). A predictive model of asymmetric morphogenesis from 3D reconstructions of mouse heart looping dynamics. *Elife* *6*, 1–35.
- Garrity, D.M., Childs, S., and Fishman, M.C. (2002). The heartstrings mutation in zebrafish causes heart/fin Tbx5 deficiency syndrome. *Dev.* *129*, 4635–4645.
- Gauvrit, S., Bossaer, J., Lee, J., and Collins, M.M. (2022). Modeling Human Cardiac Arrhythmias : Insights from Zebrafish. *J. Cardiovasc. Dev. Dis.* *9*, 1–22.
- Gelbart, M.A., He, B., Martin, A.C., Thiberge, S.Y., Wieschaus, E.F., and Kaschube, M. (2012). Volume conservation principle involved in cell lengthening and nucleus movement during tissue morphogenesis. *Proc. Natl. Acad. Sci. U. S. A.* *109*, 19298–19303.
- Gentile, A., Bensimon-Brito, A., Priya, R., Maischein, H.M., Piesker, J., Guenther, S., Gunawan, F., and Stainier, D.Y.R. (2021). The EMT transcription factor Snai1 maintains myocardial wall integrity by repressing intermediate filament gene expression. *Elife* *10*, 1–22.
- George, V., Colombo, S., and Targoff, K.L. (2015). An Early Requirement for nkx2.5 Ensures First and Second Heart Field Ventricular Identity and Cardiac Function into Adulthood. *Dev Biol* *400*, 10–22.
- Glasauer, S.M.K., and Neuhauss, S.C.F. (2014). Whole-genome duplication in teleost fishes and its evolutionary consequences. *Mol. Genet. Genomics* *289*, 1045–1060.
- Grande, M.T., Sánchez-Laorden, B., López-Blau, C., De Frutos, C.A., Boutet, A., Arévalo, M., Rowe, R.G., Weiss, S.J., López-Novoa, J.M., and Nieto, M.A. (2015). Snail1-induced partial epithelial-to-mesenchymal transition drives renal fibrosis in mice and can be targeted to reverse established disease. *Nat. Med.* *21*, 989–997.
- Grant, M.G., Patterson, V.L., Grimes, D.T., and Burdine, R.D. (2017). Chapter One: Modeling Syndromic Congenital Heart Defects in Zebrafish. In *Current Topics in Developmental Biology*, (Elsevier Inc.), pp. 1–40.
- Grimes, A.C., and Kirby, M.L. (2009). The outflow tract of the heart in fishes: Anatomy, genes and evolution. *J. Fish Biol.* *74*, 983–1036.

- Grimes, D.T., and Burdine, R.D. (2017). Left–Right Patterning: Breaking Symmetry to Asymmetric Morphogenesis. *Trends Genet.* 33, 616–628.
- Grimes, D.T., Patterson, V.L., Luna-Arvizu, G., Schottenfeld-Roames, J., Irons, Z.H., and Burdine, R.D. (2020). Left-right asymmetric heart jogging increases the robustness of dextral heart looping in zebrafish. *Dev. Biol.* 459, 79–86.
- Gros, J., Feistel, K., Viebahn, C., Blum, M., and Tabin, J.C. (2009). Cell movements at Hensen’s Node establish left/right asymmetric gene expression in the chick. *Sci. (New York)* 324, 941–944.
- Gu, Z., Steinmetz, L.M., Gu, X., Scharfe, C., Davis, R.W., and Li, W.H. (2003). Role of duplicate genes in genetic robustness against null mutations. *Nature* 421, 63–66.
- Guaita, S., Puig, I., Francí, C., Garrido, M., Domínguez, D., Batlle, E., Sancho, E., Dedhar, S., De Herreros, A.G., and Baulida, J. (2002). Snail induction of epithelial to mesenchymal transition in tumor cells is accompanied by MUC1 repression and ZEB1 expression. *J. Biol. Chem.* 277, 39209–39216.
- Guerra, A., Germano, R.F.V., Stone, O., Arnaout, R., Guenther, S., Ahuja, S., Uribe, V., Vanhollebeke, B., Stainier, D.Y.R., and Reischauer, S. (2018). Distinct myocardial lineages break atrial symmetry during cardiogenesis in zebrafish. *Elife* 7, 1–26.
- Guner-Ataman, B., Paffett-Lugassy, N., Adams, M.S., Nevis, K.R., Jahangiri, L., Obregon, P., Kikuchi, K., Poss, K.D., Burns, C.E., and Burns, C.G. (2013). Zebrafish second heart field development relies on progenitor specification in anterior lateral plate mesoderm and *nkx2.5* function. *Dev.* 140, 1353–1363.
- Hamada, H. (2020). Molecular and cellular basis of left-right asymmetry in vertebrates. *Proc. Japan Acad. Ser. B Phys. Biol. Sci.* 96, 273–296.
- Hamada, H., and Tam, P. (2020). Diversity of left-right symmetry breaking strategy in animals. *F1000Research* 9, 1–8.
- Hami, D., Grimes, A.C., Tsai, H.J., and Kirby, M.L. (2011). Zebrafish cardiac development requires a conserved secondary heart field. *Dev.* 138, 2389–2398.
- Hashimoto, H., Rebagliati, M., Ahmad, N., Muraoka, O., Kurokawa, T., Hibi, M., and Suzuki, T. (2004). The Cerberus/Dan-family protein Charon is a negative regulator of Nodal signaling during left-right patterning in zebrafish. *Dev.* 131, 1741–1753.
- Hashimoto, M., Shinohara, K., Wang, J., Ikeuchi, S., Yoshida, S., Meno, C., Nonaka, S., Takada, S., Hatta, K., Wynshaw-Boris, A., et al. (2010). Planar polarization of node cells determines the rotational axis of node cilia. *Nat. Cell Biol.* 12, 170–176.

Bibliography

- Hernandez-Huertas, L., Kushawah, G., Diaz-Moscoso, A., Tomas-Gallardo, L., Moreno-Sanchez, I., da Silva Pescador, G., Bazzini, A.A., and Moreno-Mateos, M.A. (2022). Optimized CRISPR-RfxCas13d system for RNA targeting in zebrafish embryos. *STAR Protoc.* *3*, 1–31.
- Hernández-Vega, A., and Minguillón, C. (2011). The Prx1 limb enhancers: Targeted gene expression in developing zebrafish pectoral fins. *Dev. Dyn.* *240*, 1977–1988.
- Hill, C.S. (2018). Spatial and temporal control of NODAL signaling. *Curr. Opin. Cell Biol.* *51*, 50–57.
- Hill, J.T., Demarest, B., Gorski, B., Smith, M., and Yost, H.J. (2017). Heart morphogenesis gene regulatory networks revealed by temporal expression analysis. *Dev.* *144*, 3487–3498.
- Hinitz, Y., Pan, L., Walker, C., Dowd, J., Moens, C.B., and Hughes, S.M. (2012). Zebrafish Mef2ca and Mef2cb are essential for both first and second heart field cardiomyocyte differentiation. *Dev. Biol.* *369*, 199–210.
- Holowiecki, A., Linstrum, K., Ravisankar, P., Chetal, K., Salomonis, N., and Waxman, J.S. (2020). Pbx4 limits heart size and fosters arch artery formation by partitioning second heart field progenitors and restricting proliferation. *Dev.* *147*, 1–15.
- Hoshijima, K., Jurynek, M.J., Klatt Shaw, D., Jacobi, A.M., Behlke, M.A., and Grunwald, D.J. (2019). Highly Efficient CRISPR-Cas9-Based Methods for Generating Deletion Mutations and F0 Embryos that Lack Gene Function in Zebrafish. *Dev. Cell* *51*, 645-657.e4.
- Hoyle, C., Brown, N.A., and Wolpert, L. (1992). Development of left/right handedness in the chick heart. *Dev.* *115*, 1071–1078.
- Hsu, D.S.S., Wang, H.J., Tai, S.K., Chou, C.H., Hsieh, C.H., Chiu, P.H., Chen, N.J., and Yang, M.H. (2014). Acetylation of snail modulates the cytokinome of cancer cells to enhance the recruitment of macrophages. *Cancer Cell* *26*, 534–548.
- Hwang, W.Y., Fu, Y., Reyon, D., Maeder, M.L., Tsai, S.Q., Sander, J.D., Peterson, R.T., Yeh, J.R.J., and Joung, J.K. (2013). Efficient genome editing in zebrafish using a CRISPR-Cas system. *Nat. Biotechnol.* *31*, 227–229.
- Ihida-Stansbury, K., McKean, D.M., Gebb, S.A., Martin, J.F., Stevens, T., Nemenoff, R., Akeson, A., Vaughn, J., and Jones, P.L. (2004). Paired-related homeobox gene Prx1 is required for pulmonary vascular development. *Circ. Res.* *94*, 1507–1514.
- Isaac, A., Sargent, M.G., and Cooke, J. (1997). Control of vertebrate left-right asymmetry by a snail-related zinc finger gene. *Sci. (New York)* *275*, 1301–1304.

- Itasaki, N., Nakamura, H., Sumida, H., and Yasuda, M. (1991). Actin bundles on the right side in the caudal part of the heart tube play a role in dextro-looping in the embryonic chick heart. *Anat. Embryol. (Berl)*. *183*, 29–39.
- Ivanovitch, K., Temiño, S., and Torres, M. (2017). Live imaging of heart tube development in mouse reveals alternating phases of cardiac differentiation and morphogenesis. *Elife* *5*, 1–30.
- Jakutis, G., and Stainier, D.Y.R. (2021). Genotype–Phenotype Relationships in the Context of Transcriptional Adaptation and Genetic Robustness. *Annu. Rev. Genet.* *55*, 1–21.
- Ji, Y., Buel, S.M., and Amack, J.D. (2016). Mutations in zebrafish *pitx2* model congenital malformations in Axenfeld-Rieger syndrome but do not disrupt left-right placement of visceral organs. *Dev. Biol.* *416*, 69–81.
- Jiang, R., Lan, Y., Norton, C.R., Sundberg, J.P., and Gridley, T. (1998). The slug gene is not essential for mesoderm or neural crest development in mice. *Dev. Biol.* *198*, 277–285.
- Jiménez-Amilburu, V., Rasouli, S.J., Staudt, D.W., Nakajima, H., Chiba, A., Mochizuki, N., and Stainier, D.Y.R. (2016). In Vivo Visualization of Cardiomyocyte Apicobasal Polarity Reveals Epithelial to Mesenchymal-like Transition during Cardiac Trabeculation. *Cell Rep.* *17*, 2687–2699.
- Jung, H.Y., Fattet, L., Tsai, J.H., Kajimoto, T., Chang, Q., Newton, A.C., and Yang, J. (2019). Apical–basal polarity inhibits epithelial–mesenchymal transition and tumour metastasis by PAR-complex-mediated SNAI1 degradation. *Nat. Cell Biol.* *21*, 359–371.
- Kajikawa, E., Horo, U., Ide, T., Mizuno, K., Minegishi, K., Hara, Y., Ikawa, Y., Nishimura, H., Uchikawa, M., Kiyonari, H., et al. (2020). Nodal paralogues underlie distinct mechanisms for visceral left–right asymmetry in reptiles and mammals. *Nat. Ecol. Evol.* *4*, 261–269.
- Katsuno, Y., and Derynck, R. (2021). Epithelial plasticity, epithelial-mesenchymal transition, and the TGF- β family. *Dev. Cell* *56*, 726–746.
- Kawahira, N., Ohtsuka, D., Kida, N., Hironaka, K., and Morishita, Y. (2020). Quantitative Analysis of 3D Tissue Deformation Reveals Key Cellular Mechanism Associated with Initial Heart Looping. *Cell Rep.* *30*, 3889–3903.
- Kawakami, Y., Raya, Á., Raya, R.M., Rodriguez-Esteban, C., and Izpisua Belmonte, J.C. (2005). Retinoic acid signalling links left-right asymmetric patterning and bilaterally symmetric somitogenesis in the zebrafish embryo. *Nature* *435*, 165–171.
- Keegan, B.R., Meyer, D., and Yelon, D. (2004). Organization of cardiac chamber progenitors in the zebrafish blastula. *Dev.* *131*, 3081–3091.

Bibliography

- Kelly, R.G. (2012). Chapter Two: The Second Heart Field. In *Current Topics in Developmental Biology*, (Elsevier Inc.), pp. 33–65.
- Kelly, R.G., Brown, N.A., and Buckingham, M.E. (2001). The Arterial Pole of the Mouse Heart Forms from Fgf10-Expressing Cells in Pharyngeal Mesoderm. *Dev. Cell* *1*, 435–440.
- Kelly, R.G., Buckingham, M.E., and Moorman, A.F. (2014). Heart fields and cardiac morphogenesis. *Cold Spring Harb. Perspect. Med.* *4*, 1–11.
- Kemmler, C.L., Riemsdijk, F.W., Moran, H.R., and Mosimann, C. (2021). From stripes to a beating heart: Early cardiac development in zebrafish. *J. Cardiovasc. Dev. Dis.* *8*, 1–21.
- Kennaway, R., Coen, E., Green, A., and Bangham, A. (2011). Generation of diverse biological forms through combinatorial interactions between tissue polarity and growth. *PLoS Comput. Biol.* *7*, 1–22.
- Kidokoro, H., Okabe, M., and Tamura, K. (2008). Time-lapse analysis reveals local asymmetrical changes in C-looping heart tube. *Dev. Dyn.* *237*, 3545–3556.
- Kimmel, C.B., Ballard, W.W., Kimmel, S.R., Ullmann, B., and Schilling, T.F. (1995). Stages of embryonic development of the zebrafish. *Dev. Dyn.* *203*, 253–310.
- Kinder, S.J., Tsang, T.E., Quinlan, G.A., Hadjantonakis, A., Nagy, A., and Tam, P.P.L. (2017). The orderly allocation of mesodermal cells to the extraembryonic structures and the anteroposterior axis during gastrulation of the mouse embryo. *Dev.* *114*, 2705–2710.
- Kirby, L. (2007). Chapter 7: Molecular Control of Looping. In *Cardiac Development*, (Oxford University Press), pp. 87–101.
- Knight, H.G., and Yelon, D. (2016). Chapter 25: Utilizing Zebrafish to Understand Second Heart Field Development. In *Etiology and Morphogenesis of Congenital Heart Disease: From Gene Function and Cellular Interaction to Morphology*, pp. 193–199.
- Kok, F.O., Shin, M., Ni, C.W., Gupta, A., Grosse, A.S., vanImpel, A., Kirchmaier, B.C., Peterson-Maduro, J., Kourkoulis, G., Male, I., et al. (2015). Reverse genetic screening reveals poor correlation between morpholino-induced and mutant phenotypes in zebrafish. *Dev. Cell* *32*, 97–108.
- Komiyama, M., Ito, K., and Shimada, Y. (1987). Origin and development of the epicardium in the mouse embryo. *Anat. Embryol. (Berl.)* *176*, 183–189.
- Kramer-Zucker, A.G., Olale, F., Haycraft, C.J., Yoder, B.K., Schier, A.F., and Drummond, I.A. (2005). Cilia-driven fluid flow in the zebrafish pronephros, brain and Kupffer's vesicle is required for normal organogenesis. *Dev.* *132*, 1907–1921.
- Krebs, A.M., Mitschke, J., Losada, M.L., Schmalhofer, O., Boerries, M., Busch, H.,

- Boettcher, M., Mougiakakos, Di., Reichardt, W., Bronsert, P., et al. (2017). The EMT-activator Zeb1 is a key factor for cell plasticity and promotes metastasis in pancreatic cancer. *Nat. Cell Biol.* *19*, 518–529.
- Kreiling, J.A., Prabhat, Williams, G., and Creton, R. (2007). Analysis of Kupffer's vesicle in zebrafish embryos using a cave automated virtual environment. *Dev. Dyn.* *236*, 1963–1969.
 - Kuratani, S., Martin, J.F., Wawersik, S., Lilly, B., Eichele, G., and Olson, E.N. (1994). The Expression Pattern of the Chick Homeobox Gene gMHox Suggests a Role in Patterning of the Limbs and Face and in Compartmentalization of Somites. *Dev. Biol.* *161*, 357–369.
 - Kushawah, G., Hernandez-Huertas, L., Abugattas-Nuñez del Prado, J., Martinez-Morales, J.R., DeVore, M.L., Hassan, H., Moreno-Sanchez, I., Tomas-Gallardo, L., Diaz-Moscoco, A., Monges, D.E., et al. (2020). CRISPR-Cas13d Induces Efficient mRNA Knockdown in Animal Embryos. *Dev. Cell* *54*, 805–817.
 - de la Cruz, M. V., and Markwald, R.R. (1998). Chapter 4: Torsion and looping of the cardiac tube and primitive cardiac segments. Anatomical manifestations. In *Living Morphogenesis of the Heart*, pp. 99–120.
 - De La Cruz, M. V, Sánchez-Gómez, C., and Palomino, M.A. (1989). The primitive cardiac regions in the straight tube heart (Stage 9) and their anatomical expression in the mature heart: An experimental study in the chick embryo. *J. Anat.* *165*, 121–131.
 - Lai, J.K.H., Galalova, K.K., Kuenne, C., El-Brolosy, M.A., and Stainier, D.Y.R. (2019). Induction of interferon-stimulated genes and cellular stress pathways by morpholinos in zebrafish. *Dev. Biol.* *454*, 21–28.
 - Lalonde, S., Stone, O.A., Lessard, S., Lavertu, A., Desjardins, J., Beaudoin, M., Rivas, M., Stainier, Di.Y.R., and Lettre, G. (2017). Frameshift indels introduced by genome editing can lead to in-frame exon skipping. *PLoS One* *12*, 1–13.
 - Laurent, F., Girdziusaite, A., Gamart, J., Barozzi, I., Osterwalder, M., Akiyama, J.A., Lincoln, J., Lopez-Rios, J., Visel, A., Zuniga, A., et al. (2017). HAND2 Target Gene Regulatory Networks Control Atrioventricular Canal and Cardiac Valve Development. *Cell Rep.* *19*, 1602–1613.
 - Lawson, K.A., Meneses, J.J., and Pedersen, R.A. (1991). Clonal analysis of epiblast fate during germ layer formation in the mouse embryo. *Dev.* *113*, 891–911.
 - Lazic, S., and Scott, I.C. (2011). Mef2cb regulates late myocardial cell addition from a second heart field-like population of progenitors in zebrafish. *Dev. Biol.* *354*, 123–133.

Bibliography

- Lee, J.D., and Anderson, K. V. (2008). Morphogenesis of the node and notochord: The cellular basis for the establishment and maintenance of left-right asymmetry in the mouse. *Dev. Dyn.* 237, 3464–3476.
- Lee, K.-W., Shin, D., Kim, S.-H., Cho, K.-H., An, S., and Yeo, S.-Y. (2018). A positive feedback loop bi-stably activates fibroblasts. *Nat. Commun.* 9, 1–16.
- Lenhart, K.F., Lin, S.Y., Titus, T.A., Postlethwait, J.H., and Burdine, R.D. (2011). Two additional midline barriers function with midline *lefty1* expression to maintain asymmetric Nodal signaling during left-right axis specification in zebrafish. *Dev.* 138, 4405–4410.
- Lenhart, K.F., Holtzman, N.G., Williams, J.R., and Burdine, R.D. (2013). Integration of Nodal and BMP Signals in the Heart Requires FoxH1 to Create Left-Right Differences in Cell Migration Rates That Direct Cardiac Asymmetry. *PLoS Genet.* 9, 1–11.
- Leptin, M. (1991). *twist* and *snail* as positive and negative regulators during *Drosophila* mesoderm development. *Genes Dev.* 5, 1568–1576.
- Leussink, B., Brouwer, A., El Khattabi, M., Poelmann, R.E., Gittenberger-de Groot, A.C., and Meijlink, F. (1995). Expression patterns of the paired-related homeobox genes *MHox Prx1* and *S8 Prx2* suggest roles in development of the heart and the forebrain. *Mech. Dev.* 52, 51–64.
- Leventea, E., Hazime, K., Zhao, C., and Malicki, J. (2016). Analysis of cilia structure and function in zebrafish. In *Methods in Cell Biology*, (Elsevier Ltd), pp. 179–227.
- Levin, M., Klar, A.J.S., and Ramsdell, A.F. (2016). Introduction to provocative questions in left - right asymmetry. *Philos. Trans. R. Soc. B Biol. Sci.* 371, 1–7.
- Lewis, N.L., and Rossant, J. (1982). Mechanism of size regulation in mouse embryo aggregates. *J. Embryol. Exp. Morphol.* 72, 169–181.
- Li, M., Zhao, L., Page-McCaw, P.S., and Chen, W. (2016). Zebrafish Genome Engineering Using the CRISPR–Cas9 System. *Trends Genet.* 32, 815–827.
- Lieschke, G.J., and Currie, P.D. (2007). Animal models of human disease: Zebrafish swim into view. *Nat. Rev. Genet.* 8, 353–367.
- Lin, A.E., Krikov, S., Riehle-Colarusso, T., Frías, J.L., Belmont, J., Anderka, M., Geva, T., Getz, K.D., and Botto, L.D. (2014). Laterality defects in the national birth defects prevention study (1998–2007): Birth prevalence and descriptive epidemiology. *Am. J. Med. Genet. Part A* 164, 2581–2591.
- Lin, C.R., Kloussi, C., O’Connell, S., Briata, P., Szeto, D., Liu, F., Izpisua-Belmonte, J.C., and

- Rosenfeld, M.G. (1999). Pitx2 regulates lung asymmetry, cardiac positioning and pituitary and tooth morphogenesis. *Nature* *401*, 279–282.
- Lin, Q., Schwarz, J., Bucana, C., and Olson, E.N. (1997). Control of mouse cardiac morphogenesis and myogenesis by transcription factor MEF2C. *Sci. (New York)* *276*, 1404–1407.
 - Linask, K.K. (1992). N-cadherin localization in early heart development and polar expression of Na⁺, K⁺-ATPase, and integrin during pericardial coelom formation and epithelialization of the differentiating myocardium. *Dev. Biol.* *151*, 213–224.
 - Liu, J., and Stainier, D.Y.R. (2010). Tbx5 and Bmp Signaling Are Essential for Proepicardium Specification in Zebrafish. *Circ. Res.* *106*, 1818–1828.
 - Liu, Y., Morley, M., Brandimarto, J., Hannenhalli, S., Hu, Y., Ashley, E.A., Tang, W.H.W., Moravec, C.S., Margulies, K.B., Cappola, T.P., et al. (2015). RNA-Seq identifies novel myocardial gene expression signatures of heart failure. *Genomics* *105*, 83–89.
 - Locascio, A., Manzanares, M., Blanco, M.J., and Nieto, M.A. (2002). Modularity and reshuffling of snail and slug expression during vertebrate evolution. *Proc. Natl. Acad. Sci. U. S. A.* *99*, 16841–16846.
 - Lombardo, V.A., Heise, M., Moghtadaei, M., Bornhorst, D., Männer, J., and Abdelilah-Seyfried, S. (2019). Morphogenetic control of zebrafish cardiac looping by Bmp signaling. *Dev.* *146*, 1–13.
 - Long, S., Ahmad, N., and Rebagliati, M. (2003). The zebrafish nodal-related gene southpaw is required for visceral and diencephalic left-right asymmetry. *Dev.* *130*, 2303–2316.
 - Lovisa, S., LeBleu, V.S., Tampe, B., Sugimoto, H., Vадnagara, K., Carstens, J.L., Wu, C.C., Hagos, Y., Burckhardt, B.C., Pentcheva-Hoang, T., et al. (2015). Epithelial-to-mesenchymal transition induces cell cycle arrest and parenchymal damage in renal fibrosis. *Nat. Med.* *21*, 998–1009.
 - Lozano-Velasco, E., Hernández-Torres, F., Daimi, H., Serra, S.A., Herraiz, A., Hove-Madsen, L., Aránega, A., and Franco, D. (2016). Pitx2 impairs calcium handling in a dose-dependent manner by modulating Wnt signalling. *Cardiovasc. Res.* *109*, 55–66.
 - Lozano-Velasco, E., Franco, D., Aranega, A., and Daimi, H. (2020). Genetics and epigenetics of atrial fibrillation. *Int. J. Mol. Sci.* *21*, 1–30.
 - Lu, M.F., Cheng, H.T., Kern, M.J., Potter, S.S., Tran, B., Diekwisch, T.G.H., and Martin, J.F. (1999). Prx-1 Functions Cooperatively With Another Paired-Related Homeobox Gene,

Bibliography

- Prx-2, To Maintain Cell Fates Within the Craniofacial Mesenchyme. *Dev.* 126, 495–504.
- Luna-Zurita, L., Stirnimann, C.U., Glatt, S., Pollard, K.S., Mu, C.W., Bruneau, B.G., Luna-zurita, L., Stirnimann, C.U., Glatt, S., Kaynak, B.L., et al. (2016). Complex Interdependence Regulates Heterotypic Transcription Factor Distribution and Coordinates Complex Interdependence Regulates Heterotypic Transcription Factor Distribution and Coordinates Cardiogenesis. *Cell* 164, 999–1014.
 - Ma, Z., Zhu, P., Shi, H., Guo, L., Zhang, Q., Chen, Y., Chen, S., Zhang, Z., Peng, J., and Chen, J. (2019). PTC-bearing mRNA elicits a genetic compensation response via Upf3a and COMPASS components. *Nature* 568, 259–263.
 - MacArthur, R.H., and Wilson, E.O. (1967). The Theory of Island Biogeography.
 - MacNeil, L.T., and Walhout, A.J.M. (2011). Gene regulatory networks and the role of robustness and stochasticity in the control of gene expression. *Genome Res.* 21, 645–657.
 - Macrae, C.A., and Seidman, C.E. (2017). Closing the Genotype-Phenotype Loop for Precision Medicine. *Circulation* 136, 1492–1494.
 - Maitra, M., Schluterman, M.K., Nichols, H.A., Richardson, J.A., Lo, C.W., Srivastava, D., and Garg, V. (2009). Interaction of Gata4 and Gata6 with Tbx5 is critical for normal cardiac development. *Dev. Biol.* 326, 368–377.
 - Männer, J. (2000). Cardiac looping in the chick embryo: A morphological review with special reference to terminological and biomechanical aspects of the looping process. *Anat. Rec.* 259, 248–262.
 - Männer, J. (2004). On Rotation, Torsion, Lateralization, and Handedness of the Embryonic Heart Loop: New Insights from a Simulation Model for the Heart Loop of Chick Embryos. *Anat. Rec. - Part A Discov. Mol. Cell. Evol. Biol.* 278, 481–492.
 - Männer, J. (2009). The anatomy of cardiac looping: A step towards the understanding of the morphogenesis of several forms of congenital cardiac malformations. *Clin. Anat.* 22, 21–35.
 - Manning, A., and McLachlan, J.C. (1990). Looping of chick embryo hearts in vitro. *J. Anat.* 168, 257–263.
 - Manzanares, M., and Nieto, M.Á. (2003). A celebration of the new head and an evaluation of the new mouth. *Neuron* 37, 895–898.
 - Manzanares, M., Blanco, M.J., and Nieto, M.Á. (2004). Snail3 orthologues in vertebrates: Divergent members of the Snail zinc-finger gene family. *Dev. Genes Evol.* 214, 47–53.

- Mao, L.M.F., Boyle Anderson, E.A.T., and Ho, R.K. (2021). Anterior lateral plate mesoderm gives rise to multiple tissues and requires *tbx5a* function in left-right asymmetry, migration dynamics, and cell specification of late-addition cardiac cells. *Dev. Biol.* 472, 52–66.
- Markwald, R.R., Fitzharris, T.P., and Manasek, F.J. (1977). Structural development of endocardial cushions. *Am. J. Anat.* 148, 85–119.
- Martik, M.L., and Bronner, M.E. (2017). Regulatory Logic Underlying Diversification of the Neural Crest. *Trends Genet.* 33, 715–727.
- Martin, K.E., and Waxman, J.S. (2021). Atrial and sinoatrial node development in the zebrafish heart. *J. Cardiovasc. Dev. Dis.* 8, 1–17.
- Martin, R.T., and Bartman, T. (2009). Analysis of heart valve development in larval zebrafish. *Dev. Dyn.* 238, 1796–1802.
- Martin, J.F., Bradley, A., and Olson, E.N. (1995). The paired-like homeo box gene *MHox* is required for early events of skeletogenesis in multiple lineages. *Genes Dev.* 9, 1237–1249.
- Martínez-Estrada, O.M., Lettice, L.A., Essafi, A., Guadix, J.A., Slight, J., Velecela, V., Hall, E., Reichmann, J., Devenney, P.S., Hohenstein, P., et al. (2010). *Wt1* is required for cardiovascular progenitor cell formation through transcriptional control of *Snail* and *E-cadherin*. *Nat. Genet.* 42, 89–93.
- Masel, J., and Siegal, M.L. (2009). Robustness: mechanisms and consequences. *Trends Genet.* 25, 395–403.
- Maya-Ramos, L., Cleland, J., Bressan, M., and Mikawa, T. (2013). Induction of the proepicardium. *J. Dev. Biol.* 1, 82–91.
- McCormack, N., and O’Dea, S. (2013). Regulation of epithelial to mesenchymal transition by bone morphogenetic proteins. *Cell. Signal.* 25, 2856–2862.
- McCulley, D.J., and Black, B.L. (2012). Chapter Nine: Transcription Factor Pathways and Congenital Heart Disease. In *Current Topics in Developmental Biology*, (Elsevier Inc.), pp. 253–277.
- McElhinney, D.B., Geiger, E., Blinder, J., Benson, D.W., and Goldmuntz, E. (2003). *NKX2.5* Mutations in Patients with Congenital Heart Disease. *J. Am. Coll. Cardiol.* 42, 1650–1655.
- McGrath, J., Somlo, S., Makova, S., Tian, X., and Brueckner, M. (2003). Two populations of node monocilia initiate left-right asymmetry in the mouse. *Cell* 114, 61–73.
- Meilhac, S.M., and Buckingham, M.E. (2018). The deployment of cell lineages that form

Bibliography

- the mammalian heart. *Nat. Rev. Cardiol.* *15*, 705–724.
- Meilhac, S.M., Esner, M., Kelly, R.G., Nicolas, J.F., and Buckingham, M.E. (2004). The clonal origin of myocardial cells in different regions of the embryonic mouse heart. *Dev. Cell* *6*, 685–698.
 - Mendes, R. V., Martins, G.G., Cristovão, A.M., and Saúde, L. (2014). N-cadherin locks left-right asymmetry by ending the leftward movement of hensen’s node cells. *Dev. Cell* *30*, 353–360.
 - Meno, C., Shimono, A., Saijoh, Y., Yashiro, K., Mochida, K., Ohishi, S., Noji, S., Kondoh, H., and Hamada, H. (1998). Lefty-1 Is Required for Left-Right Determination As a Regulator of Lefty-2 and Nodal. *Cell* *94*, 287–297.
 - Minegishi, K., Hashimoto, M., Ajima, R., Takaoka, K., Shinohara, K., Ikawa, Y., Nishimura, H., McMahon, A.P., Willert, K., Okada, Y., et al. (2017). A Wnt5 Activity Asymmetry and Intercellular Signaling via PCP Proteins Polarize Node Cells for Left-Right Symmetry Breaking. *Dev. Cell* *40*, 439–452.
 - Misfeldt, A.M., Boyle, S.C., Tompkins, K.L., Bautch, V.L., Labosky, P.A., and Baldwin, H.S. (2009). Endocardial cells are a distinct endothelial lineage derived from Flk1+ multipotent cardiovascular progenitors. *Dev. Biol.* *333*, 78–89.
 - Mjaatvedt, C.H., Nakaoka, T., Moreno-Rodriguez, R., Norris, R.A., Kern, M.J., Eisenberg, C.A., Turner, D., and Markwald, R.R. (2001). The outflow tract of the heart is recruited from a novel heart-forming field. *Dev. Biol.* *238*, 97–109.
 - Mogi, K., and Toyozumi, R. (2010). Invasion by matrix metalloproteinase-expressing cells is important for primitive streak formation in early chick blastoderm. *Cells Tissues Organs* *192*, 1–16.
 - Moreno-Ayala, R., Olivares-Chauvet, P., Schäfer, R., and Junker, J.P. (2021). Variability of an Early Developmental Cell Population Underlies Stochastic Laterality Defects. *Cell Rep.* *34*, 1–8.
 - Mosimann, C., Panáková, D., Werdich, A.A., Musso, G., Burger, A., Lawson, K.L., Carr, L.A., Nevis, K.R., Sabeh, M.K., Zhou, Y., et al. (2015). Chamber identity programs drive early functional partitioning of the heart. *Nat. Commun.* *6*, 1–10.
 - Moskowitz, I.P.G., Pizard, A., Patel, V. V., Bruneau, B.G., Kim, J.B., Kupersmidt, S., Roden, D., Berul, C.I., Seidman, C.E., and Seidman, J.G. (2004). The T-Box transcription factor Tbx5 is required for the patterning and maturation of the murine cardiac conduction system. *Dev.* *131*, 4107–4116.

- Moskowitz, I.P.G., Kim, J.B., Moore, M.L., Wolf, C.M., Peterson, M.A., Shendure, J., Nobrega, M.A., Yokota, Y., Berul, C., Izumo, S., et al. (2007). A Molecular Pathway Including Id2, Tbx5, and Nkx2-5 Required for Cardiac Conduction System Development. *Cell* 129, 1365–1376.
- Mou, H., Smith, J.L., Peng, L., Yin, H., Moore, J., Zhang, X.O., Song, C.Q., Sheel, A., Wu, Q., Ozata, D.M., et al. (2017). CRISPR/Cas9-mediated genome editing induces exon skipping by alternative splicing or exon deletion. *Genome Biol.* 18, 4–11.
- Mulas, C., Chaigne, A., Smith, A., and Chalut, K.J. (2021). Cell state transitions: definitions and challenges. *Dev.* 148, 1–6.
- Müller, P., Rogers, K.W., Jordan, B.M., Lee, J.S., Robson, D., Ramanathan, S., and Schier, A.F. (2012). Differential diffusivity of nodal and lefty underlies a reaction-diffusion patterning system. *Sci. (New York)* 336, 721–724.
- Murray, S.A., and Gridley, T. (2006). Snail family genes are required for left-right asymmetry determination, but not neural crest formation, in mice. *Proc. Natl. Acad. Sci. U. S. A.* 103, 10300–10304.
- Nakamura, T., and Hamada, H. (2012). Left-right patterning: Conserved and divergent mechanisms. *Dev.* 139, 3257–3262.
- Nakamura, T., Mine, N., Nakaguchi, E., Mochizuki, A., Yamamoto, M., Yashiro, K., Meno, C., and Hamada, H. (2006). Generation of Robust Left-Right Asymmetry in the Mouse Embryo Requires a Self-Enhancement and Lateral-Inhibition System. *Dev. Cell* 11, 495–504.
- Nakamura, T., Saito, D., Kawasumi, A., Shinohara, K., Asai, Y., Takaoka, K., Dong, F., Takamatsu, A., Belo, J.A., Mochizuki, A., et al. (2012). Fluid flow and interlinked feedback loops establish left-right asymmetric decay of Cerl2 mRNA. *Nat. Commun.* 3, 1–13.
- Nattel, S., Heijman, J., Zhou, L., and Dobrev, D. (2020). Molecular Basis of Atrial Fibrillation Pathophysiology and Therapy: A Translational Perspective. *Circ. Res.* 51–72.
- Nevis, K., Obregon, P., Walsh, C., Guner-Ataman, B., Burns, C.G., and Burns, C.E. (2013). Tbx1 is required for second heart field proliferation in zebrafish. *Dev. Dyn.* 242, 550–559.
- Newbury-Ecob, R., Leanage, R., Raeburn, J.A., and Young, I.D. (1996). Holt-Oram syndrome: a clinical genetic study. *F. Med Genet* 33, 300–307.
- Nicoli, S., Standley, C., Walker, P., Hurlstone, A., Fogarty, K.E., and Lawson, N.D. (2010). MicroRNA-mediated integration of haemodynamics and Vegf signalling during angiogenesis. *Nature* 464, 1196–1200.

Bibliography

- Nielsen, J.B., Thorolfsson, R.B., Fritsche, L.G., Zhou, W., Skov, M.W., Graham, S.E., Herron, T.J., McCarthy, S., Schmidt, E.M., Sveinbjornsson, G., et al. (2018). Biobank-driven genomic discovery yields new insight into atrial fibrillation biology. *Nat. Genet.* *50*, 1234–1239.
- Nieto, M.A. (2013). Epithelial plasticity: A common theme in embryonic and cancer cells. *Sci. (New York)* *342*, 1–7.
- Nieto, M.A. (2017). Context-specific roles of EMT programmes in cancer cell dissemination. *Nat. Cell Biol.* *19*, 416–418.
- Nieto, M.A., Bennett, M.F., Sargent, M.G., and Wilkinson, D.G. (1992). Cloning and developmental expression of *Sna*, a murine homologue of the *Drosophila* snail gene. *Dev.* *116*, 227–237.
- Nieto, M.A., Huang, R.Y.Y.J., Jackson, R.A.A., and Thiery, J.P.P. (2016). EMT: 2016. *Cell* *166*, 21–45.
- Nieto, M.Á., Sargent, M.G., Wilkinson, D.G., and Cooke, J. (1994). Control of Cell Behavior During Vertebrate Development by *Slug*, a Zinc Finger Gene. *Sci. (New York)* *264*, 835–839.
- Noël, E.S., Verhoeven, M., Lagendijk, A.K., Tessadori, F., Smith, K., Choorapoikayil, S., Den Hertog, J., and Bakkers, J. (2013). A Nodal-independent and tissue-intrinsic mechanism controls heart-looping chirality. *Nat. Commun.* *4*, 1–9.
- Nonaka, S., Yoshida, S., Watanabe, D., Ikeuchi, S., Goto, T., Marshall, W.F., and Hamada, H. (2005). De novo formation of left-right asymmetry by posterior tilt of nodal cilia. *PLoS Biol.* *3*, 1467–1472.
- Norris, D.P. (2012). Cilia, calcium and the basis of left-right asymmetry. *BMC Biol.* *10*, 1–8.
- Norris, R.A., and Kern, M.J. (2001). The Identification of *Prx1* Transcription Regulatory Domains Provides a Mechanism for Unequal Compensation by the *Prx1* and *Prx2* Loci. *J. Biol. Chem.* *276*, 26829–26837.
- Novodvorsky, P., Watson, O., Gray, C., Wilkinson, R.N., Reeve, S., Smythe, C., Beniston, R., Plant, K., Maguire, R., Rothman, A.M.K., et al. (2015). *Klf2ash317* mutant zebrafish do not recapitulate morpholino-induced vascular and haematopoietic phenotypes. *PLoS One* *10*, 1–22.
- Ocaña, O.H., Córcoles, R., Fabra, Á., Moreno-Bueno, G., Acloque, H., Vega, S., Barralío-Gimeno, A., Cano, A., and Nieto, M.A. (2012). Metastatic Colonization Requires the

- Repression of the Epithelial-Mesenchymal Transition Inducer Prrx1. *Cancer Cell* 22, 709–724.
- Ocaña, O.H., Coskun, H., Minguillón, C., Murawala, P., Tanaka, E.M., Galcerán, J., Muñoz-Chápuli, R., and Nieto, M.A. (2017). A right-handed signalling pathway drives heart looping in vertebrates. *Nature* 549, 86–90.
 - Okabe, N., Xu, B., and Burdine, R.D. (2008). Fluid dynamics in zebrafish Kupffer's vesicle. *Dev. Dyn.* 237, 3602–3612.
 - Okada, Y., Takeda, S., Tanaka, Y., Belmonte, J.C.I., and Hirokawa, N. (2005). Mechanism of nodal flow: A conserved symmetry breaking event in left-right axis determination. *Cell* 121, 633–644.
 - Oki, S., Hashimoto, R., Okui, Y., Shen, M.M., Mekada, E., Otani, H., Saijoh, Y., and Hamada, H. (2007). Sulfated glycosaminoglycans are necessary for Nodal signal transmission from the node to the left lateral plate in the mouse embryo. *Dev.* 134, 3893–3904.
 - Oteiza, P., Köppen, M., Concha, M.L., and Heisenberg, C.P. (2008). Origin and shaping of the laterality organ in zebrafish. *Dev.* 135, 2807–2813.
 - Van Ouwerkerk, A.F., Hall, A.W., Kadow, Z.A., Lazarevic, S., Reyat, J.S., Tucker, N.R., Nadadur, R.D., Bosada, F.M., Bianchi, V., Ellinor, P.T., et al. (2020). Epigenetic and Transcriptional Networks Underlying Atrial Fibrillation. *Circ. Res.* 34–50.
 - Paffett-Lugassy, N., Novikov, N., Jeffrey, S., Abrial, M., Guner-Ataman, B., Sakthivel, S., Burns, C.E., and Burns, C.G. (2017). Unique developmental trajectories and genetic regulation of ventricular and outflow tract progenitors in the zebrafish second heart field. *Dev.* 144, 4616–4624.
 - Parker, L.H., Schmidt, M., Jin, S.W., Gray, A.M., Beis, D., Pham, T., Frantz, G., Palmieri, S., Hillan, K., Stainier, D.Y.R., et al. (2004). The endothelial-cell-derived secreted factor Egf17 regulates vascular tube formation. *Nature* 428, 754–758.
 - Pastushenko, I., and Blanpain, C. (2019). EMT Transition States during Tumor Progression and Metastasis. *Trends Cell Biol.* 29, 212–226.
 - Patel, K., Isaac, A., and Cooke, J. (1999). Nodal signalling and the roles of the transcription factors Snr and Pitx2 in vertebrate left-right asymmetry. *Curr. Biol.* 9, 609–612.
 - de Pater, E., Clijsters, L., Marques, S.R., Lin, Y.F., Garavito-Aguilar, Z. V., Yelon, D., and Bakkens, J. (2009). Distinct phases of cardiomyocyte differentiation regulate growth of the zebrafish heart. *Dev.* 136, 1633–1641.
 - Patten, B.M. (1922). The formation of the cardiac loop in the chick. *Am. J. Anat* 30, 373–

Bibliography

397.

- Peng, W., Song, R., and Acar, M. (2016). Noise reduction facilitated by dosage compensation in gene networks. *Nat. Commun.* 7, 1–8.
- Peralta, M., Steed, E., Harlepp, S., González-Rosa, J.M., Monduc, F., Ariza-Cosano, A., Cortés, A., Rayón, T., Gómez-Skarmeta, J.L., Zapata, A., et al. (2013). Heartbeat-driven pericardiac fluid forces contribute to epicardium morphogenesis. *Curr. Biol.* 23, 1726–1735.
- Pi-Roig, A., Martin-Blanco, E., and Minguillon, C. (2014). Distinct tissue-specific requirements for the zebrafish *tbx5* genes during heart, retina and pectoral fin development. *Open Biol.* 4.
- Pierpont, M.E., Brueckner, M., Chung, W.K., Garg, V., Lacro, R. V., McGuire, A.L., Mital, S., Priest, J.R., Pu, W.T., Roberts, A., et al. (2018). Genetic Basis for Congenital Heart Disease: Revisited: A Scientific Statement from the American Heart Association. *Circulation* 138, 653–711.
- Popp, M.W., and Maquat, L.E. (2016). Leveraging rules of nonsense-mediated mRNA decay for genome engineering and personalized medicine. *Cell* 165, 1319–1322.
- Prall, O.W.J., Menon, M.K., Solloway, M.J., Watanabe, Y., Zaffran, S., Bajolle, F., Biben, C., McBride, J.J., Robertson, B.R., Chaulet, H., et al. (2007). An *Nkx2-5/Bmp2/Smad1* Negative Feedback Loop Controls Heart Progenitor Specification and Proliferation. *Cell* 128, 947–959.
- Priya, R., Allanki, S., Gentile, A., Mansingh, S., Uribe, V., Maischein, H.M., and Stainier, D.Y.R. (2020). Tension heterogeneity directs form and fate to pattern the myocardial wall. *Nature* 588, 130–134.
- Prummel, K.D., Nieuwenhuize, S., and Mosimann, C. (2020). The lateral plate mesoderm. *Dev.* 147, 1–10.
- Puisieux, A., Brabletz, T., and Caramel, J. (2014). Oncogenic roles of EMT-inducing transcription factors. *Nat. Cell Biol.* 16, 488–494.
- De Putte, T. Van, Maruhashi, M., Francis, A., Nelles, L., Kondoh, H., Huylebroeck, D., and Higashi, Y. (2003). Mice lacking *Zfhx1b*, the gene that codes for Smad-interacting protein-1, reveal a role for multiple neural crest cell defects in the etiology of hirschsprung disease-mental retardation syndrome. *Am. J. Hum. Genet.* 72, 465–470.
- Qiao, L., Gao, H., Zhang, T., Jing, L., Xiao, C., Xiao, Y., Luo, N., Zhu, H., Meng, W., Xu, H., et al. (2014). Snail modulates the assembly of fibronectin via $\alpha 5$ integrin for myocardial

- migration in zebrafish embryos. *Sci. Rep.* 4, 1–6.
- Qiu, D., Cheng, S.M., Wozniak, L., McSweeney, M., Perrone, E., and Levin, M. (2005). Localization and loss-of-function implicates ciliary proteins in early, cytoplasmic roles in left-right asymmetry. *Dev. Dyn.* 234, 176–189.
 - Rago, L., Castroviejo, N., Fazilaty, H., Garcia-Asencio, F., Ocaña, O.H., Galcerán, J., and Nieto, M.A. (2019). MicroRNAs Establish the Right-Handed Dominance of the Heart Laterality Pathway in Vertebrates. *Dev. Cell* 51, 446-459.e5.
 - Ramasubramanian, A., Chu-Lagraff, Q.B., Buma, T., Chico, K.T., Carnes, M.E., Burnett, K.R., Bradner, S.A., and Gordon, S.S. (2013). On the role of intrinsic and extrinsic forces in early cardiac S-looping. *Dev. Dyn.* 242, 801–816.
 - Ramsdell, A.F. (2005). Left-right asymmetry and congenital cardiac defects: Getting to the heart of the matter in vertebrate left-right axis determination. *Dev. Biol.* 288, 1–20.
 - Rana, M.S., Théveniau-Ruissy, M., De Bono, C., Mesbah, K., Francou, A., Rammah, M., Domínguez, J.N., Roux, M., Laforest, B., Anderson, R.H., et al. (2014). Tbx1 coordinates addition of posterior second heart field progenitor cells to the arterial and venous poles of the heart. *Circ. Res.* 115, 790–799.
 - Ray, P., Chin, A.S., Worley, K.E., Fan, J., Kaur, G., Wu, M., and Wan, L.Q. (2018). Intrinsic cellular chirality regulates left–right symmetry breaking during cardiac looping. *Proc. Natl. Acad. Sci. U. S. A.* 115, 11568–11577.
 - Reichert, M., Takano, S., Von Burstin, J., Kim, S.B., Lee, J.S., Ihida-Stansbury, K., Hahn, C., Heeg, S., Schneider, G., Rhim, A.D., et al. (2013). The Prrx1 homeodomain transcription factor plays a central role in pancreatic regeneration and carcinogenesis. *Genes Dev.* 27, 288–300.
 - Reik, W. (2007). Stability and flexibility of epigenetic gene regulation in mammalian development. *Nature* 447, 425–432.
 - Reiter, J.F., Alexander, J., Rodaway, A., Yelon, D., Patient, R., Holder, N., and Stainier, D.Y.R. (1999). Gata5 is required for the development of the heart and endoderm in zebrafish. *Genes Dev.* 13, 2983–2995.
 - Rembold, M., Ciglar, L., Omar Yáñez-Cuna, J., Zinzen, R.P., Girardot, C., Jain, A., Welte, M.A., Stark, A., Leptin, M., and Furlong, E.E.M. (2014). A conserved role for Snail as a potentiator of active transcription. *Genes Dev.* 28, 167–181.
 - Risebro, C.A., Smart, N., Dupays, L., Breckenridge, R., Mohun, T.J., and Riley, P.R. (2006). Hand1 regulates cardiomyocyte proliferation versus differentiation in the developing

Bibliography

- heart. *Dev.* *133*, 4595–4606.
- Roberts, R.M., Katayama, M., Magnuson, S.R., Falduto, M.T., and Torres, K.E.O. (2011). Transcript profiling of individual twin blastomeres derived by splitting two-cell stage murine embryos. *Biol. Reprod.* *84*, 487–494.
 - Rochais, F., Mesbah, K., and Kelly, R.G. (2009). Signaling pathways controlling second heart field development. *Circ. Res.* *104*, 933–942.
 - Rodriguez-Boulan, E., and Macara, I.G. (2014). Organization and execution of the epithelial polarity programme. *Nat. Rev. Mol. Cell Biol.* *15*, 225–242.
 - Rohr, S., Otten, C., and Abdelilah-Seyfried, S. (2008). Asymmetric involution of the myocardial field drives heart tube formation in zebrafish. *Circ. Res.* *102*, 12–19.
 - Roselli, C., Roselli, C., Rienstra, M., Ellinor, P.T., and Ellinor, P.T. (2020). Genetics of Atrial Fibrillation in 2020: GWAS, Genome Sequencing, Polygenic Risk, and beyond. *Circ. Res.* 21–33.
 - Rosenquist, G.C. (1970). Location and movements of cardiogenic cells in the chick embryo: The heart-forming portion of the primitive streak. *Dev. Biol.* *22*, 461–475.
 - Rossi, A., Kontarakis, Z., Gerri, C., Nolte, H., Hölper, S., Krüger, M., and Stainier, D.Y.R. (2015). Genetic compensation induced by deleterious mutations but not gene knockdowns. *Nature* *524*, 230–233.
 - Ryan, K., and Chin, A.J. (2003). T-box genes and cardiac development. *Birth Defects Res. Part C - Embryo Today Rev.* *69*, 25–37.
 - Ryan, A.K., Blumberg, B., Rodriguez-Esteban, C., Yonei-Tamura, S., Tamura, K., Tsukui, T., De La Peña, J., Sabbagh, W., Greenwald, J., Choe, S., et al. (1998). Pitx2 determines left-right asymmetry of internal organs in vertebrates. *Nature* *394*, 545–551.
 - Ryckebusch, L., Wang, Z., Bertrand, N., Lin, S.C., Chi, X., Schwartz, R., Zaffran, S., and Niederreither, K. (2008). Retinoic acid deficiency alters second heart field formation. *Proc. Natl. Acad. Sci. U. S. A.* *105*, 2913–2918.
 - Sage, J., Miller, A.L., Pérez-Mancera, P.A., Wysocki, J.M., and Jacks, T. (2003). Acute mutation of retinoblastoma gene function is sufficient for cell cycle re-entry. *Nature* *424*, 223–228.
 - Saijoh, Y., Oki, S., Ohishi, S., and Hamada, H. (2003). Left-right patterning of the mouse lateral plate requires Nodal produced in the node. *Dev. Biol.* *256*, 161–173.
 - Sampaio, P., Ferreira, R.R., Guerrero, A., Pintado, P., Tavares, B., Amaro, J., Smith, A.A., Montenegro-Johnson, T., Smith, D.J., and Lopes, S.S. (2014). Left-right organizer flow

- dynamics: How much cilia activity reliably yields laterality? *Dev. Cell* 29, 716–728.
- Sauer, S., and Klar, A.J.S. (2012). Left-right symmetry breaking in mice by left-right dynein may occur via a biased chromatid segregation mechanism, without directly involving the Nodal gene. *Front. Oncol.* 2, 1–10.
 - Scarpa, E., and Mayor, R. (2016). Collective cell migration in development. *J. Cell Biol.* 212, 143–155.
 - Schaks, M., Giannone, G., and Rottner, K. (2019). Actin dynamics in cell migration. *Essays Biochem.* 63, 483–495.
 - Schindler, Y.L., Garske, K.M., Wang, J., Firulli, B.A., Firulli, A.B., Poss, K.D., and Yelon, D. (2014). Hand2 elevates cardiomyocyte production during zebrafish heart development and regeneration. *Dev.* 141, 3112–3122.
 - Schlueter, J., and Brand, T. (2013). Left-right asymmetrical development of the proepicardium. *J. Dev. Biol.* 1, 126–140.
 - Schlueter, J., Männer, J., and Brand, T. (2006). BMP is an important regulator of proepicardial identity in the chick embryo. *Dev. Biol.* 295, 546–558.
 - Schottenfeld, J., Sullivan-Brown, J., and Burdine, R.D. (2007). Zebrafish curly up encodes a Pkd2 ortholog that restricts left-side-specific expression of southpaw. *Dev.* 134, 1605–1615.
 - Schulte, I., Schlueter, J., Abu-Issa, R., Brand, T., and Männer, J. (2007). Morphological and molecular left-right asymmetries in the development of the proepicardium: A comparative analysis on mouse and chick embryos. *Dev. Dyn.* 236, 684–695.
 - Schweickert, A., Ott, T., Kurz, S., Tingler, M., Maerker, M., Fuhl, F., and Blum, M. (2017). Vertebrate Left-Right Asymmetry: What Can Nodal Cascade Gene Expression Patterns Tell Us? *J. Cardiovasc. Dev. Dis.* 5, 1–12.
 - Sefton, M., Sánchez, S., and Nieto, M.A. (1998). Conserved and divergent roles for members of the Snail family of transcription factors in the chick and mouse embryo. *Dev.* 125, 3111–3121.
 - Serluca, F.C. (2008). Development of the proepicardial organ in the zebrafish. *Dev. Biol.* 315, 18–27.
 - Shi, L., Tang, X., Qian, M., Liu, Z., Meng, F., Fu, L., Wang, Z., Zhu, W.G., Huang, J.D., Zhou, Z., et al. (2018). A SIRT1-centered circuitry regulates breast cancer stemness and metastasis. *Oncogene* 37, 6299–6315.
 - Shi, Y., Yao, J., Xu, G., and Taber, L.A. (2014). Bending of the looping heart: Differential

Bibliography

- growth revisited. *J. Biomech. Eng.* *136*, 1–15.
- Shimozaki, K., Clemenson, G.D., and Gage, F.H. (2013). Paired related homeobox protein 1 is a regulator of stemness in adult neural stem/progenitor cells. *J. Neurosci.* *33*, 4066–4075.
 - Shiratori, H., and Hamada, H. (2006). The left-right axis in the mouse: From origin to morphology. *Dev.* *133*, 2095–2104.
 - Shiratori, H., Yashiro, K., Shen, M.M., and Hamada, H. (2006). Conserved regulation and role of Pitx2 in situs-specific morphogenesis of visceral organs. *Dev.* *133*, 3015–3025.
 - Singleman, C., and Holtzman, N.G. (2012). Analysis of postembryonic heart development and maturation in the zebrafish, *Danio rerio*. *Dev. Dyn.* *241*, 1993–2004.
 - Smith, K.A., and Uribe, V. (2021). Getting to the heart of left–right asymmetry: Contributions from the zebrafish model. *J. Cardiovasc. Dev. Dis.* *8*, 1–12.
 - Smith, K.A., Uribe, V., Hamada, H., Grimes, D.T., Burdine, R.D., Ferreira, R.R., Vermot, J., Coutelis, J., González-Morales, N., Géminard, C., et al. (2006). Molecular and cellular basis of left-right asymmetry in vertebrates. *J. Cardiovasc. Dev. Dis.* *5*, 273–296.
 - Smith, K.A., Chocron, S., von der Hardt, S., de Pater, E., Soufan, A., Bussmann, J., Schulte-Merker, S., Hammerschmidt, M., and Bakkers, J. (2008). Rotation and Asymmetric Development of the Zebrafish Heart Requires Directed Migration of Cardiac Progenitor Cells. *Dev. Cell* *14*, 287–297.
 - Smith, K.A., Noël, E., Thurlings, I., Rehmann, H., Chocron, S., and Bakkers, J. (2011). Bmp and Nodal independently regulate *lefty1* expression to maintain unilateral Nodal activity during left-right axis specification in zebrafish. *PLoS Genet.* *7*, 1–13.
 - Snow, M.H.L., and Tam, P.P.L. (1979). Is compensatory growth a complicating factor in mouse teratology? *Nature* *279*, 555–557.
 - Soo, K., O’Rourke, M.P., Khoo, P.L., Steiner, K.A., Wong, N., Behringer, R.R., and Tam, P.P.L. (2002). Twist function is required for the morphogenesis of the cephalic neural tube and the differentiation of the cranial neural crest cells in the mouse embryo. *Dev. Biol.* *247*, 251–270.
 - Stainier, D.Y.R., Lee, R.K., and Fishman, M.C. (1993). Cardiovascular development in the zebrafish: I. Myocardial fate map and heart tube formation. *Dev.* *119*, 31–40.
 - Stainier, D.Y.R., Raz, E., Lawson, N.D., Ekker, S.C., Burdine, R.D., Eisen, J.S., Ingham, P.W., Schulte-Merker, S., Yelon, D., Weinstein, B.M., et al. (2017). Guidelines for morpholino use in zebrafish. *PLoS Genet.* *13*, 6–10.

- Stalsberg, H., and Dehaan, R.L. (1969). The Precardiac Areas and Formation of the Tubular Heart in the Chick Embryo. *Dev. Biol.* *19*, 128–159.
- Stark, K., Vainio, S., Vassileva, G., and McMahon, A.P. (1994). Epithelial transformation of metanephric mesenchyme in the developing kidney regulated by Wnt-4. *Nature* *372*, 679–683.
- Staudt, D., and Stainier, D. (2012). Uncovering the molecular and cellular mechanisms of heart development using the zebrafish. *Annu. Rev. Genet.* *46*, 397–418.
- Staudt, D.W., Liu, J., Thorn, K.S., Stuurman, N., Liebling, M., and Stainier, D.Y.R. (2014). High-resolution imaging of cardiomyocyte behavior reveals two distinct steps in ventricular trabeculation. *Dev.* *141*, 585–593.
- Steimle, J.D., and Moskowitz, I.P. (2017). Chapter seven: TBX5: A Key Regulator of Heart Development. In *Current Topics in Developmental Biology*, (Elsevier Inc.), pp. 195–221.
- Stemmler, M.P., Eccles, R.L., Brabletz, S., and Brabletz, T. (2019). Non-redundant functions of EMT transcription factors. *Nat. Cell Biol.* *21*, 102–112.
- Sulaiman, F.A., Nishimoto, S., Murphy, G.R.F., Kucharska, A., Butterfield, N.C., Newbury-Ecob, R., and Logan, M.P.O. (2016). Tbx5 Buffers Inherent Left/Right Asymmetry Ensuring Symmetric Forelimb Formation. *PLoS Genet.* *12*, 1–18.
- Sun, J.H., Zhang, Y., Yin, B.Y., Li, J.X., Liu, G.S., Xu, W., and Tang, S. (2012). Differential expression of Axin1, Cdc25c and Cdkn2d mRNA in 2-cell stage mouse blastomeres. *Zygote* *20*, 305–310.
- Suster, M.L., Abe, G., Schouw, A., and Kawakami, K. (2011). Transposon-mediated BAC transgenesis in zebrafish. *Nat. Protoc.* *6*, 1998–2021.
- Taber, L.A., Lin, I.-En, and Clark, E.B. (1995). Mechanics of cardiac looping. *Dev. Dyn.* *203*, 42–50.
- Taber, L.A., Voronov, D.A., and Ramasubramanian, A. (2010). The role of mechanical forces in the torsional component of cardiac looping. *Ann. N. Y. Acad. Sci.* *1188*, 103–110.
- Tabin, C.J., and Vogon, K.J. (2003). A two-cilia model for vertebrate left-right axis specification. *Genes Dev.* *17*, 1–6.
- Tam, P.P.L., and Beddington, R.S.P. (1987). The formation of mesodermal tissues in the mouse embryo during gastrulation and early organogenesis. *Dev.* *99*, 109–126.
- Tam, P.P.L., Parameswaran, M., Kinder, S.J., and Weinberger, R.P. (1997). The allocation of epiblast cells to the embryonic heart and other mesodermal lineages: The role of ingression and tissue movement during gastrulation. *Dev.* *124*, 1631–1642.

Bibliography

- Tanaka, Y., Okada, Y., and Hirokawa, N. (2005). FGF-induced vesicular release of Sonic hedgehog and retinoic acid in leftward nodal flow is critical for left-right determination. *Nature* 435, 172–177.
- Tao, G., Levay, A.K., Gridley, T., and Lincoln, J. (2011). Mmp15 is a direct target of Snai1 during endothelial to mesenchymal transformation and endocardial cushion development. *Dev. Biol.* 359, 209–221.
- Tessadori, F., van Weerd, J.H., Burkhard, S.B., Verkerk, A.O., de Pater, E., Boukens, B.J., Vink, A., Christoffels, V.M., and Bakkers, J. (2012). Identification and Functional Characterization of Cardiac Pacemaker Cells in Zebrafish. *PLoS One* 7, 1–9.
- Tessadori, F., de Bakker, D.E.M., Barske, L., Nelson, N., Algra, H.A., Willekers, S., Nichols, J.T., Crump, J.G., and Bakkers, J. (2020). Zebrafish *prrx1a* mutants have normal hearts. *Nature* 585, E14–E16.
- Tessadori, F., Tsingos, E., Colizzi, E.S., Kruse, F., Van Den Brink, S.C., Van Den Boogaard, M., Christoffels, V.M., Merks, R.M.H., and Bakkers, J. (2021). Twisting of the zebrafish heart tube during cardiac looping is a *tbx5*-dependent and tissue-intrinsic process. *Elife* 10, 1–34.
- Thiery, J.P., Acloque, H., Huang, R.Y.J., and Nieto, M.A. (2009). Epithelial-Mesenchymal Transitions in Development and Disease. *Cell* 139, 871–890.
- Thisse, B., Stoetzel, C., Gorostiza-Thisse, C., and Perrin-Schmitt, F. (1988). Sequence of the twist gene and nuclear localization of its protein in endomesodermal cells of early *Drosophila* embryos. *EMBO J.* 7, 2175–2183.
- Tondeleir, D., Lambrechts, A., Müller, M., Jonckheere, V., Doll, T., Vandamme, D., Bakkali, K., Waterschoot, D., Lemaistre, M., Debeir, O., et al. (2012). Cells lacking β -actin are genetically reprogrammed and maintain conditional migratory capacity. *Mol. Cell. Proteomics* 11, 255–271.
- Tran, D.D., Corsa, C.A.S., Biswas, H., Aft, R.L., and Longmore, G.D. (2011). Temporal and spatial cooperation of Snail1 and Twist1 during epithelial-mesenchymal transition predicts for human breast cancer recurrence. *Mol. Cancer Res.* 9, 1644–1657.
- Tran, H.D., Luitel, K., Kim, M., Zhang, K., Longmore, G.D., and Tran, D.D. (2014). Transient SNAIL1 expression is necessary for metastatic competence in breast cancer. *Cancer Res.* 74, 6330–6340.
- Triedman, J.K., and Newburger, J.W. (2016). Trends in congenital heart disease. *Circulation* 133, 2716–2733.

- Trinh, L.A., and Stainier, D.Y.R. (2004). Cardiac development. *Methods Cell Biol.* 2004, 455–473.
- Tucker, N.R., Dolmatova, E. V., Lin, H., Cooper, R.R., Ye, J., Hucker, W.J., Jameson, H.S., Parsons, V.A., Weng, L.C., Mills, R.W., et al. (2017). Diminished PRRX1 Expression Is Associated with Increased Risk of Atrial Fibrillation and Shortening of the Cardiac Action Potential. *Circ. Cardiovasc. Genet.* 10, 1–12.
- Tyser, R.C.V., Ibarra-Soria, X., McDole, K., Jayaram, S.A., Godwin, J., Brand, T.A.H.V. Den, Miranda, A.M.A., Scialdone, A., Keller, P.J., Marioni, J.C., et al. (2021). Characterization of a common progenitor pool of the epicardium and myocardium. *Sci. (New York)* 371, 1–17.
- Tzouanacou, E., Wegener, A., Wymeersch, F.J., Wilson, V., and Nicolas, J.F. (2009). Redefining the Progression of Lineage Segregations during Mammalian Embryogenesis by Clonal Analysis. *Dev. Cell* 17, 365–376.
- Vakulskas, C.A., Dever, D.P., Rettig, G.R., Turk, R., Jacobi, A.M., Collingwood, M.A., Bode, N.M., McNeill, M.S., Yan, S., Camarena, J., et al. (2018). A high-fidelity Cas9 mutant delivered as a ribonucleoprotein complex enables efficient gene editing in human hematopoietic stem and progenitor cells. *Nat. Med.* 24, 1216–1224.
- Vandenberg, L.N., and Levin, M. (2013). A unified model for left-right asymmetry? Comparison and synthesis of molecular models of embryonic laterality. *Dev. Biol.* 379, 1–15.
- Veerkamp, J., Rudolph, F., Cseresnyes, Z., Priller, F., Otten, C., Renz, M., Schaefer, L., and Abdelilah-Seyfried, S. (2013). Unilateral Dampening of Bmp Activity by Nodal Generates Cardiac Left-Right Asymmetry. *Dev. Cell* 24, 660–667.
- Vega, S., Morales, A. V., Ocaña, O.H., Valdés, F., Fabregat, I., and Nieto, M.A. (2004). Snail blocks the cell cycle and confers resistance to cell death. *Genes Dev.* 18, 1131–1143.
- Verschuere, K., Remacle, J.E., Collart, C., Kraft, H., Baker, B.S., Tylzanowski, P., Nelles, L., Wuytens, G., Su, M.T., Bodmer, R., et al. (1999). SIP1, a novel zinc finger/homeodomain repressor, interacts with Smad proteins and binds to 5'-CACCT sequences in candidate target genes. *J. Biol. Chem.* 274, 20489–20498.
- Victorino, J., Alvarez-Franco, A., and Manzanares, M. (2021). Functional genomics and epigenomics of atrial fibrillation. *J. Mol. Cell. Cardiol.* 157, 45–55.
- Vincent, S.D., and Buckingham, M.E. (2010). How to make a heart. The origin and regulation of cardiac progenitor cells. *Curr. Top. Dev. Biol.* 90, 1–41.

Bibliography

- Vincent, S.D., Norris, D.P., Ann Le Good, J., Constam, D.B., and Robertson, E.J. (2004). Asymmetric Nodal expression in the mouse is governed by the combinatorial activities of two distinct regulatory elements. *Mech. Dev.* *121*, 1403–1415.
- Viotti, M., Niu, L., Shi, S.H., and Hadjantonakis, A.K. (2012). Role of the gut endoderm in relaying left-right patterning in mice. *PLoS Biol.* *10*, 1–16.
- Voronov, D.A., Alford, P.W., Xu, G., and Taber, L.A. (2004). The role of mechanical forces in dextral rotation during cardiac looping in the chick embryo. *Dev. Biol.* *272*, 339–350.
- Wagner, D.E., Weinreb, C., Collins, Z.M., Briggs, J.A., Megason, S.G., and Klein, A.M. (2018). Single-cell mapping of gene expression landscapes and lineage in the zebrafish embryo. *Sci. (New York)* *360*, 981–987.
- Waldo, K.L., Kumiski, D.H., Wallis, K.T., Stadt, H.A., Hutson, M.R., Platt, D.H., and Kirby, M.L. (2001). Conotruncal myocardium arises from a secondary heart field. *Dev.* *128*, 3179–3188.
- Wang, X., and Yost, H.J. (2008). Initiation and propagation of posterior to anterior (PA) waves in zebrafish left-right development. *Dev. Dyn.* *237*, 3640–3647.
- Wang, G., Cadwallader, A.B., Jang, D.S., Tsang, M., Yost, H.J., and Amack, J.D. (2011). The Rho kinase *rock2b* establishes anteroposterior asymmetry of the ciliated Kupffer’s vesicle in zebrafish. *Dev.* *138*, 45–54.
- Wang, G., Manning, M.L., and Amack, J.D. (2012). Regional cell shape changes control form and function of Kupffer’s vesicle in the zebrafish embryo. *Dev. Biol.* *370*, 52–62.
- Wang, Y., Wang, X., Wohland, T., and Sampath, K. (2016). Extracellular interactions and ligand degradation shape the nodal morphogen gradient. *Elife* *5*, 1–19.
- White, J.K., Gerdin, A.K., Karp, N.A., Ryder, E., Buljan, M., Bussell, J.N., Salisbury, J., Clare, S., Ingham, N.J., Podrini, C., et al. (2013). Genome-wide generation and systematic phenotyping of knockout mice reveals new roles for many genes. *Cell* *154*, 452.
- Wilkinson, M.F. (2019). Genetic paradox explained by nonsense. *Nature* *568*, 179–180.
- Witzel, H.R., Jungblut, B., Choe, C.P., Crump, J.G., Braun, T., and Dobрева, G. (2012). The LIM Protein Ajuba Restricts the Second Heart Field Progenitor Pool by Regulating *Isl1* Activity. *Dev. Cell* *23*, 58–70.
- Witzel, H.R., Cheedipudi, S., Gao, R., Stainier, D.Y.R., and Dobрева, G.D. (2017). *Isl2b* regulates anterior second heart field development in zebrafish. *Sci. Rep.* *7*, 1–9.
- Wolf, F.A., Angerer, P., and Theis, F.J. (2018). SCANPY: large-scale single-cell gene expression data analysis. *Genome Biol.* *19*, 1–5.

- Wu, L., Chu, M., and Zhuang, W. (2021). Association between ZFH3 and PRRX1 Polymorphisms and Atrial Fibrillation Susceptibility from Meta-Analysis. *Int. J. Hypertens.* 2021, 1–13.
- Wu, M., Smith, C.L., Hall, J.A., Lee, I., Luby-Phelps, K., and Tallquist, M.D. (2010). Epicardial Spindle Orientation Controls Cell Entry into the Myocardium. *Dev. Cell* 19, 114–125.
- Wu, R.S., Lam, I.I., Clay, H., Duong, D.N., Deo, R.C., and Coughlin, S.R. (2018). A Rapid Method for Directed Gene Knockout for Screening in G0 Zebrafish. *Dev. Cell* 46, 112–125.
- Xie, L., Hoffmann, A.D., Burnicka-Turek, O., Friedland-Little, J.M., Zhang, K., and Moskowitz, I.P. (2012). Tbx5-Hedgehog Molecular Networks Are Essential in the Second Heart Field for Atrial Septation. *Dev. Cell* 23, 280–291.
- Xu, Y., Lee, D.K., Feng, Z., Xu, Y., Bu, W., Li, Y., Liao, L., and Xu, J. (2017). Breast tumor cell-specific knockout of Twist1 inhibits cancer cell plasticity, dissemination, and lung metastasis in mice. *Proc. Natl. Acad. Sci. U. S. A.* 114, 11494–11499.
- Yang, J., Antin, P., Berx, G., Blanpain, C., Brabletz, T., Bronner, M., Campbell, K., Cano, A., Casanova, J., Christofori, G., et al. (2020). Guidelines and definitions for research on epithelial–mesenchymal transition. *Nat. Rev. Mol. Cell Biol.* 21, 341–352.
- Yelon, D., Horne, S.A., and Stainier, D.Y.R. (1999). Restricted expression of cardiac myosin genes reveals regulated aspects of heart tube assembly in zebrafish. *Dev. Biol.* 214, 23–37.
- Yoshida, S., Shiratori, H., Kuo, I.Y., Kawasumi, A., Kyosuke, Shinohara Shigenori, N., Asai, Y., Sasaki, G., Belo, J.A., Sasaki, H., Nakai, J., et al. (2012). Cilia at the Node of Mouse Embryos Sense Fluid Flow for Left-Right Determination via Pkd2. *Sci. (New York)* 338, 226–231.
- Yoshida, M., Kajikawa, E., Yamamoto, D., Kurokawa, D., Yonemura, S., Kobayashi, K., Kiyonari, H., and Aizawa, S. (2016). Conserved and divergent expression patterns of markers of axial development in the laboratory opossum, *Monodelphis domestica*. *Dev. Dyn.* 245, 1176–1188.
- Yoshioka, H., Meno, C., Koshiba, K., Sugihara, M., Itoh, H., Ishimaru, Y., Inoue, T., Ohuchi, H., Semina, E. V., Murray, J.C., et al. (1998). Pitx2, a bicoid-type homeobox gene, is involved in a lefty-signaling pathway in determination of left-right asymmetry. *Cell* 94, 299–305.
- Yuan, S., Zhao, L., Brueckner, M., and Sun, Z. (2015). Intraciliary calcium oscillations initiate vertebrate left-right asymmetry. *Curr. Biol.* 25, 556–567.

Bibliography

- Zaffran, S., Kelly, R.G., Meilhac, S.M., Buckingham, M.E., and Brown, N.A. (2004). Right ventricular myocardium derives from the anterior heart field. *Circ. Res.* 95, 261–268.
- Zeng, X.X.I., and Yelon, D. (2014). *Cadm4* restricts the production of cardiac outflow tract progenitor cells. *Cell Rep.* 7, 951–960.
- Zheng, X., Carstens, J.L., Kim, J., Scheible, M., Kaye, J., Sugimoto, H., Wu, C.C., Lebleu, V.S., and Kalluri, R. (2015). Epithelial-to-mesenchymal transition is dispensable for metastasis but induces chemoresistance in pancreatic cancer. *Nature* 527, 525–530.
- Zhou, Y., Cashman, T.J., Nevis, K.R., Obregon, P., Carney, S.A., Liu, Y., Gu, A., Mosimann, C., Sondalle, S., Peterson, R.E., et al. (2011). Latent TGF- β binding protein 3 identifies a second heart field in zebrafish. *Nature* 474, 645–648.
- Zimmer, A.M., Pan, Y.K., Chandrapalan, T., Kwong, R.W.M., and Perry, S.F. (2019). Loss-of-function approaches in comparative physiology: Is there a future for knockdown experiments in the era of genome editing? *J. Exp. Biol.* 222.
- Zimmerman, M.S., Smith, A.G.C., Sable, C.A., Echko, M.M., Wilner, L.B., Olsen, H.E., Atalay, H.T., Awasthi, A., Bhutta, Z.A., Boucher, J.L.A., et al. (2020). Global, regional, and national burden of congenital heart disease, 1990–2017: a systematic analysis for the Global Burden of Disease Study 2017. *Lancet Child Adolesc. Heal.* 4, 185–200.

ANNEX |

Matters arising

Reply to: Zebrafish *prrx1a* mutants have normal hearts

Noemi Castroviejo¹, Oscar H. Ocaña^{1,2}, Luciano Rago^{1,3}, Hakan Coskun^{1,4}, Aida Arcas^{1,5}, Joan Galcerán¹ & M. Angela Nieto¹ ✉

¹Instituto de Neurociencias (CSIC-UMH), Sant Joan d'Alacant, Alicante, Spain. ²Present address: Centro Nacional de Investigaciones Cardiovasculares (CNIC), Madrid, Spain. ³Present address: Department of Oncogenomics, Academic Medical Center, Amsterdam, The Netherlands. ⁴Present address: Boston Children's Hospital, Harvard Medical School, Harvard University, Boston, MA, USA. ⁵Present address: Centro de Investigación Médica Aplicada (CIMA), University of Navarra, Pamplona, Spain. ✉e-mail: anieto@umh.es

Replying to F. Tessadori et al. *Nature* <https://doi.org/10.1038/s41586-020-2674-1> (2020)

Published online: 23 September 2020

<https://doi.org/10.1038/s41586-020-2675-0>

In our original paper we showed that left–right (L–R) asymmetric cell movements towards the midline produced differential forces that lead to a leftward displacement of the cardiac posterior pole, initiating heart laterality¹. We also showed that the cell movements were mediated by the L–R asymmetric activation (higher on the right) of transcription factors (Snail and/or *Prrx*) that induce epithelial–mesenchymal transition (EMT), and that this cellular behaviour is conserved in zebrafish, chicken and mouse¹. In the accompanying Comment, Tessadori et al.² question the role of *Prrx1a* in heart laterality in zebrafish, after generating mutants that do not present heart laterality defects. Injection of one of the morpholinos we used (MO1) into zygotic *prrx1a*^{el558} and *prrx1a*^{hu13685} mutant embryos led to a cardiac phenotype that was considered to result from off-target mediated effects that act early in development and alter the structure of the left–right organizer (LRO) (also known as Kupffer's vesicle) in zebrafish^{3–5}. Thus, two questions arise. First, whether the mesocardia phenotype that we observed in *prrx1a*-MO1 embryos was due to non-specific off-target effects; and second, whether *Prrx1a* is dispensable for heart laterality in zebrafish. Here we provide new data indicating that *Prrx1a* has a role in heart laterality in zebrafish (Fig. 1).

We also show that although *Prrx1a* may be dispensable, as seen in genetic knockout experiments, other EMT transcription factors (namely *Twist1a* and *Snail1b*) are also expressed in a L–R asymmetric manner in the relevant region of the anterior lateral plate mesoderm (ALPM). Furthermore, GO CRISPR-induced mutant (crisprant) embryos for *twist1a* and *snail1b* also show

mesocardia (Fig. 2), raising the possibility that they may cooperate with and/or compensate for the loss of Prrx1a and, if so, explaining the absence of cardiac laterality defects in *prrx1a* zebrafish mutants.

To further examine the specificity of the heart phenotype, we generated *prrx1a*-crispr embryos (G0) with an additional set of guides (Fig. 1a), and using a Cas9 protein optimized to prevent off-target function^{6,7}, in conditions that have been shown to generate mutagenized G0 embryos that lack confounding non-specific traits⁶. Prrx1a protein cannot be detected in these embryos, confirming the efficiency of the guides (Fig. 1b) and showing that mutations are induced in virtually all copies of the targeted gene in the zebrafish G0 crispr embryos⁶. These embryos show the same defects that we described previously¹—namely mesocardia (although at a lower penetrance) and a reduction in the size of the atrium (Fig. 1c, d). Other defects, such as a smaller head, were also previously observed in *prrx1a* and *prrx1b* double mutants⁸. Notably, both the cilia in the LRO and the expression of *spaw* appear normal (Fig. 1e, f), indicating that the crispr embryos do not have the early defects in the LRO that were observed in the morpholino-induced mutant embryos and that could non-specifically influence heart laterality. Moreover, the decision of the posterior pole of the heart to move from the midline to the left occurs late—independent of the formation of the LRO and heart jogging^{9,10}. This is also in agreement with our photoablation experiments that were performed after jogging¹.

We generated a *prrx1a*-mutant allele (*prrx1a*^{*in69*}) using the set of guides that was also used for the generation of crispr embryos (yellow in Fig. 1a, g). This mutant allele generates a *prrx1a* transcript that lacks the splice site at exon 1 and hence cannot encode a functional Prrx1a protein (Fig. 1g). Thus, the *in69* mutation is equivalent to a *prrx1a* loss-of-function mutation. This mutant—like the *prrx1a* null mutants *hu13685*, *hu13762* and *el803*—does not show mesocardia, indicating that Prrx1a may be dispensable, as suggested by Tessadori et al.². However, this does not necessarily mean that Prrx1a is not involved in heart laterality. The *in69* mutant allows us to directly examine the specificity of the RNA guides in targeting *prrx1a*, as the corresponding guide sequences are not present in its genome. As expected for a bona fide specificity control, when *prrx1a*^{*in69*} homozygous mutant embryos are injected with these guides they do not show any detectable defect, whereas the injection of these guides into wild-type sibling embryos leads to mesocardia (Fig. 1g). Thus, although we cannot formally exclude the existence of an off-target effect, all of this evidence supports that the mesocardia phenotype we observe in G0 crispr embryos is a specific effect of targeting the *prrx1a* gene.

Germline mutations might compensate for deficiencies that cannot be compensated after acute losses such as the somatic mutations induced by CRISPR–Cas9, with the latter revealing putative gene redundancy⁶. Compensatory mechanisms include transcriptional adaptation through mRNA nonsense-mediated decay^{11,12} or activation of paralogues, but these mechanisms are rejected by Tessadori et al.². Notably, compensation can also be achieved by non-paralogous genes, provided they have similar functions¹³. We have now found a transient L–R asymmetric expression pattern similar to that of *prrx1a* for two other EMT transcription factor genes—*snail1b* and *twist1a*—in the ALPM, in which the precursor cells of the second heart field are located (Fig. 2a). G0 crispant embryos for *snail1b* or *twist1a* also showed a heart laterality phenotype (Fig. 2b), and we have previously shown that Twist transcription factors can cooperate with Prrx1 in zebrafish and in cancer cells¹⁴. Thus, all of these data are compatible with a scenario in which the three EMT transcription factors cooperate in the regulation of heart laterality, and in which Snail1b and/or Twist1a might compensate for the loss of Prrx1a.

With respect to the mechanism we described for heart lateralization in vertebrates, we showed that a similar mechanism operates in the chick embryo (using short interfering RNA (siRNA)), and in the mouse embryo (using conditional mutants)¹. Furthermore, this mechanism is compatible with previous studies that proposed a L–R asymmetric contribution to the posterior pole of the heart for heart laterality^{15,16}. In addition, with regard to the conservation of the Nodal pathway in vertebrates⁵, we have shown that the transient L–R asymmetric expression of EMT transcription factors that leads to differential L–R cell movements is established by a Nodal-mediated transient activation of microRNAs in the LPM. Deregulation of these microRNAs by gain and CRISPR–Cas9-mediated loss of function, or by genetic deletion of their binding sites in Prrx1 or Snail1 3' untranslated regions, led to bilateral symmetric expression of Prrx1 and Snail1 and mesocardia in both zebrafish and mice¹⁷.

All of the data above, together with previous comprehensive morphological, functional and computational studies of cardiac development in mice^{18,19}, support our conclusion that the displacement of the posterior pole of the vertebrate heart from the midline implies a differential L–R EMT¹. Whether other EMT transcription factors compensate for Prrx1a loss, and how the right-handed heart looping occurs after the leftward displacement of the posterior pole, deserve further investigation, although the latter is probably driven by intrinsic cues, as previously suggested^{9,10}.

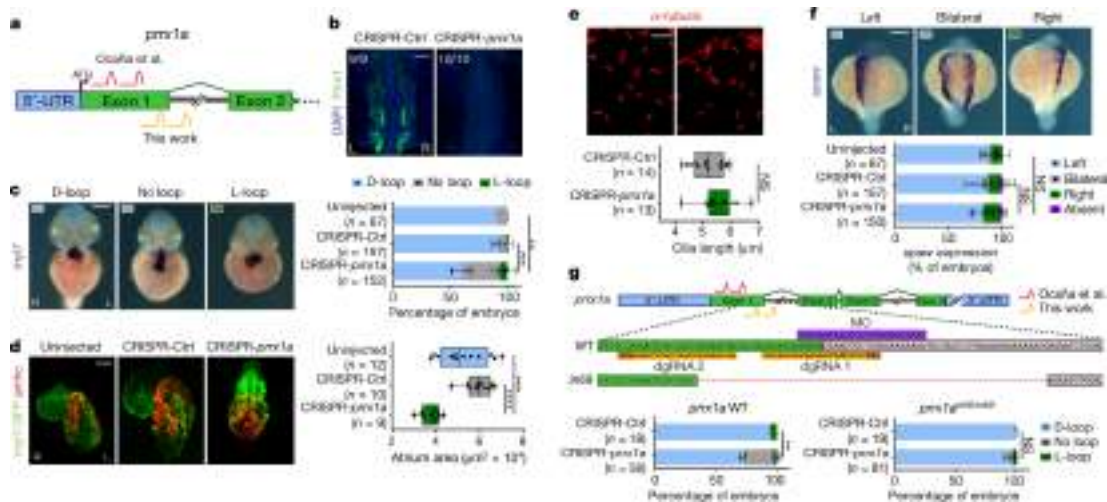


Fig. 1 | *prrx1a*-crispant embryos show mesocardia and a smaller atrium without early defects in the LRO. **a**, Schematic representation of the *prrx1a* gene and the RNA guides used previously¹ (pink) or in this work (yellow). UTR, untranslated region. **b**, Immunofluorescence at the 18-somite stage shows the absence of Prrx1a protein in *prrx1a*-crispant embryos (dorsal view). **c**, Analysis of heart position at 52 hours post-fertilization (hpf) shows mesocardia (no loop) in *prrx1a*-crispant embryos. Images are shown in ventral view. D-loop, posterior pole to the left and dextral loop; L-loop, posterior pole to the right and sinistral loop. **d**, Whole-mount *in situ* hybridization for *amhc* (atrial marker) in *Tg(myl7:GFP)* embryos (in which a *myl7* promoter drives GFP expression in cardiomyocytes) at 52 hpf. *prrx1a*-crispant embryos show a reduction in the size of the atrium. Images are shown in ventral view. **e**, Immunofluorescence of acetylated α -tubulin shows that cilia in the Kupffer's vesicle are not affected in 8-somite-stage *prrx1a*-crispant embryos. **f**, Normal left-sided *spaw* transcripts in 20-somite-stage *prrx1a*-crispant embryos (dorsal view). **g**, The *prrx1a* gene, with coding sequences highlighted in green and intron sequences in grey. The *prrx1a*ⁱⁿ⁶⁹ allele contains a 69-nucleotide deletion generated using the new CRISPR-*prrx1a* guides (yellow). Protospacer adjacent motif (PAM) sequences are highlighted in orange and the predicted sites of Cas9 digestion are marked with red dotted lines. The *in69* allele lacks both of the guide sequences (yellow) at the *prrx1a* locus. The position of the morpholino (MO) in our original study¹ is highlighted in purple. As expected from the lack of the guide sequences in the mutant and for a bona fide specificity control, only the embryos with wild-type (WT) alleles present a mesocardia phenotype after injection of CRISPR-Cas9 *prrx1a* reagents. dgRNA, dual-guide RNA. Data in **c**, **f**, **g** are mean percentage \pm s.d. In box plots (**d**, **e**), centre lines, medians; box limits, second and third quartiles; whiskers, first and fourth quartiles. n = number of embryos analysed from one (**d**, **e**), two (**b**, **g**) or three (**c**, **f**) independent experiments. Statistical analysis: two-way analysis of variance (ANOVA) (**c**, **f**, **g**); one-way ANOVA (**d**); unpaired Student's t-test (two-tailed) (**e**). NS, not significant, **P < 0.01, ***P < 0.001, ****P < 0.0001. Scale bars, 200 μ m (**b**), 250 μ m (**c**, **f**), 50 μ m (**d**) and 40 μ m (**e**). See Supplementary Methods.

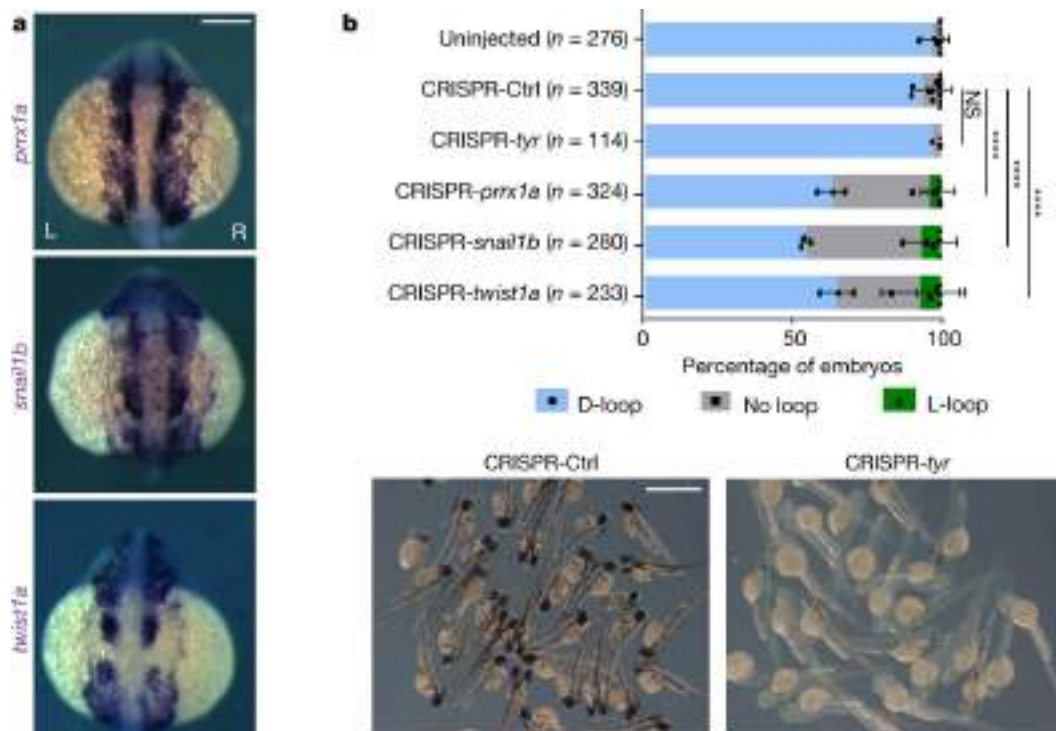


Fig. 2 | EMT transcription factors in heart laterality in zebrafish. a, L–R asymmetric expression of the EMT transcription factors *prrx1a*, *snail1b* and *twist1a* in the ALPM of 20-somite-stage embryos (dorsal view). Representative images from two independent experiments (total number of embryos, n = 60). **b**, Heart position at 52 hpf in crisprant embryos for *prrx1a*, *snail1b*, *twist1a* and *tyr* (tyrosinase; negative control). Note the efficacy of editing in the zebrafish population, as assessed by the level of pigmentation. Data are mean percentage \pm s.d. n = number of embryos analysed from one independent experiment (CRISPR-tyr) or three independent experiments (for each EMT transcription factor). Statistical analysis (shown for the mesocardia phenotype; grey): two-way ANOVA. NS, not significant, ****P < 0.0001. Scale bars, 250 μ m (**a**) and 1.5 mm (**b**). See Supplementary Methods.

Reporting summary

Further information on research design is available in the Nature Research Reporting Summary linked to this paper.

Data availability

All of the raw data that support the findings of this study are available within the manuscript and its associated files. Source data are provided with this paper.

1. Ocaña, O. H. et al. A right-handed signalling pathway drives heart looping in vertebrates. *Nature* **549**, 86–90 (2017).
2. Tessadori, F. et al. Zebrafish *prrx1a* mutants have normal hearts. *Nature* <https://www.nature.com/articles/s41586-020-2674-1>(2020).
3. Collignon, J., Varlet, I. & Robertson, E. J. Relationship between asymmetric nodal expression and the direction of embryonic turning. *Nature* **381**, 155–158 (1996).
4. Long, S., Ahmad, N. & Rebagliati, M. The zebrafish nodal-related gene southpaw is required for visceral and diencephalic left-right asymmetry. *Development* **130**, 2303–2316 (2003).
5. Montague, T. G., Gagnon, J. A. & Schier, A. F. Conserved regulation of Nodal-mediated left–right patterning in zebrafish and mouse. *Development* **145**, dev171090 (2018).
6. Hoshijima, K. et al. Highly efficient CRISPR–Cas9-based methods for generating deletion mutations and F0 embryos that lack gene function in zebrafish. *Dev. Cell* **51**, 645–657 (2019).
7. Vakulskas, C. A. et al. A high-fidelity Cas9 mutant delivered as a ribonucleoprotein complex enables efficient gene editing in human hematopoietic stem and progenitor cells. *Nat. Med.* **24**, 1216–1224 (2018).
8. Barske, L. et al. Competition between Jagged–Notch and endothelin1 signaling selectively restricts cartilage formation in the zebrafish upper face. *PLoS Genet.* **12**, e1005967 (2016).
9. Noël, E. S. et al. A Nodal-independent and tissue-intrinsic mechanism controls heart-looping chirality. *Nat. Commun.* **4**, 2754 (2013).
10. Grimes, D. T. et al. Left–right asymmetric heart jogging increases the robustness of dextral heart looping in zebrafish. *Dev. Biol.* **459**, 79–86 (2020).
11. El-Brolosy, M. A. et al. Genetic compensation triggered by mutant mRNA degradation. *Nature* **568**, 193–197 (2019).
12. Ma, Z. et al. PTC-bearing mRNA elicits a genetic compensation response via Upf3a and COMPASS components. *Nature* **568**, 259–263 (2019).
13. Pasek, S., Risler, J. L. & Brézellec, P. The role of domain redundancy in genetic robustness against null mutations. *J. Mol. Biol.* **362**, 184–191 (2006).
14. Ocaña, O. H. et al. Metastatic colonization requires the repression of the epithelial–mesenchymal transition inducer *Prrx1*. *Cancer Cell* **22**, 709–724 (2012).

15. Taber, L. A., Voronov, D. A. & Ramasubramanian, A. The role of mechanical forces in the torsional component of cardiac looping. *Ann. NY Acad. Sci.* **1188**, 103–110 (2010).
16. Domínguez, J. N., Meilhac, S. M., Bland, Y. S., Buckingham, M. E. & Brown, N. A. Asymmetric fate of the posterior part of the second heart field results in unexpected left/right contributions to both poles of the heart. *Circ. Res.* **111**, 1323–1335 (2012).
17. Rago, L. et al. MicroRNAs establish the right-handed dominance of the heart laterality pathway in vertebrates. *Dev. Cell* **51**, 446–459 (2019).
18. Tautz, D. Redundancies, development and the flow of information. *BioEssays* **14**, 263–266 (1992).
19. Garrec, J. F. et al. A predictive model of asymmetric morphogenesis from 3D reconstructions of mouse heart looping dynamics. *eLife* **6**, e28951 (2017).

Acknowledgements Work in the laboratory is supported by grants from the Ministry of Science and Innovation through the Spanish State Research Agency (AEI) (MICIU RTI2018-096501-B-I00) and from Generalitat Valenciana (PROMETEOII/2017/150). M.A.N. also acknowledges the ‘Severo Ochoa’ Programme for Centres of Excellence in R&D (SEV-2017-0273) to Instituto de Neurociencias.

Author contributions N.C. performed the majority of the experiments, analysed the data and prepared the figures; L.R. performed CRISPR injections and collaborated on the scoring of heart positioning; and A.A. performed bioinformatics analyses. N.C., L.R. and A.A. did not contribute to the original publication but they contributed to this Matters Arising, mainly because O.H.O. and H.C., the main authors of the previous study, moved to the National Centre for Cardiovascular Diseases (CNIC, Spain) and Harvard University, respectively. C. Minguillón, P. Murawala, E. M. Tanaka and R. Muñoz-Chápuli, the other co-authors of the previous study¹, did not contribute to the issues raised in this Reply. They have been informed, and agreed. J.G. designed the CRISPR guides and performed the mutant selection. M.A.N. conceived the study, interpreted the data and wrote the manuscript.

Competing interests The authors declare no competing interests.

Additional information

Supplementary information is available for this paper at <https://doi.org/10.1038/s41586-020-2675-0>.

Correspondence and requests for materials should be addressed to M.A.N.

Reprints and permissions information is available at <http://www.nature.com/reprints>.

Publisher's note Springer Nature remains neutral with regard to jurisdictional claims in published maps and institutional affiliations.

© The Author(s), under exclusive licence to Springer Nature Limited 2020

Supplementary Methods

Animals and Ethical Issues

Zebrafish strain AB wild type and *Tg(myl7:GFP)* were maintained at 28 °C under standard conditions, and the embryos were staged as previously described¹. All animal procedures were conducted in compliance with the European Community Council Directive (2010/63/EU) and Spanish legislation. The protocols were approved by the CSIC Ethical Committee and the Animal Welfare Committee at the Instituto de Neurociencias (CSICUMH), Alicante.

CRISPR Injection

Alt-RR S.r. Cas9 Nuclease V3 (IDT) enzyme and equimolar amounts of crRNA:tracrRNA (Alt- RR CRISPR-Cas9 crRNA and Alt-RR CRISPR-Cas9 tracrRNA IDT) were mixed and incubated to form RNP complexes. The complexes were injected (1 pL containing RNPs at 5µM in 100 mM KCl) into the cytoplasm of one-cell stage embryos and incubated at 28 °C up to the indicated stage. The specific sequence for each crRNA is as follows: *prrx1a* gRNA1 cacagcaggagagtaagtgc, *prrx1a* gRNA2 tcgctcccgtggtgagtcc, *twist1a* gRNA1 tgaggaagaggcgatgcacg, *twist1a* gRNA2 agactgtccaccggagactc, *twist1a* gRNA3 attccgacagtcccacgccc, *snail1b* gRNA1 ttcttgacaagaaatgagcg, *snail1b* gRNA2 gaagccaaactacagtgaac, *tyr* cRNA1 ggactggaggacttctgggg, Control cRNA1 tagagggggcatacaacgca.

Mutant Generation

Wild type AB embryos were injected with Cas9:crRNA:tracrRNA RNP at one cell stage targeting the following genomic sequences tcgctcccgtggtgagtcc and cacagcaggagagtaagtgc at the 3' end of exon 1 of *prrx1a* (see extended legend for Fig. 1g below for details). Guides were designed to induce double strand breaks both upstream and downstream of the exon 1 splice site. Location of PAM is indicated in orange and the predicted cut site is shown in red in Figure 1g. Progeny of the G0 crispants was individually screened by PCR amplification using primers 5'-gccacactaccaaaccgact-3' and 5'-ccattttcccctgtgtgac-3'. Those that showed alterations in the size of the PCR fragment were selected to establish a line, and the region comprising the end of exon 1 and the beginning of intron 1 was sequenced to characterize the nature of the mutation.

*prrx1a*ⁱⁿ⁶⁹ was identified as bearing a 69 nt deletion that included the last 25 nt of exon1 and the first 44 nt of intron 1, therefore containing the sequences of MO binding (Fig 1g).

Whole Mount *in situ* Hybridization and Immunofluorescence

Whole-mount *in situ* hybridization using DIG-labelled probes and fluorescence *in situ* hybridization was performed as described before². Probes for zebrafish *twist1a*, *myl7*, *snail1b*, *spaw*, *amhc* and *prrx1a* were previously described³⁻⁵. For immunofluorescence, whole-mounted embryos were fixed with 4 % PFA overnight at 4 °C and were treated as described before¹. Embryos were incubated with Prrx1 antibody¹ and detected with Alexa Fluor 488 goat anti-rabbit (1:500; Invitrogen, A11008), with mouse anti-acetylated α - tubulin (1:600; Sigma, T6793) and detected with Alexa Fluor 568 goat anti-mouse (1:500; Invitrogen, A11004).

Microscopy and Image Analysis

Pictures of whole-mounted embryos subjected to *in situ* hybridization were taken with a Leica M125 stereoscope, using the Leica suite software with a Leica DFC 7000T digital camera. Immunofluorescence images (Figure 1b) and *in situ* hybridization (Figure 1d) were obtained with a Zeiss lightsheet Z.1 microscope using the following acquisition parameters: Dual side illumination with LSM 5x/0.1 illumination optics, and detection with a PApo 10x/0.5 objective. The excitation and collection of the light was performed as follows: DAPI was excited with laser line 405 nm and collected with a BP 420-470 filter; Alexa 488 was excited with laser line 488 nm and collected with a BP 505-545 filter; and Alexa 568 was excited with laser line 561 nm and collected with a BP575-615 filter. All images were acquired at 16-bit with sCMOS PCO.Edge cameras. Immunofluorescence of Figure 1e was obtained with an Olympus FV1200 microscope with a 40x objective (UPLFLN 1.30 oil). The fluorophore Alexa Fluor 568 was excited with a 559nm laser line and was collected at 570– 620nm.

Statistical Analysis

Statistical analysis was performed using the GraphPad Prism software. Results were expressed as mean \pm SD (standard deviation). Differences between groups were tested by Student's t-test, One-way ANOVA and Two-way ANOVA.

Supplementary References

1. Kimmel, C.B. et al. Stages of embryonic development of the zebrafish. *Dev Dyn* **203**, 253-310 (1995)
2. Nieto, M.A. et al. In situ hybridization analysis of chick embryos in whole mount and tissue sections. *Methods Cell Biol* **51**, 219-235 (1996)
3. Ocana, O.H. et al. A right-handed pathway drives heart looping in vertebrates. *Nature* **549**, 86-90 (2017)
4. Ocana, O.H. et al. Metastatic colonization requires the repression of the epithelial mesenchymal transition inducer Prrx1. *Cancer Cell* **22**, 709-724 (2012)
5. Rago, L et al. MicroRNAs Establish the Right-Handed Dominance of the Heart Laterality Pathway in Vertebrates. *Dev Cell* **51**, 446-459 (2019)

ACKNOWLEDGEMENTS |

No creo que los agradecimientos sea lo que más me cueste escribir de la tesis, pero desde luego no quiero dejarme a ninguna de las personas a las que les debo el bonito tiempo que me han hecho pasar durante estos años en el Instituto de Neurociencias. Quizás este apartado se alargue más de lo aceptable, pero es que sin duda lo mejor que me llevo de aquí es la gente que he conocido, os debo muchísimo, y unas pocas palabras es lo mínimo que puedo hacer por vosotros.

He crecido muchísimo durante estos años, tanto profesional como personalmente. Creo que la Prof. Ángela Nieto puede dar fe de ello. Salí de la carrera creyendo que sabía mucho, pero al final cuando empiezas a trabajar en tu carrera investigadora vives la paradoja de cuanto más sabes, más te das cuenta de lo que te queda por aprender. Me has ayudado a madurar, a tener una mente mucho más crítica y a saber defender mis ideas y mis experimentos. Creo que sale una versión mucho más completa y mejorada de mí gracias al haber estado en este laboratorio. Muchas gracias por todo. También a Joan Galcerán. Gracias por tu ayuda y aprendizaje durante estos años. Por poder ir a preguntarte dudas y ayudarme a sacar adelante mi proyecto. Por saber llegarnos a entender. He aprendido lo importante del poder de la comunicación. Gracias. A Berta, quizás no hayamos coincidido tanto profesionalmente, pero no tengo duda de que me habrías ayudado en caso de necesitarlo. He visto como ha crecido muchísimo tu lab en estos años, y deseo que así siga.

Otro gran apoyo durante esta etapa ha sido Khalil. Muchas gracias por siempre sacar un hueco para ayudarme, por hacerme reflexionar sobre mi proyecto y no quedarme en la superficie. Tienes siempre muy buenas ideas, aunque algunas un poco locas jajaja, pero siempre estás dispuesto a ayudar, incluso cuando tienes mil cosas más que hacer. Realmente te deseo que todo el esfuerzo que pones te sea recompensado, porque sé que te lo mereces. A Oscar por estar en gran parte de mi primera etapa predoctoral, cuando aún me quedaba mucho por aprender. Me alegré mucho por tu salto profesional al CNIC, y como a Khalil también te deseo que encontréis vuestro lugar.

También quiero dar las gracias a Luciano, contigo he aprendido mucho sobre tomarse la vida con filosofía, a ver la otra cara de la moneda. La vida es relativa, y es muy de grises y no tanto de blancos y negros. A Verona, persona a la que admiro muchísimo. Siempre recordaré tus presentaciones, me quedaba embobada viendo la calidad de tus imágenes, y pensaba que me encantaría llegar a “ser como tú de mayor”. Gracias por los cafés y tu escucha activa, eres una

Agradecimientos

persona que vale muchísimo. To Hassan, you have been my spiritual guide: *“Nothing is impossible, somethings just require more time”*. You were completely right. I missed you a lot when you started to work as a posdoc. It is always very nice to hear your voice, even more if you are singing. A Aida Arcas, por siempre estar dispuesta a sacar lo mejor de mis datos y hacerme un hueco, aunque estuvieras ocupada. He aprendido mucho de ti a dar prioridad al tiempo de uno mismo y poner límites. To Hakan. I have learned a lot from you in the lab. Unluckily for me, you have only met the "clumsy" version of Noemi in the lab, I swear I've improved hahaha. I wish you well in the other side of the sea.

A Cris mi mamá metalera. Me has aportado tantísimo durante estos años. Me has formado en lo mejorcito del metal, te debo conocer unos grupos y subgéneros increíbles, a aprender a tocar la guitarra cada día un poquito menos robot, me has salvado en conciertos y festivales donde tenía como ir, pero no como volver. En el lab eres fundamental para todos, y me da mucha pena no haber trabajado contigo porque sé que habría aprendido un montón mientras me lo habría pasado genial. Nos seguiremos viendo allá donde el metal suene. A Diana. No ha pasado persona más dulce por el lab. Gracias por tus sonrisas y tu ayuda, generabas muy buen ambiente en el laboratorio y se te echa mucho de menos. Te deseo lo mejor. A Sonia, que siempre está dispuesta a ayudarnos a todos. Da gusto tratar con gente como tú, que siempre vas a decir las cosas con respecto y con la mejor de las maneras, aunque sea “para echarnos la bronca”. Consigues que en el lab estemos mucho mejor. A Cristina Minaya, gracias de verdad por ayudarme en el último empujón de mi doctorado. Muchas gracias a ti Auxi, que siempre vas detrás de todos nosotros. Te mereces mucho porque se nota todo lo que te importamos.

A Fran García. Creo que eres de las personas más especiales que he conocido durante estos años. Si hay una palabra que te define es particular. He pasado muchísimas cosas contigo con muchos altibajos, pero hemos crecido y para bien jajaja. Me alegra tanto no haber perdido el contacto contigo aun después de irte a Suiza, eres una de esas personas que quiero seguir manteniendo en mi vida. A Ainara, gracias a ti he integrado en mi el verdadero significado de la palabra sororidad. Me alegra mucho el punto en el que estamos las dos. Espero que sigas creciendo profesionalmente. A Sandy Brownie. Flipé contigo desde el día uno que te conocí. Siempre que me acuerdo de ti me viene a la mente tu risa. Eres de esas personas que están y alegran muchísimo el ambiente. Me encantó vivir contigo. Feliz por el pedazo enfermera que sé que vas a ser, triste por verte tan poco. A Sergio Cano, el que va a 1000 revoluciones por segundo. Como Sandra eres de esas personas que alegra el ambiente cuando estás. Te deseo a ti también lo

mejor. A Juan Medrano. Siempre me alegra tanto saber de ti, eres una personita que merece muchísimo la pena, random pero se te quiere. Me hace feliz que hayas vuelto a aparecer en nuestras quedadas.

A Javi. Sé que vas siempre muy liado, pero los huecos que me buscas siempre me lo paso genial contigo. Te debo muchos momentos muy buenos y de muy buena calidad, y eso casi siempre pesa más. Te quiero mucho y te deseo a ti también que todo el curro que te estás pegando en esta vida te sea recompensado. A Marta. Te adoro Marta. Me encanta tomarme cafés contigo, que vengas a buscarme, salir de fiesta contigo. Me encanta esa naturalidad, esa inocencia. Estas loquísima y te quiero un montón. Me falta hacer un viaje contigo jajajaja. A Fran Quiles, por favor nunca cambies. AMO como eres de único. Gracias a ti conozco el verdadero y único camino en la vida: ir con flow. Orgullosa de tener como amigo al más guapo del INA. A Andrea, hemos pasado muchas cosas. Nos podemos dar la mano porque creo que vamos por caminos muy paralelos, en el fondo nos entendemos perfectamente. Espero que la vida te aporte todo lo que te mereces, y me harías muy feliz con... ya tú sabes jajajaja. Nunca es tarde para ser tia por segunda vez jajajaja. A Fran Cabello, mi Pachi que va como pollo sin cabeza. Te hemos echado en falta en más de una fiesta. Espero verte por lo menos en el Resu. A David. Otra personita que me encanta. Te conozco de hace poco, pero vayámonos a vivir juntos jajaja. La vida son dos días.

A Marilyn siempre tan mona. Tenemos que visitarte más, que tus hijos te tienen secuestrada jajaja. A Mari Ángeles, a la que deseo de corazón que te vaya genial. To Sanjay. I would have like to work with you more, but I rather prefer to see you smiling again. To Nitin, who like Hassan I strongly believe that is a good person. The world needs more people like you. A Andrés mi viejoven, Noelia, Pablo y Raúl. Gracias a todos por crear un buen ambiente de laboratorio.

También quiero dar las gracias a la gente que trabajaba o ha trabajado en el centro como Selene y Laura del animalario. Sois geniales. A Giovanna, muchísimas gracias por tanta ayuda. Tienes el cielo ganado con tanta paciencia. A Antonio que contagias esa alegría. A Maite y a Ruth, por poner las cosas tan fáciles. A todos los conserjes. Da gusto entran al centro. Y a muchísima más gente que trabajan en el Instituto de Neurociencias.

Aysha. Mi bombón canario. Eres de esas personas que no pasa desapercibida. Me acordaré del primer día que te conocí que pensé: *¿por qué esta chica es tan extrovertida y contagia tan buen rollo?, me encanta ¿de dónde ha salido?* También sé que siempre vas muy liada y tienes una agenda social muy apretada, pero que cuando necesito contarte mis dramas estás ahí.

Agradecimientos

Literalmente te conoces todos mis dramas. Eres reina por fuera y por dentro. Te quiero mucho, y espero poder conservar contigo la amistad, aunque estemos lejos.

Lucia, has sido sin duda una de las personas más especiales también durante mi doctorado. Me has visto en mis momentos más turbios y también en los más felices. Te debo muchísimas cosas, pero desde luego quizás lo que más es la búsqueda de la paz mental. El darles importancia a todos los aspectos de mi vida, a la familia, a los amigos, a mí misma. Como ya te dije, eres la persona más pequeñita y grande que conozco. Gracias, por tanto. Te quiero se queda corto. No te preocupes, nos veremos en el camino para convertirnos en ninjas jajajja.

Es que de verdad que lo mejor de este centro es la gente que hay en él. Bea, Alicia, Sofia, Carina, Chrysa, Ernesto, Pablo, Alejandro, Francesco, Irene, Juan Carranza y Juan Paraíso. En general Angel's Barco Lab. Muchísimas gracias por tantos días de buenos recuerdos, por tantas risas. Por sentirme tan a gusto con vosotros. Me va a costar mucho despegar de este sitio, ahora que conozco a tanta gente especial.

También quiero dar las gracias a gente que ha contribuido en este camino desde fuera. A Cris, mi mejor amiga. He compartido tantísimo contigo. Lo que escriba aquí sé que no es suficiente, lo tengo clarísimo. Siempre que he querido contar contigo has estado ahí. No matter what. Quiero vivir muchos más conciertos contigo y compartir nuestras aficiones. Si me mudo necesito que te vengas conmigo, es requisito indispensable. Te amo Cris. A Vicente, con el que pasé muy buenas tardes en el local ensayando. Me abstraía de mis problemas y me ayudó mucho en una época muy mala. Gracias de corazón. A Jose Isidro, gracias por ser tú. Me encantan las personas así de especiales y de auténticas. Por más cervezas y aprender de ti. Eres pura fantasía.

A vosotros Adrian, Andrés, Caru y Sergio. Siempre me pone muy feliz cuando nos juntamos. Me alegra mucho haber mantenido el contacto con vosotros después de la carrera. Por la competición sana que teníamos por sacar la mejor nota. Me da pena no haber podido pasar tanto tiempo con vosotros durante la carrera como me habría gustado. Pero nunca es tarde, siempre podremos sacar algún hueco para seguir aprendiendo uno de los otros. Os deseo lo mejor en vuestra vida y espero manteneros en la mía. Os quiero mucho.

A Cristina que nunca me dejó echar la toalla. Tú sí que me has visto crecer y creo que puedes sentirte orgullosa de mí. Creo que conocerte ha sido una de las mejores cosas que me ha podido pasar en la vida. Creo que todas las Cristinas de mi vida son muy especiales. Gracias por todo.

Agradecimientos

A mi familia. A mis padres que nunca me han presionado o han esperado de mí, me han dejado ser. Y aun así me han apoyado a acabar porque sabían que es lo que yo quería. Gracias por darme mi espacio. A mis hermanas, gracias por inspirarme a mejorar. Gracias por creer en mí. Os quiero mucho. A Jordi, gracias por siempre abrirme las puertas de tu casa y encima con una cerveza jajaja. Y ya la personita que ha hecho que me vuelva loca, con la que he aprendido que es el amor del bueno. A ti Marc, que de momento no te enteras de la película pero que me has dado fuerzas para acabar. Eres de las cosas más bonitas de mi vida.

Gracias se me queda corto, os quiero mucho. A todos. Lo más bonito de esta etapa sois vosotros.

PD: Espero no haber caído en tópicos. Es muy difícil verbalizar todo lo bonito que me aportáis.

Con mucho amor,

Noemi :)

